

Spectral Line Survey toward Young Massive Protostar NGC 2264 CMM3 in the 4 mm, 3 mm, and 0.8 mm Bands

Yoshimasa Watanabe¹, Nami Sakai¹, Ana López-Sepulcre¹, Ryuta Furuya¹, Takeshi Sakai²,
Tomoya Hirota³, Sheng-Yuan Liu⁴, Yu-Nung Su⁴

and

Satoshi Yamamoto¹

nabe@taurus.phys.s.u-tokyo.ac.jp

ABSTRACT

Spectral line survey observations are conducted toward the high-mass protostar candidate NGC 2264 CMM3 in the 4 mm, 3 mm, and 0.8 mm bands with the Nobeyama 45 m telescope and the Atacama Submillimeter Telescope Experiment (ASTE) 10 m telescope. In total, 265 emission lines are detected in the 4 mm and 3 mm bands, and 74 emission lines in the 0.8 mm band. As a result, 36 molecular species and 30 isotopologues are identified. In addition to the fundamental molecular species, many emission lines of carbon-chain molecules such as HC₅N, C₄H, CCS, and C₃S are detected in the 4 mm and 3 mm bands. Deuterated molecular species are also detected with relatively strong intensities. On the other hand, emission lines of complex organic molecules such as HCOOCH₃, and CH₃OCH₃ are found to be weak. For the molecules for which multiple transitions are detected, rotation temperatures are derived to be 7–33 K except for CH₃OH. Emission lines with high upper-state energies ($E_u > 150$ K) are detected for CH₃OH, indicating existence of a hot core. In comparison with the chemical composition of the Orion KL, carbon-chain molecules and deuterated molecules are found to be abundant in NGC 2264 CMM3, while sulfur-bearing species and complex organic molecules are deficient. These characteristics indicate chemical youth of NGC 2264 CMM3 in spite of its location at the center of the cluster forming core, NGC 2264 C.

¹Department of Physics, The University of Tokyo, 7-3-1 Hongo, Bunkyo-ku, Tokyo, 113-0033, Japan

²Graduate School of Informatics and Engineering, The University of Electro-Communications, Chofu, Tokyo 182-8585, Japan

³National Astronomical Observatory of Japan, Osawa, Mitaka, Tokyo 181-8588, Japan

⁴Academia Sinica, Institute of Astronomy and Astrophysics, PO Box 23-141, Taipei 106, Taiwan

Subject headings: stars: formation – ISM: individual(NGC 2264) – ISM: molecules

1. Introduction

Spectral line surveys are of fundamental importance in astrochemistry and astrophysics. They reveal chemical characteristics of a target source without any preconception, and the result is subject to detailed chemical and physical modeling to strengthen basic concepts of astrochemistry, as well as to explore physical conditions of the target source. In the course of the spectral line survey, many new interstellar molecules have been discovered, and new molecular tracers which highlight particular physical situations have been recognized. Since the early days of radioastronomy, spectral line surveys have been conducted toward various representative sources including star-forming regions (e.g. Blake et al. 1986; van Dishoeck et al. 1995; Schilke et al. 1997; Bergin et al. 2010; Tercero et al. 2010; Watanabe et al. 2012), cold dark clouds (Kaifu et al. 2004), shocked regions (e.g. Codella et al. 2010; Sugimura et al. 2011; Yamaguchi et al. 2012), photodissociation regions (e.g. Ginard et al. 2012; Cuadrado et al. 2015), Galactic center clouds (e.g. Cummins et al. 1986), and external galaxies (e.g. Martín et al. 2006; Watanabe et al. 2014). Thanks to recent advances in receiver and backend technologies, spectral line surveys become feasible even toward fainter sources, and are being carried out toward various kinds of sources not only with single-dish telescopes but also with interferometers (e.g. Beuther et al. 2009; Jørgensen et al. 2011; Martín et al. 2011).

For instance, Caux et al. (2011) conducted the spectral line survey of the low-mass protostar, IRAS 16293-2422, which is known as a ‘hot corino’ source (Cazaux et al. 2003) with the IRAM 30 m telescope, whereas the spectral line survey of the low-mass protostar L1527, known as a warm-carbon-chain-chemistry source (Sakai et al. 2008), was carried out with the Nobeyama 45 m telescope (Sakai et al. in prep.). Although these two sources are low-mass protostars in the Class 0 stage, their spectral patterns are significantly different from each other. This result clearly established chemical diversity of low-mass protostellar cores, whose origin and future are of great interest in relation to the origin of the Solar System (Sakai et al. 2008, 2009; Sakai & Yamamoto 2013). Watanabe et al. (2012) and Lindberg & Jørgensen (2012) reported further chemical complexity due to external UV radiation in a low-mass protostar R CrA IRS7B. Furthermore, the spectral line surveys of the shocked region L1157 B1 which is caused by the interaction between the molecular outflow and the ambient gas were performed by several telescopes including the Nobeyama 45 m telescope (Sugimura et al. 2011; Yamaguchi et al. 2012), the IRAM 30 m telescope (e.g. Codella et al. 2012; Podio et al. 2014; Mendoza et al. 2014), and Hershel HIFI (e.g.

Codella et al. 2010). It is revealed that the shocked region harbors rich organic chemistry originating from sublimation and/or sputtering of grain mantles. This reminds us of the importance of grain-surface productions of organic molecules.

Chemical evolution of high-mass protostellar sources may be much different from that of low-mass ones, and its detailed understanding is not only important for astrochemistry but also useful for finding diagnostic tools of high-mass star formation. With these motivations, we conducted spectral line survey observations toward the high-mass star-forming region NGC 2264 CMM3 in the 4, 3, and 0.8 mm bands with the Nobeyama 45 m and the Atacama Submillimeter Telescope Experiment (ASTE) 10 m telescopes to characterise its chemical nature.

NGC 2264 CMM3 is the second nearest high-mass star-forming region after Orion KL ($d = 738$ pc: Kamezaki et al. 2014). Many submillimeter-wave continuum sources (CMM1-13) are identified around IRS1, the brightest infrared source in the NGC 2264 C region (Peretto et al. 2006, 2007). Among them, CMM3 is the most massive one ($40 M_{\odot}$: Peretto et al. 2006), and it is believed that CMM3 will evolve into a massive star of $8 M_{\odot}$, according to the theoretical model by Maury et al. (2009). However, the protostar of CMM3 is deeply embedded in the protostellar core, and invisible even in the $24 \mu\text{m}$ band of *Spitzer*. Although a molecular outflow extended toward north and south directions was detected around CMM3 in the CS ($J = 5 - 4$) emission by Schreyer et al. (1997), its association with CMM3 was not evident. Saruwatari et al. (2011) detected a compact bipolar outflow definitively associated with CMM3 in the CO($2 - 1$), and CH₃OH($5_0 - 4_0$ A⁺) lines with SMA, whose dynamical age is as short as 140–2000 yr. Hence, it is very likely that CMM3 is in the earliest evolutionary stage of a high-mass star formation. Moreover Sakai et al. (2007) detected the millimeter-wave lines of one of complex organic molecules, HCOOCH₃, toward this source with the Nobeyama 45 m telescope and Nobeyama Millimeter Array, and found that its distribution is offset from the continuum emission peak of CMM3 by $5''$ – $10''$. This result implies rich chemistry in CMM3 associated with activities of a young high-mass protostar.

2. Observation

2.1. Observation with Nobeyama 45 m

NGC 2264 CMM3 was observed in the 4 mm and 3 mm bands with the Nobeyama 45 m telescope at the Nobeyama Radio Observatory (NRO)¹ in May and December, 2014. The observed position is : $(\alpha_{J2000}, \delta_{J2000}) = (6^{\text{h}} 41^{\text{m}} 12^{\text{s}}.3, +09^{\circ} 29' 11''.9)$. Eight frequency settings were observed to cover the frequency range from 67.5 to 116.0 GHz. The side-band separating (2SB) mixer receivers T70H/V and TZ1H/V (Nakajima et al. 2013) were used as frontends with the typical system noise temperature of 140 – 380 K. The image rejection ratios were measured just before each observation session by applying artificial signals, and were assured to be better than 10 dB. The beam size ranged from 22'' to 15''. The backends were 16 SMA45 autocorrelators whose band width and frequency resolution each are 1600 MHz and 0.5 MHz, respectively. The frequency resolution corresponds to a velocity resolution of 1.7 km s⁻¹ at 90 GHz. This resolution is enough for resolving spectral line profiles observed in NGC 2264 CMM3 (~ 3 km s⁻¹). The position-switching method was employed with the off-position at $(\Delta\alpha, \Delta\delta) = (-25', -25')$. The telescope pointing was checked every hour by observing the SiO maser source SY-Mon. Pointing accuracy was confirmed to be better than 5''. Intensity scale was calibrated to the antenna temperature (T_{a}^*) scale by using the chopper-wheel method, and its accuracy is estimated to be 20 %. The antenna temperature was converted to the main-beam brightness temperature (T_{mb}) by $T_{\text{mb}} = T_{\text{A}}^*/\eta_{\text{mb}}$, where η_{mb} is 0.38, 0.31, 0.26, and 0.24 at 75, 86, 110, and 115 GHz, respectively. The observation parameters are summarized in Table 1.

The observed data were reduced by using the software package, NEWSTAR, developed by NRO. Spectral baselines were subtracted by fitting a 5th - 7th order polynomial to the line-free part of spectra in a frequency range of ~ 1.5 GHz. Distorted sub-scan spectra due to bad atmospheric conditions and instabilities of the receiver system, whose baseline could not be subtracted by the polynomial fitting, were excluded in the integration procedure.

2.2. Observation with ASTE

Observations with the ASTE 10 m telescope (Ezawa et al. 2004) were carried out in May and November 2011. The observed position is the same as that in the observations with the Nobeyama 45 m telescope. Eighteen frequency settings were observed to cover the frequency

¹Nobeyama Radio Observatory is a branch of the National Astronomical Observatory of Japan, National Institutes of Natural Sciences

range from 330 to 366 GHz. In the 345 GHz band, the beam size is $\sim 22''$, and the main beam efficiency (η_{mb}) is ~ 0.6 . The side-band separating (2SB) mixer receiver CATS345 (Inoue et al. 2008) was used as a frontend, whose typical system temperature ranged from 150 to 400 K, depending on the atmospheric conditions. The backend was a bank of XF-type digital spectro-correlators MAC (Sorai et al. 2000), whose bandwidth is 512 MHz each, all having 1024 spectral channels. The frequency resolution is 0.5 MHz, which corresponds to $\sim 0.5 \text{ km s}^{-1}$ at 345 GHz. The position-switching method was employed with the off-position at $(\Delta\alpha, \Delta\delta) = (-25', -25')$. The telescope pointing was checked every hour by observing the bright point-like $^{12}\text{CO}(J = 3 - 2)$ source GX Mon. The pointing accuracy was ensured to be better than $3''$. The intensity calibration was carried out by the chopper-wheel method, and its accuracy is estimated to be $\sim 20 \%$. The antenna temperature (T_{A}^*) was converted to the main-beam brightness temperature (T_{mb}) by $T_{\text{mb}} = T_{\text{A}}^*/\eta_{\text{mb}}$. The observation parameters are summarized in Table 1.

The observed data were reduced by using NEWSTAR. Spectral baselines were subtracted by fitting a 5th order polynomial to the line-free part in a frequency range of 512 MHz. Distorted sub-scan spectra were excluded in the integration procedure, as described in Section 2.1.

In addition to the line survey, we conducted a 5-point observation toward NGC 2264 CMM3 in the 342.7 GHz in order to investigate a distribution of CH_3OH around the protostar. The grid spacings are $20''$, which is close to the beam size of $22''$. The result of this 5-point observation will be shown in the Section 4.1.

3. Result and Analysis

3.1. Detected Molecules

Figure 1 shows the overall spectra in the 4, 3, and 0.8 mm bands. Figures A.1 and A.2 show their expanded spectra. In the 3 mm and 4 mm bands, 265 emission lines are detected, while 74 emission lines are detected in the 0.8 mm band. The line detection criterion is that a peak intensity of a line exceeds three times the r.m.s. noise level at the expected frequency.

The line identifications are carried out on the basis of the spectral line databases the Cologne Database for Molecular Spectroscopy (CDMS) managed by University of Cologne (Müller et al. 2001; Müller et al. 2005) and the Submillimeter, Millimeter, and Microwave Spectral Line Catalog provided by Jet Propulsion Laboratory (Pickett et al. 1998). From the detected emission lines, 35 molecular species and 29 isotopologues are identified in the 3 mm and 4 mm bands (Table 2). In the 0.8 mm band, 17 molecular species and 13 isotopologues

are identified (Table 3). In total, 36 molecular species and 30 isotopologues are identified in this spectral line survey. For the weak emission lines, we carefully check the presence of other emission lines of the same species at other frequencies. SO^+ , NH_2CHO , HCO_2^+ , HCOOCH_3 , and CH_3OCH_3 are tentative detections, because their lines are marginally detected (Figure 2). HCOOCH_3 was identified by Sakai et al. (2007) in this source. Sakai et al. (2007) detected the HCOOCH_3 ($8_{18}-7_{17}$ A and E) lines with a peak intensity of 84 ± 15 mK. Although these lines were not detected in the present survey probably due to lower sensitivity, a few other lines were marginally detected (Figure 2). Several HCOOCH_3 lines can be seen in the E state, but most of companion HCOOCH_3 lines in the A state whose upper state energy and $S\mu^2$ are similar to those of the HCOOCH_3 in the E state are very weak. Hence, detection of HCOOCH_3 is tentative in this survey. As for CH_3OCH_3 , two weak lines were marginally detected in this survey, since four sub-states of internal rotation are almost overlapped at the frequencies. On the other hand, other transition lines of CH_3OCH_3 are not detected due to lower sensitivity and detection of CH_3OCH_3 is also tentative. The detected molecules including tentatively detected ones are summarized in the Table 4. In spite of the above identification process, 22 lines are still unidentified in the 4 and 3 mm bands. They are also listed in Table 2. The criterion of the unidentified line is that the line is detected with 3σ confidence or higher and the line width is reasonable. Since the criterion is not stringent, some of them may be spurious signals. Hence, the data of the unidentified lines should be used carefully. On the other hand, no unidentified lines are found in the 0.8 mm band. The line-of-sight velocity and FWHM line width of each line are evaluated by a single Gaussian fit. If the line profile is blended with multiple lines such as nearby hyperfine components, multiple Gaussian functions are employed to determine the line parameters. Tables 2 and 3 present lists of the line parameters of the identified molecular lines including tentatively detected ones.

In the 3 mm and 4 mm bands, we detected many lines of various carbon-chain molecules, which include C_4H , HC_3N , HC_5N , CCS , and C_3S . In general, carbon-chain molecules are less abundant in star-forming regions than in young starless cores (e.g. Suzuki et al. 1992; Hirota et al. 2009). This is particularly true for long carbon-chain molecules. Hence, detection of various carbon-chain molecules in NGC 2264 CMM3 should be noteworthy. In addition to carbon-chain molecules, saturated molecules such as CH_3OH and CH_3CHO are also detected. However, complex organic molecules such as HCOOCH_3 and CH_3OCH_3 seem to be deficient in this source, since these molecules are marginally detected. Furthermore, nitrogen bearing complex organic molecules such as $\text{C}_2\text{H}_3\text{CN}$ and $\text{C}_2\text{H}_5\text{CN}$ were not detected in the present line survey.

Another characteristic feature of the NGC 2264 CMM3 spectrum is the relatively bright emission of deuterated species such as DCO^+ , DCN , DNC , and N_2D^+ in the 4 mm band.

Even the spectral lines of CCD and DC₃N are weakly detected. Moreover, five lines of NH₂D are seen in the 0.8 mm, 3 mm, and 4 mm bands.

In the 0.8 mm band, almost all detected emission lines are higher rotational transition lines of molecular species detected in the 4 mm and 3 mm bands, except for NO (nitric oxide). SO₂ is the heaviest molecule observed in this band. No heavy molecules, which consist of more than 3 heavy atoms, were detected except for c-C₃H₂ and SO₂ in the 0.8 mm band. For larger molecules, rotational spectral lines in the 0.8 mm band generally have higher upper-state energies, and they are not well excited except for the vicinity of the protostar. Hence, these lines are usually weak in the single-dish observation in the 0.8 mm band in ordinary star-forming regions (e.g. Watanabe et al. 2012). On the other hand, higher excitation lines of CH₃OH and H₂CO, whose upper state energies (E_u) are higher than 150 K, were detected. These molecules would be abundant in a hot and dense region in the vicinity of a protostar and/or in shocked regions caused by outflows, indicating a sign of a hot core.

3.2. Rotation Temperatures and Column Densities

To investigate molecular abundances and physical conditions of the emitting region, we derive rotation temperatures and column densities for molecules for which multiple transition lines with different upper-state energies are detected. The rotation temperature and the column density are estimated under local thermodynamic equilibrium (LTE) conditions by using a least-squares method with the following formula:

$$\Delta T = \frac{h\nu}{k} \left[\frac{1}{\exp(h\nu/kT_{\text{rot}}) - 1} - \frac{1}{\exp(h\nu/kT_{\text{bg}}) - 1} \right] [1 - \exp(-\tau)], \quad (1)$$

and

$$\tau = \frac{8\pi^3 S \mu^2 N}{3k \Delta \nu Q(T_{\text{rot}})} \left[\exp\left(\frac{h\nu}{kT_{\text{rot}}}\right) - 1 \right] \exp\left(-\frac{E_u}{kT_{\text{rot}}}\right), \quad (2)$$

where ΔT , k , ν , h , T_{rot} , T_{bg} , S , μ , N , $\Delta \nu$, $Q(T)$, and E_u are line intensity, the Boltzmann constant, transition frequency, the Planck constant, rotation temperature, the cosmic microwave background temperature of 2.7 K, line strength, dipole moment, total column density, line width, partition function, and upper state energy of the transition, respectively. In order to take frequency dependence of the beam sizes into account, the observed integrated intensities are divided by the beam filling factor $\theta_{\text{source}}^2/(\theta_{\text{beam}}^2 + \theta_{\text{source}}^2)$, where θ_{source} and θ_{beam} are the assumed source size and the FWHM beamwidth of the telescopes, respectively. Here, the source size (θ_{source}) is assumed to be 15'', which is the smallest beam size of this survey. This source size is almost comparable to the size of the distribution of HCOOCH₃ (Sakai et al. 2007). The beam size θ_{beam} is evaluated at each transition frequency by extrapolating the

beam size measured at some representative frequencies. The common line width (Δv) is assumed to be 3 km s^{-1} except for SiO ($\Delta v = 6 \text{ km s}^{-1}$), and $\int T_{\text{mb}} dv / \Delta v$ is used as the line intensity of ΔT . The error of ΔT includes the r.m.s. noise and the 20 % uncertainty of the intensity calibration by chopper-wheel method. For NH_2D , H_2CO , $\text{c-C}_3\text{H}_2$, H_2CCO , and H_2CS , ortho and para species are analysed separately. For CH_3CCH and CH_3CN , A and E states are analysed separately. Although multiple transition lines of HC_3N and C_3S are detected, we failed to derive their rotation temperatures and column densities of these molecules with this method. For HC_3N , the rotation temperature and the column density could not be determined simultaneously by the least-square fit, probably because of the low excitation temperature and relatively high optical depth ($\tau \sim 1$). For C_3S , the signal-to-noise ratio is not enough to determine the excitation temperature and the column density simultaneously. Hence, column densities of these two molecules are estimated with fixed excitation temperatures in the latter section. Table 5 shows the results of the analyses.

The rotation temperatures are found to be different from molecule to molecule, ranging from 7 K to 122 K. Carbon-chain molecules and fundamental species such as H^{13}CN , HC^{18}O^+ , and CN show relatively low rotation temperatures ($< 11 \text{ K}$). HC_5N shows relatively higher rotation temperature of 25.8 K. Because the upper state energies of the HC_5N lines observed in this survey are from 44 K to 110 K, which are higher than those of the other carbon-chain molecules, the lines would preferentially trace warmer region. Deuterated species, DCN, DCO^+ and NH_2D (para), show a similar trend of low rotation temperature. On the other hand, sulfur-bearing molecules except for sulfur-bearing carbon-chain molecule (CCS) show higher rotation temperatures ($15 < T < 26 \text{ K}$). The rotation temperature of SiO is also as high as 18.2 K. This means that the sulfur-bearing molecules and SiO preferentially reside in a warmer and denser part than the other molecular species. More importantly, we found that the CH_3OH lines cannot be fitted by a single temperature, and hence, we employed the two-component model for CH_3OH with the rotation temperatures of 24 K and 122 K, as discussed later in detail. H_2CO also shows the relatively high rotation temperature ($33 \pm 13 \text{ K}$) in spite of its large uncertainty. It should be noted that the o/p ratio of NH_2D , H_2CS , H_2CCO , and $\text{c-C}_3\text{H}_2$ are close to the statistical value of 3.

For the other molecules for which only one transition line or hyperfine lines with almost the same upper-state energies are detected, the column densities are estimated under the LTE condition with excitation temperatures of 10 K, 15 K, and 20 K by using the least-squares method with equations (1) and (2). The range of the assumed excitation temperature is set on the basis of the rotation temperatures of various molecules (Table 5). In order to correct beam dilution effect, the source size of $15''$ is also assumed as in the case of the rotation diagram analysis. Uncertainties of the derived column densities include the r.m.s. noise and the intensity calibration uncertainty of 20 %. Table 6 summarizes the column densities

obtained in the LTE analysis.

The gas kinetic temperature can be estimated by using the observed intensities of the different K lines of CH_3CN , because the radiation processes between the different K ladders are almost forbidden. The gas kinetic temperature thus obtained from the K structure lines is 37 ± 10 K and 25 ± 10 K by using the $K = 0$ and 3 lines (A-state) and the $K = 1$ and 2 lines (E-state), respectively. Similarly, the excitation temperature between the different K_a levels of H_2CO is close to the gas kinetic temperature. It is as high as 66 ± 14 K and 51 ± 13 K for the $K_a = 1$ and 3 (ortho) and $K_a = 0, 2$ and 4 (para) lines, respectively. This result may further suggest that H_2CO mainly resides in a higher temperature component in the vicinity of the protostar than CH_3CN . This result indicates that NGC2264 CMM3 involves physical and chemical complexity within the beam sizes of the present observations.

4. Discussion

4.1. High Excitation Lines of CH_3OH

In the 0.8 mm band, high excitation lines of CH_3OH with the upper-state energies higher (E_u) than 150 K were detected (Figure 3). The upper-state energies of all the other molecular lines detected in this survey are lower than 150 K except for several lines of H_2CO . The rotation diagram with a single temperature model shows systematic residuals indicating coexistence of cold and warm components (Figure 4). Such a behavior in the rotation diagram is sometimes found in hot core regions. Bisschop et al. (2007) suggested that the two components can appear from sub-thermal excitation and optical depth effects. However, the optical depths estimated from the column density and rotation temperature by the rotation diagram method with a single component are 0.2–0.1 for transitions with the upper-state energies of 90–150 K, where the rotation diagram shows a knee structure. The optical depths are found to be higher for the transitions with $E_u < 60$ K. Therefore, the optical depth effect is not likely the case for NGC 2264 CMM3 as the origin of the systemic residual. Hence, we employ a two-temperature model by extending Eq. (1) for the two-components, and the rotation temperatures of the two components are derived by the least-squares fit on all the observed lines of CH_3OH . The rotation temperature are derived to be 24.3 ± 2.6 K and 122 ± 63 K. The higher temperature component seems to correspond to the hot component in the vicinity of the protostar, although the error of the temperature is large.

Figure 5 shows a profile map of CH_3OH ($13_1 - 13_0 \text{ A}^{-+}$) around NGC 2264 CMM3. The distribution of high excitation lines of the CH_3OH is concentrated at the CMM3 position.

Therefore, it is confirmed that these CH_3OH lines originate from hot molecular gas in the vicinity of the protostar CMM3. These CH_3OH lines are often detected in hot cores (e.g. van der Tak et al. 2000) and hot corinos (e.g. Maret et al. 2005). In addition to heating by radiation from the protostar, shock heating may also contribute, since the high excitation lines of CH_3OH are also detected in the shocked regions induced by the outflow driven by the protostars in L1448-mm/IRS 3 (Jiménez-Serra et al. 2004) and L1157 (Codella et al. 2010). Saruwatari et al. (2011) reported the detection of CH_3OH ($5_0 - 4_0, A^+$ and $5_3 - 4_3, A^+$) associated with the compact outflow from the protostar in this source. From these results, the detection of high excitation CH_3OH lines represents the existence of the high temperature molecular gas affected by protostellar activities of CMM3. This is consistent with the high gas kinetic temperature inferred from the excitation temperatures between the different K_a ladders of H_2CO .

4.2. Deuterium Fractionation Ratios

Seven deuterated molecular species, DCO^+ , N_2D^+ , DCN , DNC , CCD , HDCO , and DC_3N , are identified in this line survey. Ground-state transition lines in the 70 GHz band are observed for DCO^+ , N_2D^+ , DCN , DNC , and DCO^+ . Higher transition lines of DCO^+ , DCN , and DNC are also identified in the 0.8 mm band. HDCO is detected only in the 0.8 mm band. Deuterated CH_3OH and multiply deuterated molecular species such as D_2CO and CHD_2OH are not detected, although these molecules are often found in the hot corino sources and hot core sources (e.g. Mauersberger et al. 1988; Turner 1990; Ceccarelli et al. 1998; Parise et al. 2006). This non-detection would be due to insufficient sensitivity of the present line survey. For example, the intensity of CH_2DOH ($2_{02} - 1_{01} e_1$) is estimated to be 2 mK in T_{mb} with the rotation temperature of 30 K under the LTE approximation, assuming the $\text{CH}_2\text{DOH}/\text{CH}_3\text{OH}$ ratio of 1 % ($2.1 \times 10^{13} \text{ cm}^{-2}$). It is well below our sensitivity (r.m.s ~ 30 mK at the corresponding frequency).

Table 7 shows the deuterium fractionation ratios evaluated from the column densities derived in section 3.2. The ratios range from 0.01 to 0.04, and no systematic trend can be seen among molecular species: the deuterium fractionation ratios of ionic molecules are similar to those of neutral molecules. Deuterated molecules would mostly reside in a cold ambient envelope, because the rotation temperatures of DCN and NH_2D are estimated to be lower than 10 K (Table 5).

The most characteristic feature of the deuterium fractionation ratio in this source is relatively high $\text{DCO}^+/\text{HCO}^+$ and $\text{N}_2\text{D}^+/\text{N}_2\text{H}^+$ ratios in spite of the active star-forming activities. Deuterium fractionation ratios of the ionic species are generally low for a warm

region ($T > 20$ K), because the deuterium fractionation process is not efficient above 20 K and the deuterated molecular ions which had been formed in the cold stages are quickly destroyed (Sakai et al. 2012; Fontani et al. 2014). For this reason, the $\text{DCO}^+/\text{HCO}^+$ and $\text{N}_2\text{D}^+/\text{N}_2\text{H}^+$ ratios are generally low. Indeed, the DCO^+ and N_2D^+ lines are not detected in Orion KL (Section 4.3), and the $\text{DCO}^+/\text{HCO}^+$ ratio is as low as 0.008 toward the low-mass star-forming region IRAS 16293-2422 (van Dishoeck et al. 1995) (Table 7). The moderate deuterium fractionation ratios of the ionic species mean that NGC 2264 CMM3 is surrounded by a cold envelope ($T \sim 10$ K). In fact, the deuterium fractionation ratios of various molecules including neutral species are almost comparable with those reported for the cold dark cloud L134N (Tin   et al. 2000; Turner 2001), as shown in Table 7. Such a structure of NGC 2264 CMM3 seems to be related to the youth of the protostar suggested by the short dynamical age of the outflow (Saruwatari et al. 2011). Emprechtinger et al. (2009) reported that the $\text{N}_2\text{D}^+/\text{N}_2\text{H}^+$ ratio decreases as protostellar evolution. The above observational result for $\text{N}_2\text{D}^+/\text{N}_2\text{H}^+$ in NGC2264 CMM3 is consistent with theirs.

4.3. Comparison with Orion KL

In this study, we also observed Orion KL in the 3 mm and 4 mm bands with the Nobeyama 45 m telescope for comparing with the NGC 2264 CMM3 spectrum. The observed position is : $(\alpha_{\text{J2000}}, \delta_{\text{J2000}}) = (5^{\text{h}} 35^{\text{m}} 14^{\text{s}}.5, -05^{\circ} 22' 30''.4)$. The Orion KL is the nearest high-mass star-forming region to the Sun ($d = 437$ pc; Hirota et al. 2007). The chemical compositions of Orion KL have extensively been studied with single-dish telescopes (e.g. Johansson et al. 1984; Turner 1989; Schilke et al. 1997; Tercero et al. 2010, 2011) and interferometers (e.g. Blake et al. 1996; Beuther et al. 2005). The composite spectrum is shown in Figure 6. The spectral pattern of NGC 2264 CMM3 is largely different from that of Orion KL, indicating a significant chemical difference as well as different excitation conditions between these two sources. Indeed, the rotation temperatures of molecules are much higher in the Orion KL than in NGC 2264 CMM3 (e.g. Blake et al. 1987).

As shown in Figure 6 (a), the intensities of N_2H^+ and HNC relative to the intensity of CS are brighter in the NGC 2264 CMMs than Orion KL. In addition, intensities of carbon-chain molecules such as CCS, C_3S , C_4H , and HC_5N , as well as deuterium bearing species such as DCN and DNC are found to be stronger in the NGC 2264 CMM3 (Figure 6 b). Note that the DCO^+ and N_2D^+ lines are not detected in Orion KL (Figure 6b). On the other hand, intensities of the SO, SO_2 , and SiO lines are relatively stronger in Orion KL than NGC 2264 CMM3. Intensities of complex organic molecules such as CH_3CN , CH_3OCH_3 , and HCOOCH_3 are also higher in Orion KL.

The spectra of the two sources are strikingly different from each other, indicating the difference of chemical compositions between the two objects. Figure 7 shows comparison of the column densities between NGC 2264 CMM3 and Orion KL (Table 8). In this comparison, we employ the column densities of Orion KL reported in the literatures (Bell et al. 2014; Carvajal et al. 2009; Comito et al. 2005; Esplugues et al. 2013a,b; Haykal et al. 2014; Kolesníková et al. 2014; Marcelino et al. 2009; Neill et al. 2013; Tercero et al. 2010, 2011; Turner 1991), because our observation of this source is less sensitive than the previous observations and restricted within the narrow frequency range. Since Orion KL is composed of several components with different physical and chemical conditions (Blake et al. 1987), we use the average column density of these component for comparison, as employed by Fuente et al. (2014). As described in the footnote of Table 8, we calculate the column density convolved with the $15''$ beam by considering the column density and source size of each components. This enables us a fair comparison with NGC 2264 CMM3, where several components are not resolved in this study.

In general, the column densities are higher in Orion KL than NGC 2246 CMM3 for almost all the species. For comparison between the two sources, we employ $C^{34}S$ as a standard molecule, because CS is ubiquitously present under various conditions (e.g Zhou et al. 1989; Tatematsu et al. 1993; Blake et al. 1996). The abundances of carbon-chain molecules such as CCS, C_3S , and HC_5N relative to the $C^{34}S$ are higher by an order of magnitude in NGC 2264 CMM3 than in Orion KL. The abundances of SO, SO_2 , SiO, and complex organic molecules ($HCOOCH_3$ and CH_3OCH_3) are lower in NGC 2264 CMM3 by an order of magnitude or more. An exception for this is CH_3CHO , which shows little difference between the two objects.

For reference, we prepared the column density plot between NGC2264 CMM3 and the Orion hot core and that between NGC2264 CMM3 and the Orion compact ridge, as shown in Figures 8 (a) and (b), respectively. In this case, the averaging processes made for Figure 7 are not adopted. Even in this plot, we can see the same trend mentioned above, although the number of molecular species are limited, because some species only exist in the hot core or the compact ridge.

From the comparisons with Orion KL, NGC 2264 CMM3 is found to be abundant in carbon-chain molecules and deficient in complex organic molecules, SO, and SO_2 . Abundant carbon-chain molecules are usually found in young starless cores (Suzuki et al. 1992; Hirota et al. 2009), while complex organic molecules and sulfur-bearing molecules are characteristic of hot cores and hot corions (e.g. Blake et al. 1994; van Dishoeck et al. 1995; Cazaux et al. 2003). Therefore, the chemical compositions found in NGC 2264 CMM3 indicate its chemical youth, where the protostar is very young and a hot core is not yet well

developed around it. Indeed, the protostar is deeply embedded in the dense core, as indicated by high visual extinction to the protostar (Saruwatari et al. 2011). The chemical youth is also suggested by the richness in deuterated molecules: NGC 2264 CMM3 is still surrounded by cold envelope gas. Although high excitation CH_3OH lines are detected, most of molecules would reside in the protostar envelope, because the rotation temperatures in NGC 2264 CMM3 are lower than those found in hot cores (e.g. Blake et al. 1987; Favre et al. 2011).

It is very surprising that such a cold envelope gas still exists in the central part of the active cluster forming region as a parent cloud for high-mass star formation. Therefore, this result would give an important clue to understanding evolution of a cluster forming clump. It is also interesting that NGC 2264 CMM3 seems to harbor a hot and dense region around the protostar, as inferred from detection of the high excitation lines of CH_3OH . It is still controversial whether such a hot and dense region corresponds to a hot core or to a shocked region caused by the infant outflow found by Saruwatari et al. (2011). Above all, this source is a novel target to explore the early stage of high mass star formation, and high spatial resolution observations are awaited.

The authors are grateful to the Nobeyama Radio Observatory (NRO) staff for excellent support in the observation with the 45 m telescope. The 45 m radio telescope is operated by the NRO, a branch of the National Astronomical Observatory of Japan, National Institutes of Natural Sciences. The authors are also grateful to the ASTE staff for excellent support. ASTE project is driven by the NRO in collaboration with University of Chile, and Japanese institutes including University of Tokyo, Nagoya University, Osaka Prefecture University, Ibaraki University, and Hokkaido University. Observations with ASTE were in part carried out remotely from Japan by using NTT’s GEMnet2 and its partnet R&E (Research and Education) networks, which are based on AccessNova collaboration among University of Chile, NTT Laboratories, and NAOJ. This study is supported by a Grant-in-Aid from the Ministry of Education, Culture, Sports, Science, and Technology of Japan (No. 21224002, 21740132, and 25108005).

REFERENCES

- Bell, T. A., Cernicharo, J., Viti, S., et al. 2014, *A&A*, 564, AA114
- Bergin, E. A., Phillips, T. G., Comito, C., et al. 2010, *A&A*, 521, LL20
- Beuther, H., Zhang, Q., Greenhill, L. J., et al. 2005, *ApJ*, 632, 355

- Beuther, H., Zhang, Q., Bergin, E. A., & Sridharan, T. K. 2009, *AJ*, 137, 406
- Bisschop, S. E., Jørgensen, J. K., van Dishoeck, E. F., & de Wachter, E. B. M. 2007, *A&A*, 465, 913
- Blake, G. A., Masson, C. R., Phillips, T. G., & Sutton, E. C. 1986, *ApJS*, 60, 357
- Blake, G. A., Sutton, E. C., Masson, C. R., & Phillips, T. G. 1987, *ApJ*, 315, 621
- Blake, G. A., van Dishoeck, E. F., Jansen, D. J., Groesbeck, T. D., & Mundy, L. G. 1994, *ApJ*, 428, 680
- Blake, G. A., Mundy, L. G., Carlstrom, J. E., et al. 1996, *ApJ*, 472, L49
- Carvajal, M., Margulès, L., Tercero, B., et al. 2009, *A&A*, 500, 1109
- Caux, E., Kahane, C., Castets, A., et al. 2011, *A&A*, 532, AA23
- Cazaux, S., Tielens, A. G. G. M., Ceccarelli, C., et al. 2003, *ApJ*, 593, L51
- Ceccarelli, C., Castets, A., Loinard, L., Caux, E., & Tielens, A. G. G. M. 1998, *A&A*, 338, L43
- Codella, C., Lefloch, B., Ceccarelli, C., et al. 2010, *A&A*, 518, LL112
- Codella, C., Ceccarelli, C., Lefloch, B., et al. 2012, *ApJ*, 757, LL9
- Comito, C., Schilke, P., Phillips, T. G., et al. 2005, *ApJS*, 156, 127
- Cuadrado, S., Goicoechea, J. R., Pilleri, P., et al. 2015, *A&A*, 575, A82
- Cummins, S. E., Linke, R. A., & Thaddeus, P. 1986, *ApJS*, 60, 819
- Emprechtinger, M., Caselli, P., Volgenau, N. H., Stutzki, J., & Wiedner, M. C. 2009, *A&A*, 493, 89
- Esplugues, G. B., Tercero, B., Cernicharo, J., et al. 2013a, *A&A*, 556, AA143
- Esplugues, G. B., Cernicharo, J., Viti, S., et al. 2013b, *A&A*, 559, AA51
- Ezawa, H., Kawabe, R., Kohno, K., & Yamamoto, S. 2004, *Proc. SPIE*, 5489, 763
- Favre, C., Despois, D., Brouillet, N., et al. 2011, *A&A*, 532, AA32
- Fontani, F., Sakai, T., Furuya, K., et al. 2014, *MNRAS*, 440, 448

- Fuente, A., Cernicharo, J., Caselli, P., et al. 2014, *A&A*, 568, AA65
- Ginard, D., González-García, M., Fuente, A., et al. 2012, *A&A*, 543, A27
- Jiménez-Serra, I., Martín-Pintado, J., Rodríguez-Franco, A., & Marcelino, N. 2004, *ApJ*, 603, L49
- Johansson, L. E. B., Andersson, C., Ellder, J., et al. 1984, *A&A*, 130, 227
- Jørgensen, J. K., Bourke, T. L., Nguyen Luong, Q., & Takakuwa, S. 2011, *A&A*, 534, AA100
- Hirota, T., Bushimata, T., Choi, Y. K., et al. 2007, *PASJ*, 59, 897
- Hirota, T., Ohishi, M., & Yamamoto, S. 2009, *ApJ*, 699, 585
- Haykal, I., Carvajal, M., Tercero, B., et al. 2014, *A&A*, 568, AA58
- Inoue, H., Muraoka, K., Sakai, T., et al. 2008, *Nineteenth International Symposium on Space Terahertz Technology*, 281
- Kaifu, N., Ohishi, M., Kawaguchi, K., et al. 2004, *PASJ*, 56, 69
- Kamezaki, T., Imura, K., Omodaka, T., et al. 2014, *ApJS*, 211, 18
- Kolesníková, L., Tercero, B., Cernicharo, J., et al. 2014, *ApJ*, 784, LL7
- Lindberg, J. E., & Jørgensen, J. K. 2012, *A&A*, 548, A24
- Maret, S., Ceccarelli, C., Tielens, A. G. G. M., et al. 2005, *A&A*, 442, 527
- Marcelino, N., Cernicharo, J., Tercero, B., & Roueff, E. 2009, *ApJ*, 690, L27
- Martín, S., Mauersberger, R., Martín-Pintado, J., Henkel, C., & García-Burillo, S. 2006, *ApJS*, 164, 450
- Martín, S., Krips, M., Martín-Pintado, J., et al. 2011, *A&A*, 527, AA36
- Mauersberger, R., Henkel, C., Jacq, T., & Walmsley, C. M. 1988, *A&A*, 194, L1
- Maury, A. J., André, P., & Li, Z.-Y. 2009, *A&A*, 499, 175
- Mendoza, E., Lefloch, B., López-Sepulcre, A., et al. 2014, *MNRAS*, 445, 151
- Müller, H. S. P., Thorwirth, S., Roth, D. A., & Winnewisser, G. 2001, *A&A*, 370, L49
- Müller, H. S. P., Schlöder, F., Stutzki, J. & Winnewisser, G., 2005, *J. Mol. Struct.*, 742, 215

- Nakajima, T., Kimura, K., Nishimura, A., et al. 2013, PASP, 125, 252
- Neill, J. L., Crockett, N. R., Bergin, E. A., Pearson, J. C., & Xu, L.-H. 2013, ApJ, 777, 85
- Parise, B., Ceccarelli, C., Tielens, A. G. G. M., et al. 2006, A&A, 453, 949
- Peretto, N., André, P., & Belloche, A. 2006, A&A, 445, 979
- Peretto, N., Hennebelle, P., & André, P. 2007, A&A, 464, 983
- Pickett, H. M., Poynter, R. L., Cohen, E. A., Delitsky, M. L. Pearson, J. C., & Müller, H. S. P., 1998, Journal of Quantitative Spectroscopy and Radiative Transfer, 60, 883
- Podio, L., Lefloch, B., Ceccarelli, C., Codella, C., & Bachiller, R. 2014, A&A, 565, AA64
- Sakai, N., Sakai, T., & Yamamoto, S. 2007, ApJ, 660, 363
- Sakai, N., Sakai, T., Hirota, T., & Yamamoto, S. 2008, ApJ, 672, 371
- Sakai, N., Sakai, T., Hirota, T., Burton, M., & Yamamoto, S. 2009, ApJ, 697, 769
- Sakai, N., & Yamamoto, S. 2013, Chemical Reviews, 113, 8981
- Sakai, T., Sakai, N., Furuya, K., et al. 2012, ApJ, 747, 140
- Saruwatari, O., Sakai, N., Liu, S.-Y., et al. 2011, ApJ, 729, 147
- Schilke, P., Groesbeck, T. D., Blake, G. A., Phillips, & T. G. 1997, ApJS, 108, 301
- Schreyer, K., Helmich, F. P., van Dishoeck, E. F., & Henning, T. 1997, A&A, 326, 347
- Sorai, K., Sunada, K., Okumura, S. K., et al. 2000, Proc. SPIE, 4015, 86
- Sugimura, M., Yamaguchi, T., Sakai, T., et al. 2011, PASJ, 63, 459
- Suzuki, H., Yamamoto, S., Ohishi, M., et al. 1992, ApJ, 392, 551
- Tatematsu, K., Umemoto, T., Kameya, O., et al. 1993, ApJ, 404, 643
- Tercero, B., Cernicharo, J., Pardo, J. R., & Goicoechea, J. R. 2010, A&A, 517, AA96
- Tercero, B., Vincent, L., Cernicharo, J., Viti, S., & Marcelino, N. 2011, A&A, 528, AA26
- Tiné, S., Roueff, E., Falgarone, E., Gerin, M., & Pineau des Forêts, G. 2000, A&A, 356, 1039

- Turner, B. E. 1989, *ApJS*, 70, 539
- Turner, B. E. 1990, *ApJ*, 362, L29
- Turner, B. E. 1991, *ApJS*, 76, 617
- Turner, B. E. 2001, *ApJS*, 136, 579
- van der Tak, F. F. S., van Dishoeck, E. F., & Caselli, P. 2000, *A&A*, 361, 327
- van Dishoeck, E. F., Blake, G. A., Jansen, D. J., & Groesbeck, T. D. 1995, *ApJ*, 447, 760
- Yamaguchi, T., Takano, S., Watanabe, Y., et al. 2012, *PASJ*, 64, 105
- Watanabe, Y., Sakai, N., Lindberg, J. E., et al. 2012, *ApJ*, 745, 126
- Watanabe, Y., Sakai, N., Sorai, K., & Yamamoto, S. 2014, *ApJ*, 788, 4
- Zhou, S., Wu, Y., Evans, N. J., II, Fuller, G. A., & Myers, P. C. 1989, *ApJ*, 346, 168

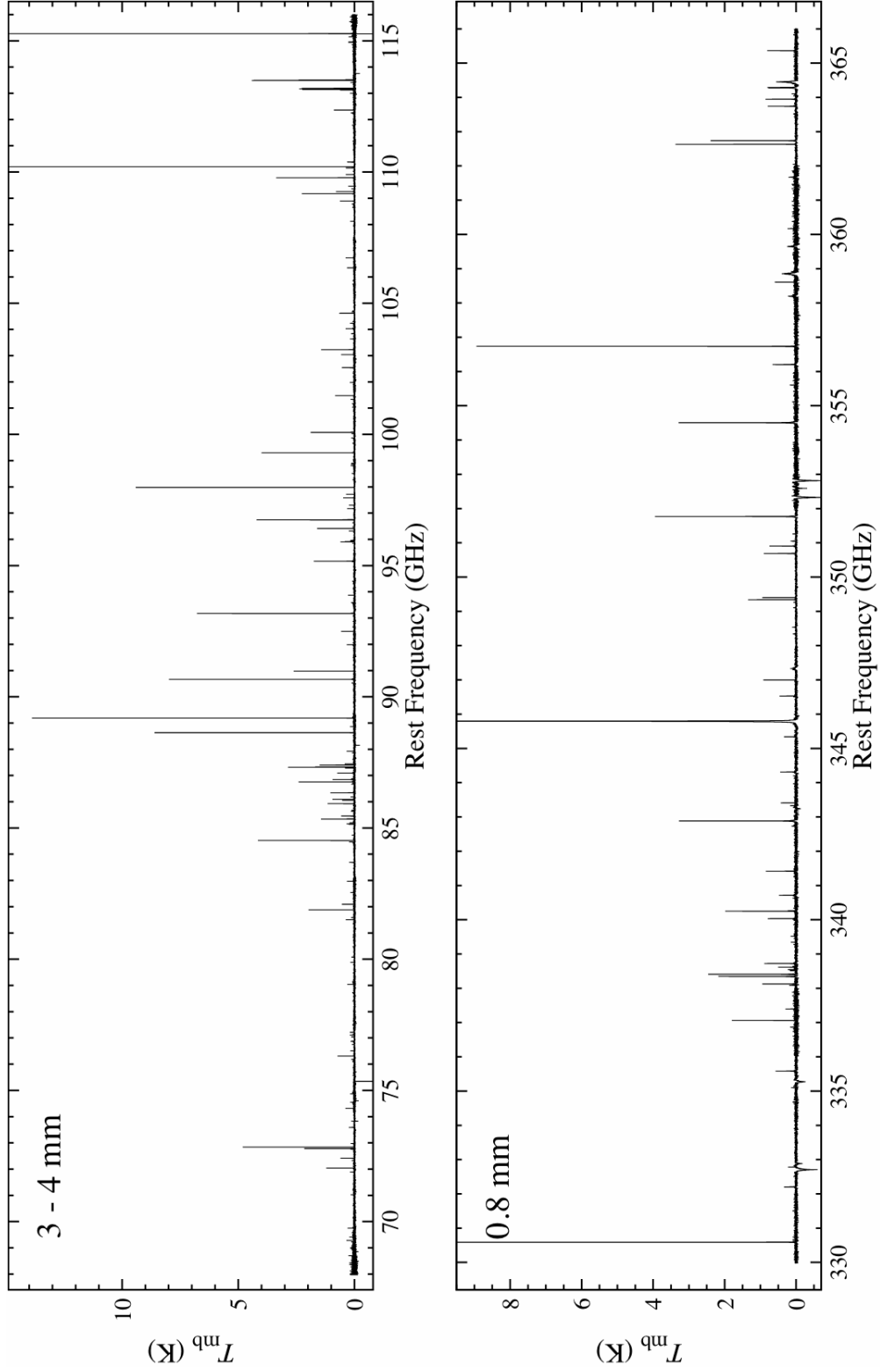


Fig. 1.— Overall spectrum observed with the NRO 45 m telescope (upper spectrum) and that with the ASTE 10 m telescope (lower spectrum). $V_{\text{LSR}} = 7.0$ is assumed as the system velocity.

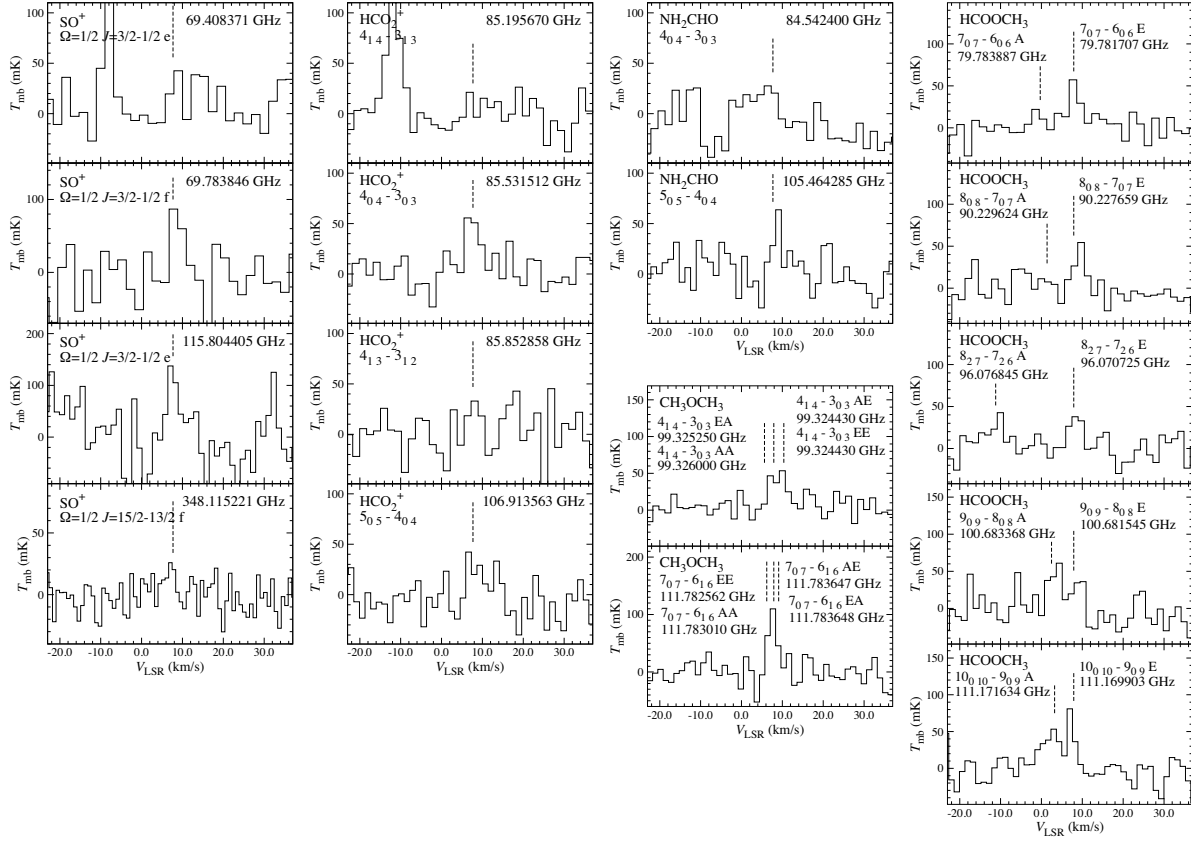


Fig. 2.— Marginal detections of SO^+ , HCO_2^+ , NH_2CHO , CH_3OCH_3 , and HCOOCH_3 . The vertical dotted lines indicate the expected line positions, where the line of sight velocity is 7.7 km s^{-1} , according to the $\text{C}^{18}\text{O}(J = 1 - 0)$ data.

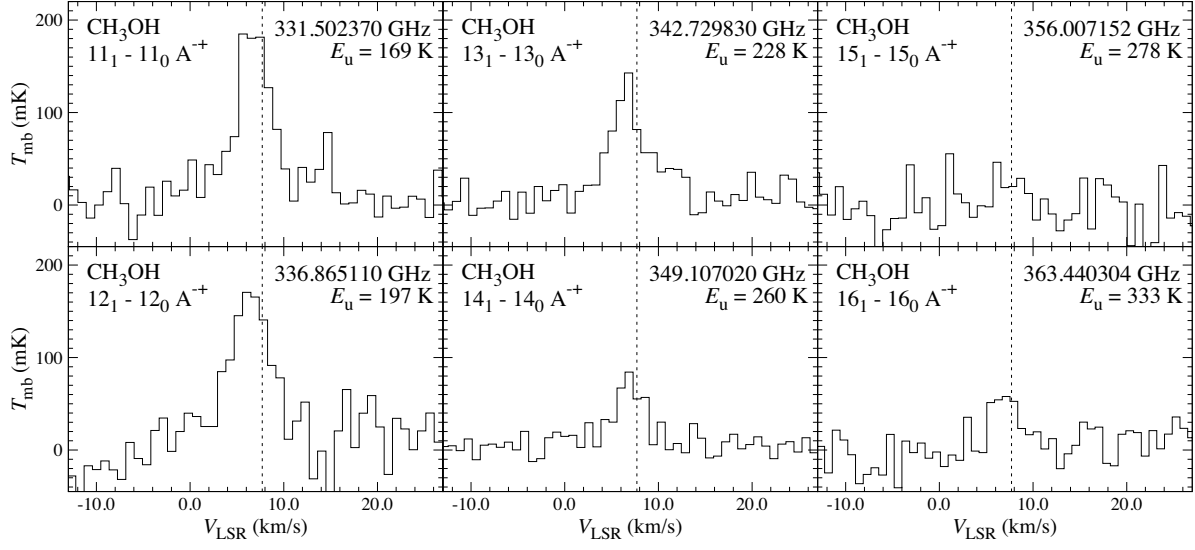


Fig. 3.— Profile of the high excitation CH_3OH lines. The vertical line indicates 7.7 km s^{-1} which is the line of sight velocity of $\text{C}^{18}\text{O}(J = 1 - 0)$.

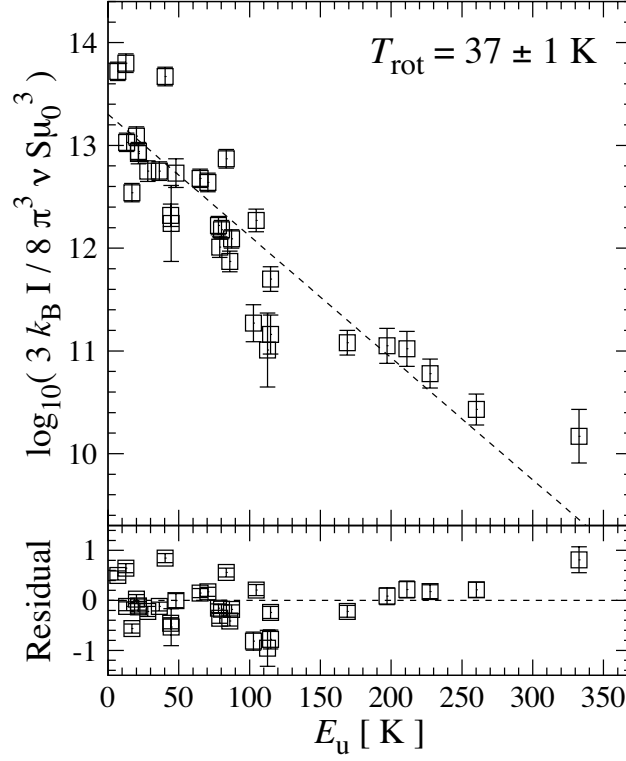


Fig. 4.— A rotation diagram of CH_3OH . A dashed line indicates a single temperature fit. Since the single temperature fit shows a ‘V-shaped’ systematic residual as shown in the bottom panel, we employ a two-component model in derivation of the column density, as described in the text.

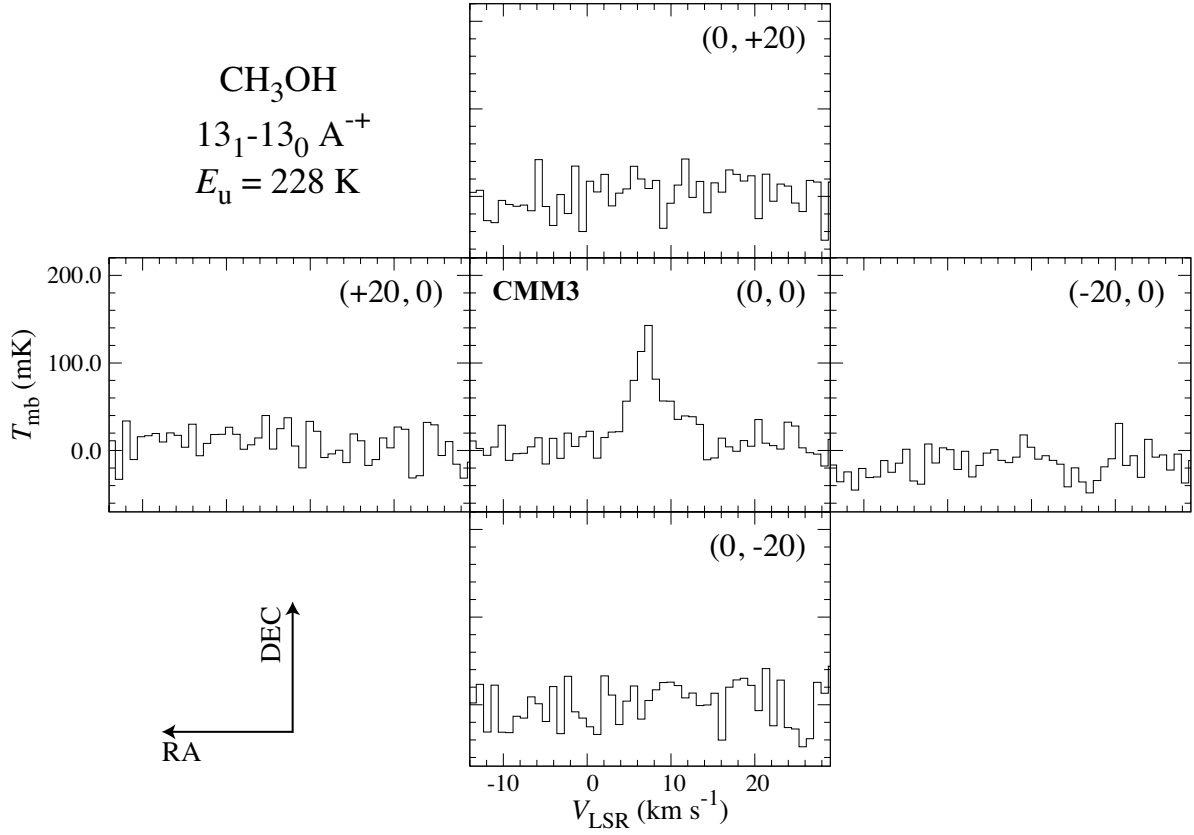


Fig. 5.— A profile map of CH₃OH($13_1 - 13_0 A^{-+}$) in NGC 2264 CMM3. The grid spacing almost corresponds to the FWHM size of the telescope beam (22''). Arrows in the bottom left corner indicate directions of the right ascension (RA) and the declination (DEC).

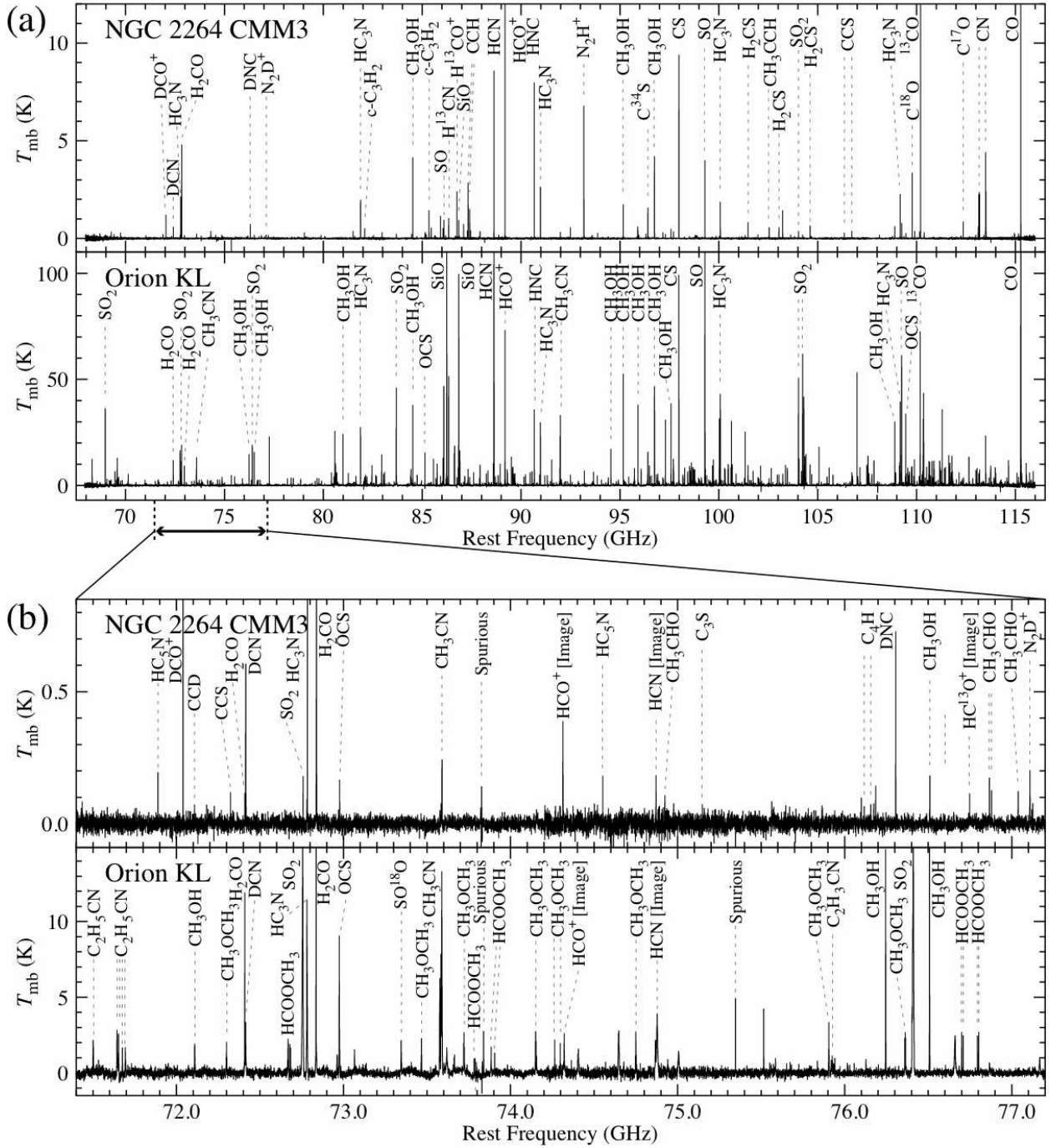


Fig. 6.— (a) Spectra of NGC 2264 CMM3 (top) and Orion KL (bottom) in the 4 and 3 mm bands. (b) The expanded spectra of the two objects in the frequency range from 71.4 GHz to 77.2 GHz. The V_{LSR} values are assumed to be 7.0 km s^{-1} and 5.5 km s^{-1} for NGC 2264 CMM3 and Orion KL, respectively.

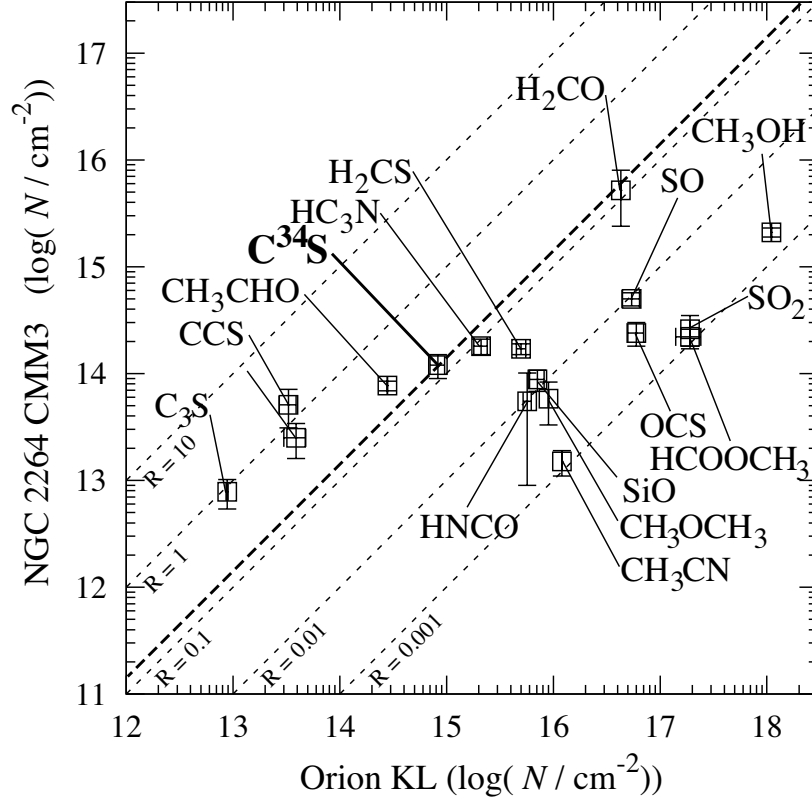


Fig. 7.— A plot of column densities between NGC 2264 CMM3 and Orion KL based on Table 8. For the column densities toward Orion KL, see the footnote of Table 8. Dotted lines indicate the column density ratios of 10, 1, 0.1, 0.01 and 0.001. The thick dashed line represents the condition that the abundances relative to C^{34}S are identical for the both sources. For molecules above this line, their abundances are higher in NGC 2264 CMM3 than Orion KL. For the molecules below this line, their abundances are lower in NGC 2264 CMM3 than Orion KL.

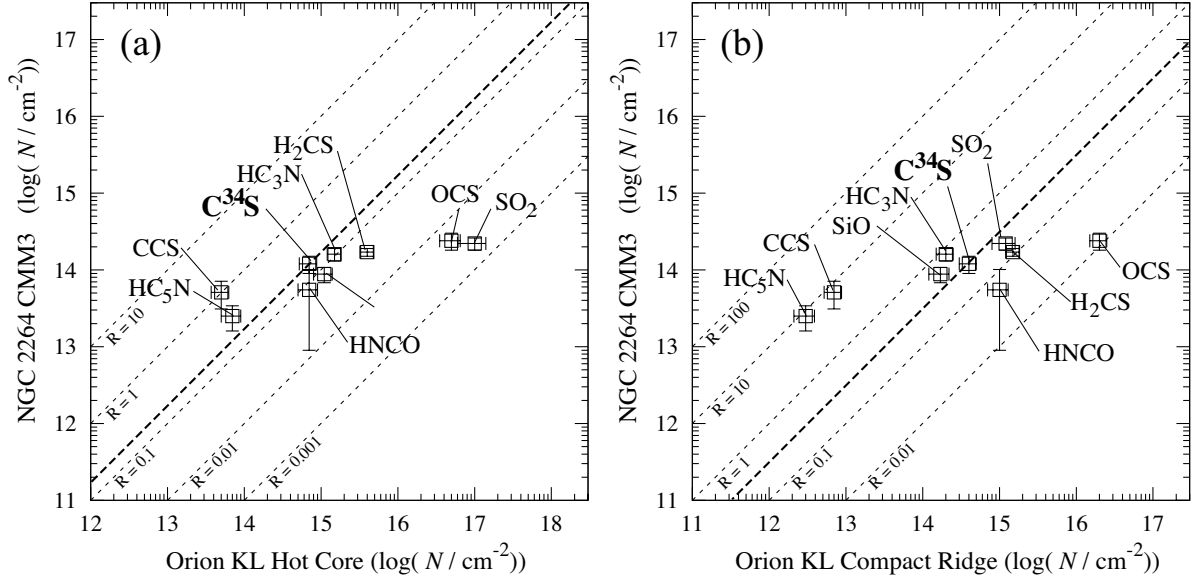


Fig. 8.— (a) A plot of column densities between NGC 2264 CMM3 and the Orion hot core. Dotted lines indicate the column density ratios of 10, 1, 0.1, 0.01 and 0.001. The thick dashed line represents the condition that the abundances relative to C^{34}S and identical for the both sources. (b) A plot of column densities between NGC 2264 CMM3 and the Orion compact ridge. Dotted lines indicate the column density ratios of 100, 10, 1, 0.1, and 0.01. The meaning of the thick dashed line is the same as (a). The column densities of Orion hot core and compact ridge are employed from Marcelino et al. (2009) (HNCO), Tercero et al. (2010) (C^{34}S , H_2CS , and OCS), Tercero et al. (2011) (SiO), Esplugues et al. (2013a) (SO and SO_2), and Esplugues et al. (2013b) (HC_3N , and HC_5N).

Table 1: Summary of observations at Nobeyama 45 m and ASTE 10 m.

Telescope	Receiver	Frequency ^a (GHz)	Res. ^b (MHz)	Tsys ^c (K)	r.m.s. ^d (mK)	FWHM ^e (arcsec)	η_{mb} ^f (%)
Nobeyama 45 m	T70H/V	67.97 – 92.43	0.5	140 – 380	13 – 51	20 – 22	31 – 38
Nobeyama 45 m	TZ1H/V	92.37 – 116.00	0.5	140 – 240	11 – 56	15 – 20	24 – 31
ASTE 10 m	CATS345	329.98 – 366.00	1.0	150 – 400	13 – 39	21 – 23	60

^aObserved frequency ranges.

^bThe spectral resolutions of the final spectra.

^cThe system noise temperatures of the receivers in the observations.

^dA typical r.m.s. noise of the final spectra at the spectral resolution.

^eThe full-width half-maximum beam width.

^fThe main-beam efficiencies of the telescopes.

Table 2. Line parameters observed in NGC 2264 CMM3 with NRO 45 m telescope.

Name ^a	Frequency ^b (GHz)	Transition	E_u (K)	$S\mu^2$ (Debye ²)	T_{mb} Peak ^c (mK)	$\int T_{mb} dv$ ^c (K km s ⁻¹)	FWHM ^d (km s ⁻¹)	V_{LSR} ^d (km s ⁻¹)
CH ₃ CCH	68.361036	4 ₂ – 3 ₂	37.1	3.6865	< 154	< 0.3		
CH ₃ CCH	68.364957	4 ₁ – 3 ₁	15.4	4.6087	222 ± 154	0.85 ± 0.66	2.9 ± 2.7	8.1 ± 0.7
CH ₃ CCH	68.366264	4 ₀ – 3 ₀	8.2	4.9158	206 ± 154	1.10 ± 0.66	4.5 ± 1.6	7.2 ± 0.6
H ₂ CS	68.699385	2 _{0 2} – 1 _{0 1}	4.9	5.4395	257 ± 141	1.15 ± 0.42	3.2 ± 0.9	7.7 ± 0.2
SO ₂	68.972159	6 _{1 5} – 6 _{0 6}	22.5	14.779	176 ± 115	0.72 ± 0.42	3.3 ± 1.0	7.2 ± 0.3
NS	69.002890	$\Omega = 1/2, J = 3/2 - 1/2, F = 5/2 - 3/2, e$	3.3	6.5557	184 ± 107	0.56 ± 0.39	2.8 ± 0.5	7.6 ± 0.3
NS	69.017953	$\Omega = 1/2, J = 3/2 - 1/2, F = 3/2 - 1/2, e$	3.3	2.4268	124 ± 107	0.26 ± 0.23	2.1 ± 1.1	7.7 ± 1.0
NS	69.037510	$\Omega = 1/2, J = 3/2 - 1/2, F = 3/2 - 3/2, e$	3.3	1.9404	115 ± 107	0.39 ± 0.32	3.1 ± 1.4	8.2 ± 0.5
U	69.0818				111 ± 105	0.29 ± 0.31		
HC ₅ N	69.227183	$J = 26 - 25$	44.9	487.51	142 ± 85	0.40 ± 0.31	2.5 ± 1.6	8.1 ± 1.0
CCS	69.281115	$N_J = 5_6 - 4_5$	11.5	49.518	350 ± 85	1.17 ± 0.31	3.1 ± 0.4	7.4 ± 0.2
NS	69.411943	$\Omega = 1/2, J = 3/2 - 1/2, F = 5/2 - 3/2, f$	3.4	6.5528	225 ± 104	0.47 ± 0.22	2.4 ± 0.5	6.8 ± 0.3
NS	69.485223	$\Omega = 1/2, J = 3/2 - 1/2, F = 3/2 - 1/2, f$	3.3	2.4218	< 92	< 0.2		
SO ₂	69.575927	1 _{1 1} – 0 _{0 0}	3.3	2.6673	120 ± 80	0.30 ± 0.29	^e	
H ₂ CS	69.746747	2 _{1 1} – 1 _{1 0}	18.2	4.0797	297 ± 74	1.00 ± 0.27	3.2 ± 0.4	7.6 ± 0.2
SO ⁺	69.783846	$\Omega = 1/2, J = 3/2 - 1/2$	3.4	1.3122	87 ± 74	0.33 ± 0.27	^f	
¹³ CH ₃ OH	70.190200	5 ₀ – 4 ₁ , E	47.1	1.8876	< 80	< 0.3		
H ₂ ¹³ CO	71.024788	1 _{0 1} – 0 _{0 0}	3.4	5.4386	162 ± 64	0.60 ± 0.26	3.3 ± 0.4	7.6 ± 0.2
U	71.4358				84 ± 66	0.49 ± 0.30		
HC ₅ N	71.889595	$J = 27 - 26$	48.3	506.18	193 ± 56	0.56 ± 0.23	2.6 ± 0.3	8.2 ± 0.2
DCO ⁺	72.039312	$J = 1 - 0$	3.5	15.211	1214 ± 60	4.3 ± 0.2	3.3 ± 0.1	7.6 ± 0.1
CCD	72.107700	$N = 1 - 0, J = 3/2 - 1/2, F = 5/2 - 3/2$	3.5	1.1859	73 ± 56	0.28 ± 0.23	3.4 ± 1.2	8.1 ± 0.5
CCS	72.323789	$N_J = 6_5 - 5_4$	19.2	39.877	119 ± 55	0.50 ± 0.19	3.0 ± 0.8	7.7 ± 0.2
H ₂ CO	72.409090	5 _{1 4} – 5 _{1 5}	65.9	1.9957	116 ± 53	0.42 ± 0.22	3.3 ± 0.3	7.5 ± 0.1
DCN	72.413504	$J = 1 - 0, F = 1 - 1$	3.5	8.9447	344 ± 53	1.12 ± 0.22	3.0 ± 0.3	7.6 ± 0.2
DCN	72.414933	$J = 1 - 0, F = 2 - 1$	3.5	14.909	604 ± 53	1.9 ± 0.2	2.9 ± 0.1	7.6 ± 0.1
DCN	72.417028	$J = 1 - 0, F = 0 - 1$	3.5	2.9814	115 ± 53	0.38 ± 0.19	2.1 ± 3.8	7.6 ± 0.9
HCC ¹³ CN	72.482055	$J = 8 - 7$	15.7	111.40	< 50	< 0.1		
SO ₂	72.758243	6 _{0 6} – 5 _{1 5}	19.2	8.0280	181 ± 55	0.76 ± 0.22	3.9 ± 0.4	7.2 ± 0.2
HC ₃ N	72.783822	$J = 8 - 7$	15.7	111.42	2143 ± 55	7.9 ± 0.3	3.3 ± 0.1	7.9 ± 0.1
H ₂ CO	72.837948	1 _{0 1} – 0 _{0 0}	3.5	5.4374	4810 ± 55	21.3 ± 0.4	3.8 ± 0.1	7.6 ± 0.1
OCS	72.976779	$J = 6 - 5$	12.3	3.0693	167 ± 52	0.63 ± 0.21	3.5 ± 0.4	7.7 ± 0.2
CH ₃ CN	73.577759	4 ₃ – 3 ₃	73.1	107.67	49 ± 48	0.21 ± 0.19	3.2 ± 2.5	8.1 ± 0.7
CH ₃ CN	73.584543	4 ₂ – 3 ₂	37.4	92.297	76 ± 48	0.45 ± 0.23	6.0 ± 5.8	7.2 ± 2.5
CH ₃ CN	73.588799	4 ₁ – 3 ₁	16.0	115.35	211 ± 48	0.87 ± 0.19	3.5 ± 0.5	7.7 ± 0.2
CH ₃ CN	73.590218	4 ₀ – 3 ₀	8.8	123.07	242 ± 48	0.83 ± 0.19	3.0 ± 0.4	7.8 ± 0.2
NH ₂ D	74.155770	2 _{1 2} , 0 _a – 2 _{0 2} , 0 _s	50.7	18.710	53 ± 41	0.20 ± 0.16	3.5 ± 1.3	8.8 ± 0.5
HC ₅ N	74.551987	$J = 28 - 27$	51.9	524.93	182 ± 85	0.49 ± 0.33	2.5 ± 0.3	8.3 ± 0.2
CH ₃ CHO	74.891677	4 _{1 4} – 3 _{1 3} , A	11.3	47.431	< 76	< 0.2		
CH ₃ CHO	74.924134	4 _{1 4} – 3 _{1 3} , E	11.3	47.347	108 ± 76	0.47 ± 0.30	4.3 ± 1.1	6.9 ± 0.5
C ₃ S	75.147927	$J = 13 - 12$	25.3	178.37	75 ± 64	0.30 ± 0.25	4.3 ± 1.7	8.1 ± 0.7
U	75.5636				83 ± 57	0.50 ± 0.27		
DC ₃ N	75.987138	$J = 9 - 8$	18.2	125.95	< 50	< 0.2		
C ₄ H	76.117431	$N = 8 - 7, J = 17/2 - 15/2, F = 8 - 7$	16.4	6.0096	65 ± 51	0.27 ± 0.17	2.4 ± 1.8	7.5 ± 0.2
C ₄ H	76.117446	$N = 8 - 7, J = 17/2 - 15/2, F = 9 - 8$	16.4	6.7677
C ₄ H	76.156027	$N = 8 - 7, J = 15/2 - 13/2, F = 7 - 6$	16.5	5.2484	74 ± 51	0.35 ± 0.17	3.7 ± 0.9	7.7 ± 0.4
C ₄ H	76.156029	$N = 8 - 7, J = 15/2 - 13/2, F = 8 - 7$	16.5	6.0066
DNC	76.305700	$J = 1 - 0$	3.7	9.3030	730 ± 44	2.2 ± 0.2	2.8 ± 0.1	7.5 ± 0.1
SO ₂	76.412165	10 _{1 9} – 9 _{2 8}	54.7	6.4105	< 41	< 0.1		
CH ₃ OH	76.509668	5 ₀ – 4 ₁ , E	47.9	1.8941	181 ± 45	1.07 ± 0.26	4.3 ± 0.4	7.5 ± 0.2
CH ₃ CHO	76.866436	4 _{0 4} – 3 _{0 3} , E	9.3	50.594	173 ± 45	0.66 ± 0.19	3.5 ± 0.3	7.6 ± 0.2
CH ₃ CHO	76.878952	4 _{0 4} – 3 _{0 3} , A	9.2	50.561	125 ± 45	0.65 ± 0.19	4.2 ± 0.5	7.7 ± 0.2
CH ₃ CHO	77.038601	4 _{2 3} – 3 _{2 2} , A	18.3	37.954	122 ± 43	0.51 ± 0.16	3.9 ± 0.7	7.6 ± 0.3
N ₂ D ⁺	77.107760	$J = 1 - 0, F_1 = 1 - 1, F = 2 - 2$	3.7	16.290	108 ± 40	0.39 ± 0.16	3.2 ± 0.6	6.6 ± 0.2
N ₂ D ⁺	77.107465	$J = 1 - 0, F_1 = 1 - 1, F = 0 - 1$	3.7	3.8533
N ₂ D ⁺	77.107760	$J = 1 - 0, F_1 = 1 - 1, F = 2 - 1$	3.7	2.9773
N ₂ D ⁺	77.107898	$J = 1 - 0, F_1 = 1 - 1, F = 1 - 0$	3.7	5.9050
N ₂ D ⁺	77.107898	$J = 1 - 0, F_1 = 1 - 1, F = 1 - 1$	3.7	1.3688
N ₂ D ⁺	77.107898	$J = 1 - 0, F_1 = 1 - 1, F = 1 - 2$	3.7	4.2867
N ₂ D ⁺	77.109611	$J = 1 - 0, F_1 = 2 - 1, F = 3 - 2$	3.7	26.971	203 ± 40	0.73 ± 0.19	2.7 ± 0.3	5.7 ± 0.1
N ₂ D ⁺	77.109315	$J = 1 - 0, F_1 = 2 - 1, F = 2 - 1$	3.7	16.290
N ₂ D ⁺	77.109315	$J = 1 - 0, F_1 = 2 - 1, F = 2 - 2$	3.7	2.9772
N ₂ D ⁺	77.109811	$J = 1 - 0, F_1 = 2 - 1, F = 1 - 0$	3.7	3.5933
N ₂ D ⁺	77.109811	$J = 1 - 0, F_1 = 2 - 1, F = 1 - 1$	3.7	7.5094
N ₂ D ⁺	77.109811	$J = 1 - 0, F_1 = 2 - 1, F = 1 - 2$	3.7	0.4572
CH ₃ CHO	77.125695	4 _{2 2} – 3 _{2 1} , E	18.4	37.905	144 ± 40	0.35 ± 0.15	3.9 ± 1.1	6.3 ± 0.4

Table 2—Continued

Name ^a	Frequency ^b (GHz)	Transition	E_u (K)	$S\mu^2$ (Debye ²)	T_{mb} Peak ^c (mK)	$\int T_{\text{mb}} dv$ ^c (K km s ⁻¹)	FWHM ^d (km s ⁻¹)	V_{LSR} ^d (km s ⁻¹)
CH ₃ CHO	77.126413	$4_2 3 - 3_2 2$, E	18.3	37.899
HC ₅ N	77.214359	$J = 29 - 28$	55.6	543.75	340 ± 46	0.58 ± 0.17	2.6 ± 0.5	8.1 ± 0.2
CH ₃ CHO	77.218291	$4_2 2 - 3_2 1$, A	18.3	37.953	51 ± 46	0.20 ± 0.15	f	
U	77.4947				99 ± 59	0.29 ± 0.22		
CCS	77.731711	$N_J = 6_5 - 5_5$	21.8	48.384	66 ± 65	0.28 ± 0.21	f	
U	78.3998				93 ± 50	0.32 ± 0.16		
CH ₃ CHO	79.099313	$4_1 3 - 3_1 2$, E	11.8	47.350	94 ± 52	0.42 ± 0.19	3.7 ± 0.8	7.7 ± 0.3
CH ₃ CHO	79.150166	$4_1 3 - 3_1 2$, A	11.8	47.426	106 ± 52	0.48 ± 0.17	3.9 ± 0.6	7.1 ± 0.3
H ¹³ CCCN	79.350463	$J = 9 - 8$	19.0	125.33	< 53	< 0.1		
HCOOCH ₃	79.781707	$7_0 7 - 6_0 6$, E	15.8	18.271	57 ± 49	0.18 ± 0.16	3.2 ± 0.8	7.5 ± 0.4
HC ₅ N	79.876710	$J = 30 - 29$	59.4	562.49	181 ± 43	0.50 ± 0.16	2.3 ± 0.3	7.9 ± 0.2
H ₂ CCO	80.076652	$4_1 4 - 3_1 3$	22.7	7.5847	112 ± 46	0.40 ± 0.15	2.5 ± 0.9	7.9 ± 0.2
U	80.4801				57 ± 48	0.23 ± 0.15		
c-C ₃ H ₂	80.723180	$4_2 2 - 3_1 3$	28.8	19.518	62 ± 58	0.19 ± 0.15	f	
H ₂ CCO	80.832117	$4_0 4 - 3_0 3$	9.7	8.0895	86 ± 54	0.40 ± 0.19	4.3 ± 0.8	7.5 ± 0.4
C ₃ S	80.928180	$J = 14 - 13$	29.1	192.08	77 ± 54	0.32 ± 0.17	3.4 ± 1.0	7.6 ± 0.4
CCS	81.505170	$N_J = 6_7 - 5_6$	15.4	57.818	378 ± 62	1.27 ± 0.27	3.0 ± 0.2	7.2 ± 0.1
H ₂ CCO	81.586230	$4_1 3 - 3_1 2$	22.8	7.5847	129 ± 61	0.57 ± 0.22	3.9 ± 0.6	7.4 ± 0.3
HC ₃ N	81.881468	$J = 9 - 8$	19.7	125.32	1977 ± 56	8.2 ± 0.3	3.2 ± 0.1	7.8 ± 0.1
c-C ₃ H ₂	82.093544	$2_0 2 - 1_1 1$	6.4	14.641	526 ± 61	1.88 ± 0.29	3.1 ± 0.1	7.4 ± 0.1
HC ₅ N	82.539039	$J = 31 - 30$	63.4	581.27	175 ± 74	0.57 ± 0.26	2.9 ± 0.4	8.1 ± 0.2
c-C ₃ H ₂	82.966200	$3_1 2 - 3_0 3$	16.1	10.446	328 ± 82	0.98 ± 0.33	2.5 ± 0.2	7.4 ± 0.2
SO ₂	83.688093	$8_1 7 - 8_0 8$	36.7	17.009	232 ± 48	1.14 ± 0.25	3.7 ± 0.4	7.3 ± 0.2
¹³ CCH	84.119329	$N = 1 - 0, J = 3/2 - 1/2, F_1 = 2 - 1, F = 5/2 - 3/2$	4.1	1.1859	< 50	< 0.1		
DC ₃ N	84.429814	$J = 10 - 9$	22.3	139.95	59 ± 54	0.18 ± 0.16	f	
CH ₃ OH	84.521169	$5_1 - 4_0$, E	40.4	3.0832	4155 ± 54	20.2 ± 0.4	3.7 ± 0.2	7.2 ± 0.1
NH ₂ CHO	84.542330	$4_0 4 - 3_0 3$	10.2	52.279	< 54	< 0.1		
c-C ₃ H ₂	84.727688	$3_2 2 - 3_1 3$	16.1	10.306	119 ± 47	0.37 ± 0.14	2.6 ± 0.4	8.1 ± 0.2
³⁰ SiO	84.746166	$J = 2 - 1$	6.1	19.195	< 47	< 0.1		
OCS	85.139103	$J = 7 - 6$	16.3	3.5805	251 ± 53	1.07 ± 0.26	2.9 ± 0.2	7.5 ± 0.1
HC ¹⁸ O ⁺	85.162223	$J = 1 - 0$	4.1	15.210	337 ± 53	1.24 ± 0.20	3.1 ± 0.2	7.8 ± 0.1
HC ₅ N	85.201340	$J = 32 - 31$	67.5	599.97	216 ± 53	0.67 ± 0.20	2.7 ± 0.1	7.5 ± 0.1
C ¹³ CH	85.229335	$N = 1 - 0, J = 3/2 - 1/2, F_1 = 2 - 1, F = 5/2 - 3/2$	4.1	1.1859	< 56	< 0.1		
c-C ₃ H ₂	85.338894	$2_1 2 - 1_0 1$	6.4	16.050	1446 ± 53	5.8 ± 0.2	3.1 ± 0.1	7.7 ± 0.1
HCS ⁺	85.347890	$J = 2 - 1$	6.1	7.6671	330 ± 53	1.20 ± 0.20	3.3 ± 0.6	8.0 ± 0.3
CH ₃ CCH	85.442601	$5_3 - 4_3$	77.4	7.8653	67 ± 50	0.14 ± 0.15	1.9 ± 1.7	7.4 ± 1.4
CH ₃ CCH	85.450766	$5_2 - 4_2$	41.2	5.1610	168 ± 50	0.54 ± 0.19	2.7 ± 3.1	8.3 ± 1.3
CH ₃ CCH	85.455667	$5_1 - 4_1$	19.5	5.8994	412 ± 50	1.47 ± 0.17	2.8 ± 0.3	8.1 ± 0.1
CH ₃ CCH	85.457300	$5_0 - 4_0$	12.3	6.1451	554 ± 50	1.74 ± 0.15	3.0 ± 0.2	7.9 ± 0.1
HCO ₂ ⁺	85.531512	$4_0 4 - 3_0 3$	10.3	15.997	56 ± 50	0.24 ± 0.19	4.0 ± 1.0	7.1 ± 0.4
C ₄ H	85.634004	$N = 9 - 8, J = 19/2 - 17/2, F = 9 - 8$	20.6	6.7708	158 ± 52	0.55 ± 0.18	3.1 ± 0.3	7.3 ± 0.2
C ₄ H	85.634015	$N = 9 - 8, J = 19/2 - 17/2, F = 10 - 9$	20.5	7.5290
c-C ₃ H ₂	85.656431	$4_3 2 - 4_2 3$	29.1	18.719	135 ± 52	0.31 ± 0.15	2.2 ± 0.4	7.3 ± 0.3
C ₄ H	85.672579	$N = 9 - 8, J = 17/2 - 15/2, F = 8 - 7$	20.6	6.0113	128 ± 52	0.45 ± 0.18	2.9 ± 0.5	7.9 ± 0.2
C ₄ H	85.672581	$N = 9 - 8, J = 17/2 - 15/2, F = 9 - 8$	20.6	6.7697
²⁹ SiO	85.759194	$J = 2 - 1$	6.2	19.197	< 53	< 0.1		
NH ₂ D	85.926278	$1_1 1 - 1_0 1$	20.7	9.5327	1154 ± 56	7.1 ± 0.3	5.5 ± 0.3	7.2 ± 0.1
HC ¹⁵ N	86.054966	$J = 1 - 0$	4.1	8.9113	530 ± 59	1.84 ± 0.25	3.0 ± 0.1	7.7 ± 0.1
SO	86.093950	$N_J = 2_2 - 1_1$	19.3	3.5341	948 ± 52	4.8 ± 0.4	3.3 ± 0.1	7.5 ± 0.1
CCS	86.181391	$N_J = 7_6 - 6_5$	23.4	48.469	171 ± 52	0.54 ± 0.20	2.7 ± 0.3	7.5 ± 0.1
H ¹³ CN	86.338733	$J = 1 - 0, F = 1 - 1$	4.1	2.9704	656 ± 57	2.74 ± 0.23	3.2 ± 0.1	7.6 ± 0.1
H ¹³ CN	86.340163	$J = 1 - 0, F = 2 - 1$	4.1	4.9510	1041 ± 57	4.1 ± 0.2	3.1 ± 0.1	7.6 ± 0.1
H ¹³ CN	86.342251	$J = 1 - 0, F = 0 - 1$	4.1	0.9900	282 ± 57	1.06 ± 0.23	3.4 ± 0.3	7.7 ± 0.1
U	86.3772				63 ± 57	0.19 ± 0.17		
HCO	86.670760	$1_0 1 - 0_0 0, J = 3/2 - 1/2, F = 2 - 1$	4.2	3.0939	143 ± 65	0.55 ± 0.27	3.5 ± 0.5	8.1 ± 0.2
C ₃ S	86.708379	$J = 15 - 14$	33.3	205.82	99 ± 65	0.31 ± 0.22	2.8 ± 0.5	8.0 ± 0.2
HCO	86.708360	$1_0 1 - 0_0 0, J = 3/2 - 1/2, F = 2 - 1$	4.2	1.8168
H ¹³ CO ⁺	86.754288	$J = 1 - 0$	4.2	15.212	2406 ± 65	9.1 ± 0.2	3.0 ± 0.0	7.6 ± 0.1
HCO	86.777460	$1_0 1 - 0_0 0, J = 1/2 - 1/2, F = 1 - 1$	4.2	1.8269	114 ± 65	0.33 ± 0.21	2.1 ± 0.9	8.1 ± 0.2
SiO	86.846985	$J = 2 - 1$	6.3	19.198	945 ± 58	9.8 ± 0.6	6.2 ± 0.6	7.4 ± 0.2
HC ¹⁷ O ⁺	87.057535	$J = 1 - 0$	4.2	15.211	< 63	< 0.2		
HN ¹³ C	87.090825	$J = 1 - 0$	4.2	9.3022	743 ± 63	2.9 ± 0.2	3.0 ± 0.1	7.8 ± 0.1
CCH	87.284105	$N = 1 - 0, J = 3/2 - 1/2, F = 1 - 1$	4.2	0.1007	406 ± 57	1.5 ± 0.2	3.2 ± 0.2	7.7 ± 0.1
CCH	87.316898	$N = 1 - 0, J = 3/2 - 1/2, F = 2 - 1$	4.2	0.9882	2861 ± 57	11.0 ± 0.3	3.2 ± 0.1	7.8 ± 0.1
CCH	87.328585	$N = 1 - 0, J = 3/2 - 1/2, F = 1 - 0$	4.2	0.4922	1695 ± 57	6.1 ± 0.3	3.1 ± 0.1	7.8 ± 0.1
CCH	87.401989	$N = 1 - 0, J = 1/2 - 1/2, F = 1 - 1$	4.2	0.4922	1503 ± 63	6.0 ± 0.2	3.2 ± 0.4	7.9 ± 0.1

Table 2—Continued

Name ^a	Frequency ^b (GHz)	Transition	E_u (K)	$S\mu^2$ (Debye ²)	T_{mb} Peak ^c (mK)	$\int T_{mb} dv$ ^c (K km s ⁻¹)	FWHM ^d (km s ⁻¹)	V_{LSR} ^d (km s ⁻¹)
CCH	87.407165	$N = 1 - 0, J = 1/2 - 1/2, F = 0 - 1$	4.2	0.1976	812 ± 63	2.6 ± 0.2	3.0 ± 1.5	7.9 ± 0.7
CCH	87.446470	$N = 1 - 0, J = 1/2 - 1/2, F = 1 - 0$	4.2	0.1007	419 ± 63	1.7 ± 0.3	3.1 ± 0.2	8.0 ± 0.1
HC ₅ N	87.863630	$J = 33 - 32$	71.7	618.75	114 ± 53	0.35 ± 0.20	2.6 ± 0.7	8.2 ± 0.3
HNCO	87.925237	$4_0 3 - 3_0 2$	10.6	9.9869	338 ± 53	1.4 ± 0.2	3.9 ± 0.2	7.5 ± 0.1
HCN	88.630416	$J = 1 - 0, F = 1 - 1$	4.3	8.9125	8588 ± 66	75.0 ± 0.6	3.9 ± 0.1	6.8 ± 0.1
HCN	88.631848	$J = 1 - 0, F = 2 - 1$	4.3	14.852
HCN	88.633936	$J = 1 - 0, F = 0 - 1$	4.3	2.9707
H ¹⁵ NC	88.865715	$J = 1 - 0$	4.3	7.2839	192 ± 66	0.74 ± 0.24	3.3 ± 0.5	7.9 ± 0.2
HCO ⁺	89.188525	$J = 1 - 0$	4.3	15.211	13886 ± 90	67.7 ± 0.9	4.4 ± 0.2	7.0 ± 0.1
HCOOCH ₃	90.227659	$8_0 8 - 7_0 7, E$	20.1	20.893	54 ± 51	0.17 ± 0.17	2.7 ± 0.8	8.9 ± 0.4
¹⁵ NNH ⁺	90.263912	$J = 1 - 0, F = 2 - 1$	4.3	11.560	79 ± 51	0.37 ± 0.20	3.4 ± 0.9	7.2 ± 0.4
¹⁵ NNH ⁺	90.263487	$J = 1 - 0, F = 1 - 1$	4.3	19.265
HC ₅ N	90.525890	$J = 34 - 33$	76.0	637.50	106 ± 55	0.28 ± 0.18	1.9 ± 1.0	8.2 ± 0.3
HCC ¹³ CN	90.601777	$J = 10 - 9$	23.9	139.25	65 ± 61	0.13 ^{+0.17} _{-0.13}	f	...
HNC	90.663568	$J = 1 - 0$	4.4	9.3020	7984 ± 61	29.4 ± 0.4	3.4 ± 0.1	7.1 ± 0.1
CCS	90.686381	$N_J = 7_7 - 6_6$	26.1	56.880	111 ± 61	0.42 ± 0.22	3.5 ± 0.6	7.8 ± 0.2
HC ₃ N	90.979023	$J = 10 - 9$	24.0	139.26	2617 ± 54	8.8 ± 0.3	3.0 ± 0.1	7.8 ± 0.1
N ¹⁵ NH ⁺	91.204262	$J = 1 - 0, F = 1 - 1$	4.4	11.561	< 60	< 0.1	e	...
N ¹⁵ NH ⁺	91.205991	$J = 1 - 0, F = 2 - 1$	4.4	19.266	< 60	< 0.1	e	...
CH ₃ CN	91.971130	$5_3 - 4_3$	77.6	196.89	86 ± 65	0.27 ± 0.18	3.1 ± 3.4	8.1 ± 1.3
CH ₃ CN	91.979994	$5_2 - 4_2$	41.8	129.19	93 ± 65	0.34 ± 0.21	3.5 ± 0.5	7.7 ± 0.2
CH ₃ CN	91.985314	$5_1 - 4_1$	20.4	147.65	226 ± 65	0.89 ± 0.23	3.0 ± 0.3	7.7 ± 0.1
CH ₃ CN	91.987088	$5_0 - 4_0$	13.2	153.81	331 ± 65	1.24 ± 0.23	3.0 ± 0.1	8.1 ± 0.1
¹³ CS	92.494308	$J = 2 - 1$	6.7	15.336	575 ± 55	1.9 ± 0.2	3.0 ± 0.1	8.1 ± 0.1
U	92.6591				67 ± 57	0.24 ± 0.18	e	...
DC ₃ N	92.872375	$J = 11 - 10$	26.7	153.94	74 ± 53	0.15 ± 0.15	e	...
N ₂ H ⁺	93.171911	$J = 1 - 0, F_1 = 1 - 1, F = 0 - 1$	4.5	37.250	7353 ± 47	16.8 ± 0.2	3.2 ± 0.1	7.6 ± 0.1
N ₂ H ⁺	93.173770	$J = 1 - 0, F_1 = 1 - 1, F = 2 - 1$	4.5	62.079	6785 ± 47	24.6 ± 0.2	3.4 ± 0.1	7.8 ± 0.1
N ₂ H ⁺	93.176260	$J = 1 - 0, F_1 = 0 - 1, F = 1 - 1$	4.5	12.416	1995 ± 47	6.5 ± 0.2	3.0 ± 0.1	7.8 ± 0.1
HC ₅ N	93.188123	$J = 35 - 34$	80.5	656.28	159 ± 47	0.33 ± 0.13	1.9 ± 0.2	7.8 ± 0.2
CH ₃ CHO	93.580909	$5_1 5 - 4_1 4, A$	15.8	60.703	122 ± 64	0.62 ± 0.20	4.2 ± 0.7	7.5 ± 0.3
U	93.5912				78 ± 69	0.25 ± 0.22	3.0 ± 0.6	7.5 ± 0.3
CH ₃ CHO	93.595235	$5_1 5 - 4_1 4, E$	15.8	60.699	146 ± 64	0.43 ± 0.20	2.8 ± 0.1	7.7 ± 0.1
CCS	93.870107	$N_J = 7_8 - 6_7$	19.9	66.110	281 ± 53	0.92 ± 0.18	3.5 ± 1.1	7.7 ± 0.5
U	94.1134				64 ± 54	0.14 ± 0.12	3.0 ± 0.9	7.8 ± 0.4
U	94.1235				72 ± 54	0.18 ± 0.15	3.0 ± 0.9	7.8 ± 0.4
¹³ CH ₃ OH	94.405163	$2_{-1} - 1_{-1}, E$	12.4	1.2137	90 ± 57	0.22 ± 0.17	3.5 ± 1.1	7.7 ± 0.5
¹³ CH ₃ OH	94.407129	$2_0 - 1_0, A^+$	6.8	1.6173	103 ± 57	0.20 ± 0.17	3.0 ± 0.9	7.8 ± 0.4
U	94.7159				56 ± 54	0.13 ± 0.14	3.8 ± 0.6	7.8 ± 0.2
C ₄ H	95.150389	$N = 10 - 9, J = 21/2 - 19/2, F = 10 - 9$	25.1	7.5316	114 ± 48	0.31 ± 0.18
C ₄ H	95.150397	$N = 10 - 9, J = 21/2 - 19/2, F = 11 - 10$	25.1	8.2906
CH ₃ OH	95.169463	$8_0 - 7_1, A^+$	83.6	7.2210	1750 ± 48	10.9 ± 0.3	4.7 ± 0.3	7.2 ± 0.1
C ₄ H	95.188946	$N = 10 - 9, J = 19/2 - 17/2, F = 9 - 8$	25.1	6.7727	99 ± 48	0.34 ± 0.17	3.3 ± 0.6	7.5 ± 0.3
C ₄ H	95.188948	$N = 10 - 9, J = 19/2 - 17/2, F = 10 - 9$	25.1	7.5312
HC ₅ N	95.850335	$J = 36 - 35$	85.1	674.98	94 ± 40	0.19 ± 0.12	2.2 ± 0.6	8.0 ± 0.1
CH ₃ OH	95.914309	$2_1 - 1_1, A^+$	21.4	1.2142	416 ± 40	2.1 ± 0.2	4.1 ± 0.3	7.6 ± 0.1
CH ₃ CHO	95.947437	$5_0 5 - 4_0 4, E$	13.9	63.228	175 ± 40	0.88 ± 0.20	3.7 ± 0.3	7.9 ± 0.1
CH ₃ CHO	95.963459	$5_0 5 - 4_0 4, A$	13.8	63.186	176 ± 40	0.82 ± 0.19	3.9 ± 0.3	7.6 ± 0.1
HCOOCH ₃	96.070725	$8_2 7 - 7_2 6, E$	23.6	19.843	38 ± 33	0.15 ± 0.09	3.5 ± 1.4	7.9 ± 0.6
HCOOCH ₃	96.076845	$8_2 7 - 7_2 6, A$	23.6	19.849	43 ± 33	0.14 ± 0.10	f	...
CH ₃ CHO	96.274252	$5_2 4 - 4_2 3, A$	22.9	53.134	59 ± 33	0.21 ± 0.10	3.5 ± 0.7	7.7 ± 0.3
CH ₃ CHO	96.367787	$5_3 3 - 4_3 2, A$	34.3	40.496	47 ± 33	0.19 ± 0.11	4.3 ± 1.0	6.5 ± 0.4
CH ₃ CHO	96.368374	$5_3 2 - 4_3 1, E$	34.3	40.496
C ³⁴ S	96.412949	$2 - 1$	6.9	7.6678	1588 ± 33	5.9 ± 0.2	3.1 ± 0.1	7.9 ± 0.1
CH ₃ CHO	96.425614	$5_2 4 - 4_2 3, E$	23.0	52.829	90 ± 33	0.32 ± 0.11	3.2 ± 0.5	7.6 ± 0.2
CH ₃ CHO	96.475524	$5_2 3 - 4_2 2, E$	23.0	52.843	87 ± 33	0.27 ± 0.11	2.9 ± 0.4	7.6 ± 0.2
CH ₃ CHO	96.632663	$5_2 2 - 4_2 2, A$	23.0	53.135	87 ± 35	0.29 ± 0.13	2.7 ± 0.5	7.1 ± 0.3
U	96.6594				67 ± 35	0.17 ± 0.11
CH ₃ OH	96.739362	$2_{-1} - 1_{-1}, E$	12.5	1.2134	3392 ± 37	16.1 ± 0.2	4.2 ± 0.2	7.7 ± 0.1
CH ₃ OH	96.741375	$2_0 - 1_0, A^+$	7.0	1.6170	4214 ± 37	17.9 ± 0.1	3.6 ± 0.1	7.7 ± 0.1
CH ₃ OH	96.744550	$2_0 - 1_0, E$	20.1	1.6166	971 ± 37	4.2 ± 0.2	4.6 ± 0.7	7.8 ± 0.3
CH ₃ OH	96.755511	$2_1 - 1_1, E$	28.0	1.2442	301 ± 37	1.5 ± 0.2	3.7 ± 0.2	7.5 ± 0.1
H ¹³ CCCN	96.983001	$J = 11 - 10$	27.9	153.18	50 ± 35	0.14 ± 0.11	f	...
C ³³ S	97.166285	$J = 2 - 1, F = 1/2 - 3/2$	7.0	0.5100	39 ± 36	0.10 ± 0.09	f	...
C ³³ S	97.169513	$J = 2 - 1, F = 3/2 - 3/2$	7.0	3.2641	51 ± 36	0.14 ± 0.11	f	...
C ³³ S	97.171840	$J = 2 - 1, F = 5/2 - 3/2$	7.0	6.4260	318 ± 36	1.02 ± 0.12	2.9 ± 0.2	7.9 ± 0.1

Table 2—Continued

Name ^a	Frequency ^b (GHz)	Transition	E_u (K)	$S\mu^2$ (Debye ²)	T_{mb} Peak ^c (mK)	$\int T_{mb} dv$ ^c (K km s ⁻¹)	FWHM ^d (km s ⁻¹)	V_{LSR} ^d (km s ⁻¹)
C ³³ S	97.171840	$J = 2 - 1, F = 7/2 - 5/2$	7.0	12.239
C ³³ S	97.171840	$J = 2 - 1, F = 1/2 - 1/2$	7.0	2.5500
C ³³ S	97.172624	$J = 2 - 1, F = 3/2 - 5/2$	7.0	0.3060
C ³³ S	97.174996	$J = 2 - 1, F = 5/2 - 5/2$	7.0	2.7537	86 ± 36	0.23 ± 0.11	2.0 ± 3.1	7.8 ± 1.1
C ³³ S	97.175271	$J = 2 - 1, F = 3/2 - 1/2$	7.0	2.5498
OCS	97.301209	$J = 8 - 7$	21.0	4.0926	235 ± 34	0.96 ± 0.14	3.6 ± 0.2	7.6 ± 0.1
CH ₃ OH	97.582804	$2_1 - 2_1, A^-$	21.6	1.2142	488 ± 34	2.3 ± 0.2	4.0 ± 0.2	7.5 ± 0.1
³⁴ SO	97.715317	$N_J = 3_2 - 2_1$	9.1	6.9152	365 ± 34	1.2 ± 0.1	3.0 ± 0.1	7.7 ± 0.1
CS	97.980953	$J = 2 - 1$	7.1	7.6687	9398 ± 38	50.3 ± 0.3	4.6 ± 0.2	7.6 ± 0.1
U	98.1251				41 ± 40	0.11 ± 0.10		
C ₃ S	98.268516	$J = 17 - 16$	42.5	233.26	80 ± 41	0.19 ± 0.12	2.0 ± 0.5	7.4 ± 0.3
³³ SO	98.493642	$N_J = 3_2 - 2_1, F = 9/2 - 7/2$	9.2	9.8788	51 ± 41	0.10 ± 0.08	f	
HC ₅ N	98.512524	$J = 37 - 36$	89.9	693.66	121 ± 35	0.31 ± 0.11	2.0 ± 0.3	8.2 ± 0.2
CH ₃ CHO	98.863314	$5_{14} - 4_{13}, E$	16.6	60.694	225 ± 51	0.78 ± 0.22	4.5 ± 0.4	7.7 ± 0.2
CH ₃ CHO	98.900944	$5_{14} - 4_{13}, A$	16.5	60.702	140 ± 51	0.56 ± 0.17	3.2 ± 0.4	7.6 ± 0.2
SO	99.299870	$N_J = 3_2 - 2_1$	9.2	6.9114	4000 ± 48	17.1 ± 0.4	3.0 ± 0.1	7.4 ± 0.0
CH ₃ OCH ₃	99.325250	$4_{14} - 3_{03}, EA$	10.2	55.274	54 ± 48	0.26 ± 0.17	5.2 ± 1.1	8.6 ± 0.5
CH ₃ OCH ₃	99.324430	$4_{14} - 3_{03}, AE$	10.2	13.821
CH ₃ OCH ₃	99.324430	$4_{14} - 3_{03}, EE$	10.2	20.732
CH ₃ OCH ₃	99.326000	$4_{14} - 3_{03}, AA$	10.2	34.548
HCC ¹³ CN	99.661467	$J = 11 - 10$	28.7	153.19	89 ± 57	0.34 ± 0.19	3.4 ± 1.0	7.1 ± 0.4
CCS	99.866521	$N = 8 - 7, J = 7 - 6$	28.1	56.979	139 ± 57	0.32 ± 0.18	2.0 ± 0.3	7.2 ± 0.2
SO	100.029640	$N_J = 4_5 - 4_4$	38.6	0.8363	127 ± 51	0.43 ± 0.16	3.3 ± 0.6	7.5 ± 0.2
HC ₃ N	100.076392	$J = 11 - 10$	28.8	153.17	1869 ± 51	7.2 ± 0.3	2.8 ± 0.1	7.7 ± 0.0
H ₂ CCO	100.094514	$5_{15} - 4_{14}$	27.5	9.7093	154 ± 51	0.42 ± 0.10	2.3 ± 0.3	7.5 ± 0.1
SO ₂	100.878105	$2_{20} - 3_{13}$	12.6	0.4294	66 ± 51	0.16 ± 0.15	1.6 ± 1.3	7.9 ± 0.7
H ₂ CCO	101.036630	$5_{05} - 4_{04}$	14.6	10.112	102 ± 54	0.30 ± 0.16	2.1 ± 0.9	7.7 ± 0.2
U	101.1394				69 ± 63	0.21 ± 0.16		
HC ₅ N	101.174677	$J = 38 - 37$	94.7	712.56	112 ± 57	0.30 ± 0.14	e	
U	101.2841				65 ± 56	0.34 ± 0.18		
H ₂ CO	101.332991	$6_{15} - 6_{16}$	87.6	1.6865	168 ± 60	0.50 ± 0.17	2.8 ± 0.4	6.9 ± 0.2
H ₂ CS	101.477810	$3_{13} - 2_{12}$	22.9	7.2520	831 ± 57	2.9 ± 0.2	3.0 ± 0.1	7.4 ± 0.0
H ₂ CCO	101.981429	$5_{14} - 4_{13}$	27.7	9.7073	201 ± 69	0.75 ± 0.25	3.3 ± 0.3	7.7 ± 0.1
CH ₃ CCH	102.530348	$6_3 - 5_3$	82.3	5.5305	99 ± 63	0.31 ± 0.18	2.6 ± 1.4	7.7 ± 0.5
CH ₃ CCH	102.540145	$6_2 - 5_2$	46.1	3.2771	199 ± 63	0.65 ± 0.20	3.0 ± 2.7	7.9 ± 1.1
CH ₃ CCH	102.546024	$6_1 - 5_1$	24.5	3.5846	449 ± 63	1.5 ± 0.2	2.7 ± 0.2	7.8 ± 0.1
CH ₃ CCH	102.547984	$6_0 - 5_0$	17.2	3.6869	545 ± 63	2.0 ± 0.2	3.0 ± 0.2	7.8 ± 0.2
H ₂ CS	103.040452	$3_{03} - 2_{02}$	9.9	8.1585	575 ± 63	2.0 ± 0.2	3.2 ± 0.1	7.7 ± 0.1
CCS	103.640759	$N = 8 - 7, J = 8 - 7$	31.1	65.318	191 ± 54	0.43 ± 0.17	1.7 ± 0.4	7.4 ± 0.2
HC ₅ N	103.836817	$J = 39 - 38$	99.7	731.28	123 ± 48	0.30 ± 0.12	2.3 ± 0.4	8.1 ± 0.2
SO ₂	104.029418	$3_{13} - 2_{02}$	7.7	5.3734	387 ± 48	1.4 ± 0.2	3.5 ± 0.2	7.5 ± 0.1
C ₃ S	104.048455	$J = 18 - 17$	47.4	246.95	94 ± 48	0.19 ± 0.12	e	
SO ₂	104.239295	$10_{19} - 10_{010}$	54.7	17.868	192 ± 45	0.81 ± 0.17	3.0 ± 0.6	7.1 ± 0.2
CH ₃ OH	104.300414	$11_{-1} - 10_{-9}, E$	158.7	3.4143	86 ± 45	0.32 ± 0.14	3.4 ± 0.7	7.3 ± 0.3
H ₂ CS	104.617040	$3_{12} - 2_{11}$	23.2	7.2517	655 ± 36	2.6 ± 0.1	3.2 ± 0.1	7.8 ± 0.0
C ₄ H	104.666572	$N = 11 - 10, J = 23/2 - 21/2, F = 11 - 10$	30.1	9.0497	119 ± 36	0.31 ± 0.10	2.3 ± 0.2	7.6 ± 0.1
C ₄ H	104.666565	$N = 11 - 10, J = 23/2 - 21/2, F = 12 - 11$	30.1	8.2915
C ₄ H	104.705109	$N = 11 - 10, J = 21/2 - 19/2, F = 10 - 9$	30.2	8.2917	96 ± 36	0.25 ± 0.09	2.4 ± 0.4	7.9 ± 0.2
C ₄ H	104.705106	$N = 11 - 10, J = 21/2 - 19/2, F = 11 - 10$	30.2	7.5326
U	104.7115				47 ± 35	0.15 ± 0.10		
NH ₂ CHO	105.464219	$5_{04} - 4_{04}$	15.2	65.322	64 ± 56	0.15 ± 0.15	1.9 ± 0.8	8.1 ± 0.4
CCS	106.347726	$N_J = 8_9 - 7_8$	25.0	74.425	300 ± 55	0.89 ± 0.17	2.6 ± 0.3	7.7 ± 0.1
HC ₅ N	106.498910	$J = 40 - 39$	104.8	749.90	67 ± 55	0.21 ± 0.13	3.3 ± 1.1	7.7 ± 0.5
³⁴ SO	106.743244	$N_J = 2_3 - 1_2$	20.9	3.5566	58 ⁺⁶⁰ ₋₅₈	0.21 ± 0.16	f	
CH ₃ OH	107.013803	$3_1 - 4_0, A^+$	28.4	3.0088	93 ± 57	0.15 ± 0.11	f	
U	107.0887				54 ± 47	0.16 ± 0.11		
U	107.4241				59 ± 51	0.23 ± 0.14		
U	107.4989				64 ± 50	0.17 ± 0.12		
¹³ CN	108.412862	$N = 1 - 0, J = 1/2 - 1/2, F_1 = 0 - 1, F = 1 - 1$	5.2	0.6340	41 ± 39	0.08 ^{+0.12} _{-0.08}	2.1 ± 0.9	9.6 ± 0.5
¹³ CN	108.426889	$N = 1 - 0, J = 1/2 - 1/2, F_1 = 0 - 1, F = 1 - 2$	5.2	1.2668	< 39	< 0.1		
¹³ CN	108.636923	$N = 1 - 0, J = 1/2 - 1/2, F_1 = 1 - 0, F = 1 - 1$	5.2	1.9320	61 ± 39	0.18 ± 0.13	4.3 ± 1.7	8.0 ± 0.7
¹³ CN	108.643590	$N = 1 - 0, J = 3/2 - 1/2, F_1 = 1 - 1, F = 2 - 1$	5.2	0.8559	60 ± 39	0.25 ± 0.15	5.3 ± 2.6	5.3 ± 1.1
¹³ CN	108.644346	$N = 1 - 0, J = 3/2 - 1/2, F_1 = 1 - 1, F = 0 - 1$	5.2	0.6416
¹³ CN	108.645064	$N = 1 - 0, J = 3/2 - 1/2, F_1 = 1 - 1, F = 1 - 1$	5.2	0.5510
¹³ CN	108.651297	$N = 1 - 0, J = 1/2 - 1/2, F_1 = 1 - 0, F = 2 - 1$	5.2	3.2764	100 ± 39	0.27 ± 0.12	3.1 ± 0.8	7.9 ± 0.3
¹³ CN	108.657646	$N = 1 - 0, J = 3/2 - 1/2, F_1 = 1 - 1, F = 2 - 2$	5.2	2.4198	45 ± 39	0.15 ± 0.09	2.6 ± 1.3	7.9 ± 0.5

Table 2—Continued

Name ^a	Frequency ^b (GHz)	Transition	E_u (K)	$S\mu^2$ (Debye ²)	T_{mb} Peak ^c (mK)	$\int T_{mb} dv$ ^c (K km s ⁻¹)	FWHM ^d (km s ⁻¹)	V_{LSR} ^d (km s ⁻¹)
HC ¹³ CCN	108.710532	$J = 12 - 11$	33.9	167.12	60 ± 39	0.18 ± 0.12	3.4 ± 1.4	8.8 ± 0.6
HCC ¹³ CN	108.720999	$J = 12 - 11$	33.9	167.11	86 ± 39	0.21 ± 0.13	3.0 ± 0.7	8.4 ± 0.3
¹³ CN	108.780201	$N = 1 - 0, J = 3/2 - 1/2, F_1 = 2 - 1, F = 3 - 2$	5.2	4.9058	160 ± 39	0.40 ± 0.12	3.2 ± 0.7	8.4 ± 0.3
¹³ CN	108.782374	$N = 1 - 0, J = 3/2 - 1/2, F_1 = 2 - 1, F = 2 - 1$	5.2	2.5864	127 ± 39	0.29 ± 0.12	2.8 ± 1.0	7.8 ± 0.4
¹³ CN	108.786982	$N = 1 - 0, J = 3/2 - 1/2, F_1 = 2 - 1, F = 1 - 0$	5.2	1.4410	60 ± 39	0.18 ± 0.12	4.1 ± 0.9	8.6 ± 0.4
¹³ CN	108.793753	$N = 1 - 0, J = 3/2 - 1/2, F_1 = 2 - 1, F = 1 - 1$	5.2	0.8937	< 39	< 0.1		
¹³ CN	108.796400	$N = 1 - 0, J = 3/2 - 1/2, F_1 = 2 - 1, F = 2 - 2$	5.2	0.9179	70 ± 39	0.17 ± 0.10	2.8 ± 0.9	8.6 ± 0.4
CH ₃ OH	108.893963	$0_0 - 1_{-1}, E$	13.1	0.9784	844 ± 41	3.2 ± 0.2	4.2 ± 0.2	7.8 ± 0.1
HC ₅ N	109.160973	$J = 41 - 40$	110.0	768.68	127 ± 42	0.22 ± 0.14	1.9 ± 0.5	7.9 ± 0.3
HC ₃ N	109.173634	$J = 12 - 11$	34.1	167.10	3040 ± 42	8.2 ± 0.2	3.0 ± 0.1	8.0 ± 0.1
SO	109.252220	$N_J = 2_3 - 1_3$	21.1	3.5585	1062 ± 42	3.7 ± 0.3	3.4 ± 0.1	7.8 ± 0.1
OCS	109.463063	$J = 9 - 8$	26.3	4.6034	360 ± 42	1.1 ± 0.2	3.5 ± 0.2	7.6 ± 0.1
C ¹⁵ N	109.689610	$N = 1 - 0, J = 1/2 - 1/2, F = 1 - 1$	5.3	1.3858	68 ± 41	0.18 ± 0.11	2.9 ± 0.7	8.2 ± 0.3
DC ₃ N	109.757133	$J = 13 - 12$	36.9	181.90	56 ± 41	0.17 ± 0.13	2.4 ± 0.8	8.4 ± 0.4
C ¹⁸ O	109.782173	$J = 1 - 0$	5.3	0.01221	4493 ± 41	12.1 ± 0.2	3.3 ± 0.1	7.7 ± 0.1
HNCO	109.905749	$5_0 5 - 4_0 4$	15.8	12.482	377 ± 39	1.4 ± 0.2	3.4 ± 0.2	7.9 ± 0.1
C ¹⁵ N	110.023540	$N = 1 - 0, J = 3/2 - 1/2, F = 1 - 0$	5.3	1.3857	75 ± 46	0.40 ± 0.17	5.5 ± 0.9	6.0 ± 0.4
C ¹⁵ N	110.024590	$N = 1 - 0, J = 3/2 - 1/2, F = 2 - 1$	5.3	3.5040
NH ₂ D	110.153594	$1_1 1, 0_a - 1_0 1, 0_s$	21.3	9.5470	358 ± 48	1.8 ± 0.2	5.4 ± 0.3	7.6 ± 0.1
¹³ CO	110.201354	$J = 1 - 0$	5.3	0.01220	20215 ± 48	83.7 ± 0.3	3.9 ± 0.1	7.5 ± 0.1
CH ₃ CN	110.364354	$6_3 - 5_3$	82.9	276.88	81 ± 48	0.40 ± 0.18	5.1 ± 2.0	7.5 ± 0.8
CH ₃ CN	110.374989	$6_2 - 5_2$	47.1	164.06	131 ± 46	0.62 ± 0.18	3.9 ± 2.6	7.5 ± 1.1
CH ₃ CN	110.381372	$6_1 - 5_1$	25.7	179.44	282 ± 46	1.21 ± 0.17	4.3 ± 0.3	7.7 ± 0.1
CH ₃ CN	110.383500	$6_0 - 5_0$	18.5	184.57	321 ± 46	1.19 ± 0.15	3.2 ± 0.2	7.7 ± 0.1
HCOOCH ₃	111.169903	$10_0 10 - 9_0 9, E$	30.3	26.188	81 ± 63	0.21 ± 0.18	g	
HCOOCH ₃	111.171634	$10_0 10 - 9_0 9, A$	30.2	26.191	53 ± 63	0.25 ± 0.18	g	
U	111.2891				61 ± 55	0.31 ± 0.18		
CH ₃ OCH ₃	111.783010	$7_0 7 - 6_1 6, AA$	25.3	86.203	110 ± 63	0.29 ± 0.14	2.5 ± 0.5	7.1 ± 0.2
CH ₃ OCH ₃	111.782562	$7_0 7 - 6_1 6, EE$	25.3	53.868
CH ₃ OCH ₃	111.783647	$7_0 7 - 6_1 6, AE$	25.3	32.324
CH ₃ OCH ₃	111.783648	$7_0 7 - 6_1 6, EA$	25.3	21.549
CH ₃ CHO	112.248716	$6_1 6 - 5_1 5, A$	21.1	73.768	133 ± 69	0.74 ± 0.25	4.5 ± 0.7	6.9 ± 0.3
CH ₃ CHO	112.254508	$6_1 6 - 5_1 5, E$	21.2	73.796	158 ± 69	0.51 ± 0.20	2.9 ± 0.8	7.5 ± 0.3
C ¹⁷ O	112.359284	$J = 1 - 0$	5.4	0.0122	868 ± 69	4.2 ± 0.3	4.6 ± 0.2	7.5 ± 0.1
U	112.8373				83 ± 68	0.33 ± 0.22		
CN	113.123370	$N = 1 - 0, J = 1/2 - 1/2, F = 1/2 - 1/2$	5.4	0.1527	620 ± 72	2.1 ± 0.2	3.0 ± 0.1	7.5 ± 0.1
CN	113.144157	$N = 1 - 0, J = 1/2 - 1/2, F = 1/2 - 3/2$	5.4	1.2492	2254 ± 72	7.9 ± 0.3	3.3 ± 0.0	7.4 ± 0.1
CN	113.170491	$N = 1 - 0, J = 1/2 - 1/2, F = 3/2 - 1/2$	5.4	1.2199	2378 ± 72	8.4 ± 0.2	3.4 ± 0.1	7.3 ± 0.1
CN	113.191279	$N = 1 - 0, J = 1/2 - 1/2, F = 3/2 - 3/2$	5.4	1.5836	2268 ± 72	8.7 ± 0.3	3.3 ± 0.1	7.3 ± 0.1
CCS	113.410186	$N = 9 - 8, J = 8 - 7$	33.6	65.427	181 ± 87	0.67 ± 0.28	3.2 ± 0.4	7.8 ± 0.2
CN	113.488120	$N = 1 - 0, J = 3/2 - 1/2, F = 3/2 - 1/2$	5.4	1.5838	2485 ± 87	9.9 ± 0.3	3.8 ± 1.5	7.2 ± 0.6
CN	113.490970	$N = 1 - 0, J = 3/2 - 1/2, F = 5/2 - 3/2$	5.4	4.2050	4421 ± 87	18.6 ± 0.3	3.7 ± 0.5	7.2 ± 0.2
CN	113.499644	$N = 1 - 0, J = 3/2 - 1/2, F = 1/2 - 1/2$	5.4	1.2491	1810 ± 87	6.3 ± 0.3	3.3 ± 0.1	7.3 ± 0.1
CN	113.508907	$N = 1 - 0, J = 3/2 - 1/2, F = 3/2 - 3/2$	5.4	1.2196	2407 ± 87	8.5 ± 0.3	3.3 ± 0.6	7.4 ± 0.2
CN	113.520432	$N = 1 - 0, J = 3/2 - 1/2, F = 1/2 - 3/2$	5.4	0.1526	392 ± 87	1.4 ± 0.2	3.1 ± 0.2	7.3 ± 0.1
C ₄ H	114.182512	$N = 12 - 11, J = 25/2 - 23/2, F = 12 - 11$	35.6	9.0522	86 ± 87	0.27 ± 0.20	3.1 ± 1.0	7.6 ± 0.4
C ₄ H	114.182518	$N = 12 - 11, J = 25/2 - 23/2, F = 13 - 12$	35.6	9.8096
C ₄ H	114.221040	$N = 12 - 11, J = 23/2 - 21/2, F = 11 - 10$	35.6	8.2926	89 ± 87	0.25 ± 0.20	2.6 ± 0.9	7.7 ± 0.4
C ₄ H	114.221042	$N = 12 - 11, J = 23/2 - 21/2, F = 12 - 11$	35.6	9.0509
H ¹³ CCCN	114.614995	$J = 13 - 12$	38.5	181.05	94 ± 78	0.22 ± 0.17	2.0 ± 0.6	7.7 ± 0.3
CH ₃ CHO	114.940175	$6_0 6 - 5_0 5, E$	19.5	75.850	267 ± 102	1.1 ± 0.2	4.2 ± 0.5	7.4 ± 0.2
CH ₃ CHO	114.959902	$6_0 6 - 5_0 5, A$	19.4	75.800	261 ± 102	1.4 ± 0.3	5.6 ± 0.6	7.9 ± 0.3
NS	115.153935	$\Omega = 1/2, J = 5/2 - 3/2, F = 7/2 - 5/2, e$	8.8	10.485	253 ± 102	0.80 ± 0.26	2.8 ± 0.5	7.8 ± 0.2
NS	115.156812	$\Omega = 1/2, J = 5/2 - 3/2, F = 5/2 - 3/2, e$	8.8	6.6049	130 ± 102	0.39 ± 0.26	2.9 ± 1.4	8.3 ± 0.6
CO	115.271202	$J = 1 - 0$	5.5	0.01212	60474 ± 114	374 ± 1	5.4 ± 0.1	7.1 ± 0.1
NS	115.556253	$\Omega = 1/2, J = 5/2 - 3/2, F = 7/2 - 5/2, f$	8.9	10.484	158 ± 123	0.38 ± 0.31	2.0 ± 0.7	7.9 ± 0.3
CH ₃ CHO	115.695051	$6_2 5 - 5_2 4, E$	28.5	66.526	159 ± 153	0.37 ± 0.34	2.3 ± 0.7	7.7 ± 0.3
CH ₃ CHO	115.910320	$6_2 4 - 5_2 3, E$	28.6	66.535	197 ± 168	0.75 ± 0.48	4.7 ± 1.3	8.1 ± 0.5

^aUnidentified lines are denoted as 'U'.^bRest frequency.^cThe errors are 3σ . The upper limit to the integrated intensity is calculated as: $\int T_{mb} dv < 3r.m.s \times \sqrt{\Delta V / \Delta v_{res}} \Delta v_{res}$, where ΔV is the assumed line width (2 km s⁻¹) and Δv_{res} is the velocity resolution per channel.^dFWHM and V_{LSR} are obtained from Gaussian fits.

^eGaussian fitting is not successful due to narrow line widths.

^fGaussian fitting is not successful due to poor S/N ratios or blending with other lines.

^gGaussian fitting is not successful due to blending with other lines.

Table 3. Line parameters observed in NGC 2264 CMM3 with ASTE.

Name	Frequency ^a (GHz)	Transition	E_u (K)	$S\mu^2$ (Debye ²)	T_{mb} Peak ^b (mK)	$\int T_{mb} dv$ ^b (K km s ⁻¹)	FWHM ^c (km s ⁻¹)	V_{LSR} ^c (km s ⁻¹)
¹³ CO	330.587965	$J = 3 - 2$	31.7	0.03653	18981 ± 78	72.2 ± 0.3	3.6 ± 0.1	7.4 ± 0.1
D ₂ CO	330.674348	$6_{16} - 5_{15}$	61.1	31.678	< 78	< 0.2		
CH ₃ OH	331.502370	$11_1 - 11_0, A^{-+}$	169.0	21.311	185 ± 62	1.07 ± 0.22	4.6 ± 0.4	7.3 ± 0.2
SO ₂	332.505242	$4_{31} - 3_{22}$	31.3	6.9211	64 ± 61	0.14 ± 0.12	d	
NH ₂ D	332.781890	$1_{01}, 0_a - 0_{00}, 0_a$	16.6	0.1640	224 ± 67	0.65 ± 0.17	2.8 ± 0.3	7.2 ± 0.1
NH ₂ D	332.822510	$1_{01}, 0_s - 0_{00}, 0_s$	16.0	0.1529	71 ± 67	0.30 ± 0.15	3.8 ± 0.9	7.6 ± 0.4
SO ₂	334.673353	$8_{26} - 7_{17}$	43.2	4.9501	98 ± 76	0.14 ± 0.12	e	
HDCO	335.096782	$5_{14} - 4_{13}$	56.3	26.055	143 ± 76	0.37 ± 0.17	2.4 ± 0.3	6.9 ± 0.1
CH ₃ OH	335.133686	$2_2 - 3_1, A^{-}$	44.7	0.3073	68 ± 76	0.23 ± 0.19	3.3 ± 1.0	6.5 ± 0.4
CH ₃ OH	335.582005	$7_1 - 6_{11}, A^{+}$	79.0	5.5501	575 ± 64	2.5 ± 0.2	3.6 ± 0.2	7.2 ± 0.1
CH ₃ OH	336.865110	$12_1 - 12_0, A^{-+}$	197.1	22.877	170 ± 98	1.1 ± 0.4	5.7 ± 0.7	6.9 ± 0.3
C ¹⁷ O	337.060988	$J = 3 - 2$	32.4	0.03645	1799 ± 102	5.2 ± 0.3	2.6 ± 0.1	7.5 ± 0.1
C ³⁴ S	337.396459	$J = 7 - 6$	64.8	26.839	297 ± 102	0.58 ± 0.24	1.8 ± 0.2	7.6 ± 0.1
H ₂ CS	338.083195	$10_{110} - 9_{19}$	102.5	26.922	192 ± 53	0.61 ± 0.13	3.1 ± 0.3	7.6 ± 0.1
CH ₃ OH	338.124502	$7_0 - 6_0, E$	78.1	5.6546	934 ± 53	4.2 ± 0.2	3.8 ± 0.2	7.3 ± 0.1
CH ₃ OH	338.344628	$7_{-1} - 6_{-1}, E$	70.6	5.5450	2178 ± 53	10.7 ± 0.3	3.9 ± 0.1	7.4 ± 0.1
CH ₃ OH	338.408681	$7_0 - 6_0, A^{+}$	65.0	5.6598	2446 ± 53	12.1 ± 0.3	4.0 ± 0.2	7.3 ± 0.1
CH ₃ OH	338.512856	$7_2 - 6_2, A^{-}$	102.7	5.2264	164 ± 60	0.48 ± 0.16	2.9 ± 0.9	7.3 ± 0.4
CH ₃ OH	338.512627	$7_4 - 6_4, A^{-}$	145.4	3.8054
CH ₃ OH	338.512639	$7_{-4} - 6_{-4}, E$	145.4	3.8054
CH ₃ OH	338.540795	$7_3 - 6_3, A^{+}$	114.8	4.6036	230 ± 60	1.0 ± 0.2	4.4 ± 0.6	6.1 ± 0.2
CH ₃ OH	338.559928	$7_{-3} - 6_{-3}, E$	127.7	4.6377	67 ± 60	0.10 ± 0.09	d	
CH ₃ OH	338.583195	$7_3 - 6_3, E$	112.7	4.6169	54 ± 60	0.21 ± 0.17	3.7 ± 1.0	7.4 ± 0.4
CH ₃ OH	338.614999	$7_1 - 6_{11}, E$	86.1	5.6807	505 ± 60	1.9 ± 0.2	3.3 ± 0.2	7.2 ± 0.1
CH ₃ OH	338.639939	$7_2 - 6_2, A^{+}$	102.7	5.2264	102 ± 60	0.44 ± 0.16	3.9 ± 0.7	7.4 ± 0.3
CH ₃ OH	338.721630	$7_2 - 6_2, E$	87.3	5.1381	893 ± 60	4.6 ± 0.3	4.1 ± 0.2	6.9 ± 0.1
CH ₃ OH	338.722940	$7_{-2} - 6_{-2}, E$	90.9	5.2024
SO	339.341459	$N_J = 3_3 - 2_3$	22.5	0.2239	152 ± 63	0.24 ± 0.11	1.5 ± 0.2	7.6 ± 0.1
CN	339.446777	$N = 3 - 2, J = 5/2 - 5/2, F = 3/2 - 3/2$	32.6	0.1989	69 ± 63	0.23 ± 0.14	3.8 ± 1.1	6.9 ± 0.5
CN	339.516635	$N = 3 - 2, J = 5/2 - 5/2, F = 7/2 - 7/2$	32.6	0.4453	156 ± 68	0.23 ± 0.15	1.2 ± 0.2	7.8 ± 0.1
CN	340.008126	$N = 3 - 2, J = 5/2 - 3/2, F = 5/2 - 5/2$	32.6	0.8127	95 ± 74	0.27 ± 0.15	2.5 ± 0.7	7.5 ± 0.3
CN	340.019626	$N = 3 - 2, J = 5/2 - 3/2, F = 3/2 - 3/2$	32.6	0.8104	97 ± 74	0.23 ± 0.16	2.1 ± 0.5	7.5 ± 0.2
CN	340.031549	$N = 3 - 2, J = 5/2 - 3/2, F = 7/2 - 5/2$	32.6	6.7218	794 ± 74	3.9 ± 0.2	2.5 ± 0.2	7.5 ± 0.1
CN	340.035408	$N = 3 - 2, J = 5/2 - 3/2, F = 3/2 - 1/2$	32.6	2.5233	2.5 ± 0.2	7.5 ± 0.1
CN	340.035408	$N = 3 - 2, J = 5/2 - 3/2, F = 5/2 - 3/2$	32.6	4.2362
C ³³ S	340.052570	$J = 7 - 6$	65.3	107.36	< 65	< 0.1		
CN	340.247770	$N = 3 - 2, J = 7/2 - 5/2, F = 7/2 - 5/2$	32.7	6.6249	1986 ± 74	6.3 ± 0.2	2.9 ± 0.1	7.2 ± 0.1
CN	340.247770	$N = 3 - 2, J = 7/2 - 5/2, F = 9/2 - 7/2$	32.7	9.0111
CN	340.248544	$N = 3 - 2, J = 7/2 - 5/2, F = 5/2 - 3/2$	32.7	4.8082
CN	340.261773	$N = 3 - 2, J = 7/2 - 5/2, F = 5/2 - 5/2$	32.7	0.5861	230 ± 74	0.9 ± 0.2	1.6 ± 0.3	8.1 ± 0.1
CN	340.264949	$N = 3 - 2, J = 7/2 - 5/2, F = 7/2 - 7/2$	32.7	0.5844	2.6 ± 0.3	8.1 ± 0.1
HC ¹⁸ O ⁺	340.630692	$J = 4 - 3$	40.9	60.839	96 ± 71	0.23 ± 0.16	2.4 ± 0.5	7.2 ± 0.2
SO	340.714155	$N_J = 8_7 - 7_6$	81.3	16.244	481 ± 71	1.6 ± 0.2	3.3 ± 0.3	7.1 ± 0.1
HCS ⁺	341.350229	$J = 8 - 7$	73.7	30.669	71 ± 73	0.20 ± 0.14	2.8 ± 1.0	6.8 ± 0.4
CH ₃ OH	341.415639	$7_1 - 6_{11}, A^{-}$	80.1	5.5501	846 ± 73	3.8 ± 0.3	4.0 ± 0.2	7.2 ± 0.1
D ₂ CO	342.522128	$6_{06} - 5_{05}$	58.1	32.420	< 78	< 0.2		
CH ₃ OH	342.729830	$13_1 - 13_0, A^{-+}$	227.5	24.378	143 ± 53	0.68 ± 0.17	5.1 ± 0.5	7.2 ± 0.2
CS	342.882850	$J = 7 - 6$	65.8	26.837	3266 ± 73	16.4 ± 0.5	3.3 ± 0.2	7.4 ± 0.1
H ₂ CS	342.946424	$10_{010} - 9_{09}$	90.6	27.197	61 ± 73	0.22 ± 0.16	4.5 ± 1.2	8.0 ± 0.5
H ₂ ¹³ CO	343.325713	$5_{15} - 4_{14}$	61.3	26.100	157 ± 73	0.54 ± 0.20	2.8 ± 0.5	7.4 ± 0.2
HC ¹⁵ N	344.200109	$J = 4 - 3$	41.3	35.650	90 ± 71	0.43 ± 0.21	6.0 ± 1.0	7.9 ± 0.4
SO	344.310612	$N_J = 8_8 - 7_7$	87.5	18.556	446 ± 71	1.4 ± 0.2	2.6 ± 0.2	7.2 ± 0.1
H ¹³ CN	345.339769	$J = 4 - 3$	41.4	106.94	327 ± 61	1.9 ± 0.3	4.2 ± 0.3	7.6 ± 0.1
CO	345.795990	$J = 3 - 2$	33.2	0.03631	33888 ± 88	264.2 ± 0.9	f	
SO	346.528481	$N_J = 8_9 - 7_8$	78.8	21.112	464 ± 55	1.5 ± 0.2	2.7 ± 0.1	7.2 ± 0.1
H ¹³ CO ⁺	346.998344	$J = 4 - 3$	41.6	60.849	906 ± 55	2.3 ± 0.1	2.4 ± 0.1	7.4 ± 0.1
SiO	347.330579	$J = 8 - 7$	75.0	76.810	166 ± 56	3.6 ± 0.4	g	
HN ¹³ C	348.340814	$J = 4 - 3$	41.8	106.94	92 ± 39	0.32 ± 0.11	2.6 ± 0.4	7.0 ± 0.2
H ₂ CS	348.534365	$10_{19} - 9_{18}$	105.2	26.921	112 ± 40	0.43 ± 0.11	3.8 ± 0.3	7.1 ± 0.1
CH ₃ OH	349.107020	$14_1 - 14_0, A^{-+}$	260.3	25.799	84 ± 39	0.34 ± 0.10	4.3 ± 0.6	7.4 ± 0.2
c-C ₃ H ₂	349.263999	$5_{50} - 4_{41}$	49.0	36.510	78 ± 39	0.24 ± 0.09	2.4 ± 0.3	7.5 ± 0.1
CCH	349.337706	$N = 4 - 3, J = 9/2 - 7/2, F = 5 - 4$	41.9	2.8987	1346 ± 39	4.6 ± 0.1	3.0 ± 0.6	7.2 ± 0.1
CCH	349.338988	$N = 4 - 3, J = 9/2 - 7/2, F = 4 - 3$	41.9	2.3163
CCH	349.399276	$N = 4 - 3, J = 7/2 - 5/2, F = 4 - 3$	41.9	2.2712	946 ± 39	3.4 ± 0.1	3.1 ± 0.1	7.1 ± 0.1
CCH	349.400671	$N = 4 - 3, J = 7/2 - 5/2, F = 3 - 2$	41.9	1.6942
CH ₃ OH	350.687730	$4_0 - 3_{-1}, E$	36.3	1.5545	907 ± 44	4.4 ± 0.2	4.0 ± 0.2	7.0 ± 0.1

Table 3—Continued

Name	Frequency ^a (GHz)	Transition	E_u (K)	$S\mu^2$ (Debye ²)	T_{mb} Peak ^b (mK)	$\int T_{\text{mb}} dv$ ^b (K km s ⁻¹)	FWHM ^c (km s ⁻¹)	V_{LSR} ^c (km s ⁻¹)
CH ₃ OH	350.905119	$1_1 - 0_0, A^+$	16.8	1.9774	746 ± 44	3.4 ± 0.2	3.4 ± 0.0	7.0 ± 0.1
NO	351.043524	$\Omega = 1/2^-, J = 7/2 - 5/2, F = 9/2 - 7/2$	36.1	0.1079	98 ± 47	0.28 ± 0.11	2.8 ± 0.6	7.5 ± 0.2
NO	351.051469	$\Omega = 1/2^-, J = 7/2 - 5/2, F = 7/2 - 5/2$	36.1	0.07928	156 ± 47	0.49 ± 0.13	3.5 ± 0.5	7.5 ± 0.2
NO	351.051705	$\Omega = 1/2^-, J = 7/2 - 5/2, F = 5/2 - 3/2$	36.1	0.05755
SO ₂	351.257223	$5_3 3 - 4_2 2$	35.9	7.3217	100 ± 47	0.28 ± 0.10	2.8 ± 0.5	7.4 ± 0.2
H ₂ CO	351.768645	$5_1 5 - 4_1 4$	62.5	26.096	3949 ± 49	18.9 ± 0.3	3.6 ± 0.1	7.3 ± 0.1
HCN	354.505477	$J = 4 - 3$	42.5	106.94	3273 ± 86	19.2 ± 0.6	^f	
CH ₃ OH	355.603110	$13_0 - 12_1, A^+$	211.1	13.059	178 ± 91	0.71 ± 0.23	4.5 ± 0.5	6.8 ± 0.2
HCO ⁺	356.734223	$J = 4 - 3$	42.8	60.840	8943 ± 81	28.4 ± 0.4	2.6 ± 0.1	6.7 ± 0.1
CH ₃ OH	358.605800	$4_1 - 3_0, E$	44.3	2.2121	586 ± 100	2.4 ± 0.4	3.5 ± 0.2	7.3 ± 0.1
DCO ⁺	360.169778	$J = 5 - 4$	51.9	76.048	240 ± 104	0.55 ± 0.21	2.2 ± 0.4	7.5 ± 0.2
CH ₃ OH	361.852251	$8_1 - 7_2, E$	104.6	2.3796	120 ± 118	0.78 ± 0.38	6.5 ± 1.3	8.2 ± 0.6
DCN	362.045754	$J = 5 - 4$	52.1	134.18	93 ± 45	0.32 ± 0.12	2.9 ± 0.4	6.8 ± 0.2
HNC	362.630303	$J = 4 - 3$	43.5	37.213	3374 ± 46	9.9 ± 0.2	2.6 ± 0.1	7.3 ± 0.1
H ₂ CO	362.736048	$5_0 5 - 4_0 4$	52.3	27.168	2382 ± 46	9.4 ± 0.2	3.2 ± 0.1	7.3 ± 0.1
CH ₃ OH	363.440304	$16_1 - 16_0, A^{++}$	332.7	28.405	58 ± 55	0.23 ± 0.13	3.6 ± 0.8	7.5 ± 0.3
CH ₃ OH	363.739820	$7_2 - 6_1, E$	87.3	4.5730	796 ± 54	3.1 ± 0.2	3.3 ± 0.2	7.2 ± 0.1
H ₂ CO	363.945894	$5_2 4 - 4_2 3$	99.6	22.834	856 ± 54	3.0 ± 0.2	3.0 ± 0.1	7.2 ± 0.1
H ₂ CO	364.103249	$5_4 2 - 4_4 1$	240.8	9.7858	128 ± 90	0.40 ± 0.20	3.0 ± 0.4	7.1 ± 0.2
H ₂ CO	364.103249	$5_4 1 - 4_4 0$	240.8	9.7858
H ₂ CO	364.275141	$5_3 3 - 4_3 2$	158.5	17.398	765 ± 69	4.2 ± 0.3	4.3 ± 0.5	7.2 ± 0.2
H ₂ CO	364.288884	$5_3 2 - 4_3 1$	158.5	17.397	806 ± 69	4.0 ± 0.3	4.2 ± 0.4	7.2 ± 0.1
H ₂ CO	365.363428	$5_2 3 - 4_2 2$	99.7	22.837	808 ± 72	3.2 ± 0.3	3.1 ± 0.1	7.2 ± 0.1

^aRest frequency.

^bThe errors are 3σ . The upper limit to the integrated intensity is calculated as: $\int T_{\text{mb}} dv < 3r.m.s \times \sqrt{\Delta V / \Delta v_{\text{res}}} \Delta v_{\text{res}}$, where ΔV is the assumed line width (2 km s⁻¹) and Δv_{res} is the velocity resolution per channel.

^cFWHM and V_{LSR} are obtained from Gaussian fits.

^dGaussian fitting is not successful due to poor S/N ratios or blending with other lines.

^eGaussian fitting is not successful due to a distorted baseline.

^fGaussian fitting is not possible due to a very broad and complex line profile.

Table 4: Identified molecules.

NH ₂ D	HNCO
CCH, CCD	NH ₂ CHO *
CN, ¹³ CN, C ¹⁵ N	HCO ₂ ⁺ *
HCN, H ¹³ CN, HC ¹⁵ N, DCN	SiO
HNC, HN ¹³ C, H ¹⁵ NC, DNC	CS, ¹³ CS, C ³³ S, C ³⁴ S
CO, ¹³ CO, C ¹⁷ O, C ¹⁸ O	HCS ⁺
HCO	H ₂ CS
HCO ⁺ , H ¹³ CO ⁺ , HC ¹⁸ O ⁺ , DCO ⁺	NS
H ₂ CO, H ₂ ¹³ CO, HDCO	SO, ³³ SO, ³⁴ SO
CH ₃ OH, ¹³ CH ₃ OH	SO ⁺ *
N ₂ H ⁺ , ¹⁵ NNH ⁺ , N ₂ D ⁺	C ₄ H
NO	HC ₃ N, H ¹³ CCCN, HC ¹³ CCN, HCC ¹³ CN, DC ₃ N
c-C ₃ H ₂	HCOOCH ₃
CH ₃ CCH	CCS
CH ₃ CN	OCS
H ₂ CCO	SO ₂
CH ₃ CHO	C ₃ S
CH ₃ OCH ₃	HC ₅ N

*Tentative detection (see text).

Table 5. Column Densities and Rotation Temperatures ^{a b}.

Molecule	N (cm ⁻²)	T_{rot} (K)	Molecule	N (cm ⁻²)	T_{rot} (K)
NH ₂ D (para)	$(1.4 \pm 0.6) \times 10^{14}$	9.7 ± 1.9	c-C ₃ H ₂ (para)	$(3.6 \pm 1.6) \times 10^{13}$	7.2 ± 3.0
NH ₂ D (ortho) ^c	$(3.3 \pm 0.8) \times 10^{14}$	9.7	A-CH ₃ CCH ^l	$(3.3 \pm 1.7) \times 10^{14}$	10.5 ± 7.0
CCH	$(3.5 \pm 0.4) \times 10^{15}$	11.2 ± 0.7	E-CH ₃ CCH ^m	$(2.9 \pm 1.9) \times 10^{14}$	9.2 ± 5.8
CCD ^d	$(1.3 \pm 1.1) \times 10^{14}$	11.2	A-CH ₃ CN ^l	$(7.9 \pm 3.2) \times 10^{12}$	9.4 ± 3.9
CN	$(1.2 \pm 0.2) \times 10^{15}$	9.0 ± 0.7	E-CH ₃ CN ^m	$(7.1 \pm 2.9) \times 10^{12}$	9.6 ± 4.5
¹³ CN ^e	$(2.7 \pm 0.6) \times 10^{13}$	9.0	H ₂ CCO (para)	$(6.1 \pm 5.8) \times 10^{13}$	6.5 ± 4.0
C ¹⁵ N ^e	$(9.2 \pm 3.6) \times 10^{12}$	9.0	H ₂ CCO (ortho) ⁿ	$(2.2 \pm 0.9) \times 10^{13}$	6.5
H ¹³ CN	$(5.8 \pm 1.1) \times 10^{13}$	9.1 ± 0.8	CH ₃ CHO	$(7.7 \pm 0.8) \times 10^{13}$	11.2 ± 2.4
HC ¹⁵ N ^f	$(1.2 \pm 0.3) \times 10^{13}$	9.1	HNCO	$(5.5 \pm 4.6) \times 10^{13}$	8.2 ± 5.8
DCN	$(3.6 \pm 0.8) \times 10^{13}$	8.1 ± 0.7	SiO ^o	$(8.8 \pm 2.0) \times 10^{13}$	18.2 ± 1.8
HN ¹³ C	$(2.4 \pm 1.4) \times 10^{13}$	6.9 ± 1.1	C ³⁴ S	$(1.2 \pm 0.3) \times 10^{14}$	17.6 ± 2.1
H ¹⁵ NC ^g	$(4.8 \pm 2.0) \times 10^{12}$	6.9	C ³³ S ^p	$(2.0 \pm 0.4) \times 10^{13}$	17.6
DNC ^g	$(2.4 \pm 0.9) \times 10^{13}$	6.9	¹³ CS ^p	$(3.1 \pm 0.7) \times 10^{13}$	17.6
C ¹⁷ O	$(1.2 \pm 0.2) \times 10^{16}$	20.0 ± 4.3	HCS ⁺	$(2.2 \pm 0.6) \times 10^{13}$	14.9 ± 2.7
C ¹⁸ O ^h	$(4.8 \pm 1.4) \times 10^{16}$	20.0	H ₂ CS (para)	$(4.5 \pm 0.9) \times 10^{13}$	18.1 ± 3.4
HC ¹⁸ O ⁺	$(4.3 \pm 1.3) \times 10^{12}$	8.1 ± 1.6	H ₂ CS (ortho)	$(1.2 \pm 0.2) \times 10^{14}$	20.5 ± 1.4
DCO ⁺ ⁱ	$(7.4 \pm 2.7) \times 10^{13}$	8.1	SO	$(5.0 \pm 0.7) \times 10^{14}$	17.6 ± 1.1
H ₂ CO (ortho)	$(3.7 \pm 2.4) \times 10^{14}$	33 ± 13	³³ SO ^q	$(1.1 \pm 0.9) \times 10^{13}$	17.6
H ₂ ¹³ CO (para) ^j	$(2.2 \pm 1.2) \times 10^{13}$	33	³⁴ SO ^q	$(4.3 \pm 1.0) \times 10^{13}$	17.6
HDCO ^j	$(1.0 \pm 0.6) \times 10^{13}$	33	C ₄ H	$(2.2 \pm 1.1) \times 10^{14}$	10.9 ± 3.3
D ₂ CO (ortho) ^j	$< 9.3 \times 10^{11}$	33	CCS	$(5.1 \pm 2.0) \times 10^{13}$	8.2 ± 1.8
CH ₃ OH (Cold) ^k	$(1.8 \pm 0.2) \times 10^{15}$	24.3 ± 2.6	OCS	$(2.4 \pm 0.6) \times 10^{14}$	16.0 ± 8.2
CH ₃ OH (Hot) ^k	$(3.4 \pm 1.2) \times 10^{14}$	122 ± 63	SO ₂	$(2.2 \pm 0.4) \times 10^{14}$	26.3 ± 5.2
c-C ₃ H ₂ (ortho)	$(1.0 \pm 0.5) \times 10^{14}$	7.4 ± 1.1	HC ₅ N	$(2.5 \pm 0.9) \times 10^{13}$	25.8 ± 4.6

^aObtained by a least-squares fit for multiple transitions. The error denotes 3σ .

^bAssumed source size and line width are $15''$ and 3 km s^{-1} , respectively.

^cThe rotation temperature is assumed to be the same as that of NH₂D (Para).

^dThe rotation temperature is assumed to be the same as that of CCH.

^eThe rotation temperature is assumed to be the same as that of CN.

^fThe rotation temperature is assumed to be the same as that of H¹³CN.

^gThe rotation temperature is assumed to be the same as that of HN¹³C.

^hThe rotation temperature is assumed to be the same as that of C¹⁷O.

ⁱThe rotation temperature is assumed to be the same as that of HC^{18}O^+ .

^jThe rotation temperature is assumed to be the same as that of H_2CO (ortho).

^kThe column densities and rotation temperatures are estimated with two component model. ‘Cold’ and ‘Hot’ indicate results for the low temperature component and the high temperature component, respectively.

^lThe column density and rotation temperature of A state are estimated from $K = 0$ lines.

^mThe column density and rotation temperature of E state are estimated from $K = 1$ lines.

ⁿThe rotation temperature is assumed to be the same as that of H_2CCO (ortho).

^oThe line width is assumed to be 6 km s^{-1} .

^pThe rotation temperature is assumed to be the same as that of C^{34}S .

^qThe rotation temperature is assumed to be the same as that of SO .

Table 6. Column Densities of Identified Molecules.^a

Molecule	N ($T=10$ K) ^b (cm^{-2}) ^c	N ($T=15$ K) ^b (cm^{-2}) ^c	N ($T=20$ K) ^b (cm^{-2}) ^c
HCO	$(3.8 \pm 1.6) \times 10^{13}$	$(5.0 \pm 2.1) \times 10^{13}$	$(6.8 \pm 2.8) \times 10^{13}$
N ₂ H ⁺	$(4.3 \pm 2.5) \times 10^{14}$	$(3.6 \pm 0.9) \times 10^{14}$	$(3.8 \pm 0.8) \times 10^{14}$
¹⁵ NNH ⁺	$(1.4 \pm 0.8) \times 10^{12}$	$(1.7 \pm 1.0) \times 10^{12}$	$(2.0 \pm 1.2) \times 10^{12}$
N ¹⁵ NH ⁺	$< 3.6 \times 10^{11}$	$< 4.3 \times 10^{11}$	$< 5.1 \times 10^{11}$
N ₂ D ⁺	$(7.8 \pm 2.2) \times 10^{12}$	$(9.2 \pm 2.5) \times 10^{12}$	$(1.1 \pm 0.3) \times 10^{13}$
NO	$(5.5 \pm 1.6) \times 10^{15}$	$(2.3 \pm 0.6) \times 10^{15}$	$(1.6 \pm 0.4) \times 10^{15}$
CH ₃ OCH ₃	$(5.2 \pm 2.4) \times 10^{13}$	$(5.8 \pm 2.5) \times 10^{13}$	$(6.6 \pm 2.8) \times 10^{13}$
NH ₂ CHO	$2.5^{+2.6}_{-2.5} \times 10^{12}$	$2.6^{+2.7}_{-2.6} \times 10^{12}$	$3.0^{+3.1}_{-3.0} \times 10^{12}$
HCO ₂ ⁺	$(5.6 \pm 4.7) \times 10^{12}$	$(6.2 \pm 5.1) \times 10^{12}$	$(7.5 \pm 6.2) \times 10^{12}$
NS	$(7.7 \pm 2.9) \times 10^{13}$	$(9.1 \pm 3.4) \times 10^{13}$	$(1.1 \pm 0.4) \times 10^{14}$
SO ⁺	$(7.6 \pm 6.6) \times 10^{13}$	$(9.0 \pm 7.8) \times 10^{13}$	$(1.1 \pm 0.9) \times 10^{14}$
HC ₃ N	$(5.4 \pm 2.6) \times 10^{14}$	$(1.6 \pm 0.3) \times 10^{14}$	$(1.2 \pm 0.1) \times 10^{14}$
H ¹³ CCCN	$(3.5 \pm 2.7) \times 10^{12}$	$(1.9 \pm 1.5) \times 10^{12}$	$(1.6 \pm 1.2) \times 10^{12}$
HC ¹³ CCN	$(5.4 \pm 3.8) \times 10^{12}$	$(2.5 \pm 1.7) \times 10^{12}$	$(1.8 \pm 1.3) \times 10^{12}$
HCC ¹³ CN	$(6.5 \pm 4.2) \times 10^{12}$	$(3.0 \pm 1.9) \times 10^{12}$	$(2.2 \pm 1.4) \times 10^{12}$
DC ₃ N	$(6.8 \pm 5.5) \times 10^{12}$	$(2.8 \pm 2.3) \times 10^{12}$	$(2.0 \pm 1.6) \times 10^{12}$
HCOOCH ₃	$(3.3 \pm 1.2) \times 10^{14}$	$(2.6 \pm 0.9) \times 10^{14}$	$(2.6 \pm 0.9) \times 10^{14}$
C ₃ S	$(1.8 \pm 0.6) \times 10^{13}$	$(7.8 \pm 2.4) \times 10^{12}$	$(5.2 \pm 1.6) \times 10^{12}$

^aErrors of the column densities are estimated by taking into account the r.m.s. noise and calibration uncertainties of the chopper-wheel method (20 %). The source size is assumed to be 15''.

^bAssumed excitation temperatures.

^cThe upper limit to the column density is estimated from the 3σ upper limit of the integrated intensity assuming the line width of 2 km/s.

Table 7: Deuterium fractionation ratios.

Molecule	NGC 2264 CMM3	L134 N	IRAS 16293
DCO ⁺ /HCO ⁺	0.030 ± 0.015 ^a	0.18 ^f	0.0086 ^h
N ₂ D ⁺ /N ₂ H ⁺	0.026 ± 0.010 ^b	0.35 ^f	
DCN/HCN	0.010 ± 0.003 ^c	0.050 ± 0.016 ^g	0.013 ^h
DNC/HNC	0.017 ± 0.012 ^c	0.047 ± 0.020 ^g	0.03 ^h
CCD/CCH	0.037 ± 0.032	0.060 ± 0.040 ^g	0.18 ^h
DC ₃ N/HC ₃ N	0.016 ± 0.013 ^b		
HDCO/H ₂ CO	0.0020 ± 0.0015 ^d	0.068 ^f	0.14 ^h
D ₂ CO/H ₂ CO	< 0.0003 ^{de}		0.05 ± 0.025 ⁱ

^aThe column density of the normal molecule is estimated from the ¹⁸O isotopologue assuming that ¹⁶O/¹⁸O = 560.

^bThe column density is estimated under the LTE approximation with T_{ex} of 15 K.

^cThe column density of the normal molecule is estimated from the ¹³C isotopologue assuming that ¹²C/¹³C = 60.

^dThe column density of the normal molecule is estimated from the H₂¹³CO (para) data assuming that the ortho to para is 3 and the ¹²C/¹³C ratio of 60.

^eThe column density of the D₂CO is estimated from the D₂CO (ortho) data assuming that the ortho to para ratio is 2.

^fTiné et al. (2000)

^gTurner (2001)

^hvan Dishoeck et al. (1995)

ⁱParise et al. (2006)

Table 8. Column Densities Observed in NGC 2264 CMM3 and Orion KL.

Molecule	NGC 2264 CMM3 N (cm ⁻²)	Orion KL ^a N (cm ⁻²)	References ^b
H ₂ CO	$(5.2 \pm 2.8) \times 10^{15}$	4.3×10^{16} ^{gh}	Neill et al. (2013)
CH ₃ OH	$(2.1 \pm 0.2) \times 10^{15}$ ^c	1.1×10^{18} ^{gh}	Kolesniková et al. (2014)
CH ₃ CN	$(1.5 \pm 0.4) \times 10^{13}$	1.2×10^{16} ^{gh}	Bell et al. (2014)
CH ₃ CHO	$(7.7 \pm 0.8) \times 10^{13}$	2.8×10^{14} ^g	Turner (1991)
CH ₃ OCH ₃	$(5.8 \pm 2.5) \times 10^{13}$ ^d	9.0×10^{15} ^g	Comito et al. (2005)
HNCO	$(5.5 \pm 4.6) \times 10^{13}$	$(5.7 \pm 0.5) \times 10^{15}$ ^e	Marcelino et al. (2009)
SiO	$(8.8 \pm 2.0) \times 10^{13}$	$(7.1 \pm 1.1) \times 10^{15}$ ^e	Tercero et al. (2011)
C ³⁴ S	$(1.2 \pm 0.3) \times 10^{14}$	$(8.3 \pm 1.3) \times 10^{14}$ ^e	Tercero et al. (2010)
H ₂ CS	$(1.7 \pm 0.2) \times 10^{14}$	$(5.0 \pm 0.5) \times 10^{15}$ ^e	Tercero et al. (2010)
SO	$(5.0 \pm 0.7) \times 10^{14}$	$(5.4 \pm 1.0) \times 10^{16}$ ^e	Esplugues et al. (2013a)
HC ₃ N	$(1.6 \pm 0.3) \times 10^{14}$ ^d	$(2.1 \pm 0.3) \times 10^{15}$ ^f	Esplugues et al. (2013b)
HCOOCH ₃	$(2.6 \pm 0.9) \times 10^{14}$ ^d	2.9×10^{17} ^{fgh}	Carvajal et al. (2009), Haykal et al. (2014)
CCS	$(5.1 \pm 2.0) \times 10^{13}$	$(3.3 \pm 0.6) \times 10^{13}$ ^e	Tercero et al. (2010)
OCS	$(2.4 \pm 0.6) \times 10^{14}$	$(6.0 \pm 1.0) \times 10^{16}$ ^e	Tercero et al. (2010)
SO ₂	$(2.2 \pm 0.4) \times 10^{14}$	$(1.9 \pm 0.5) \times 10^{17}$ ^e	Esplugues et al. (2013a)
C ₃ S	$(7.8 \pm 2.4) \times 10^{12}$ ^d	$(8.8 \pm 0.2) \times 10^{12}$ ^e	Tercero et al. (2010)
HC ₅ N	$(2.5 \pm 0.9) \times 10^{13}$	$(3.9 \pm 0.9) \times 10^{13}$ ^f	Esplugues et al. (2013b)

^aAveraged column densities are estimated with the assumption of the source diameter of 15".

^bReferences for Orion KL.

^cThe column density is estimated by summing the column density of cold and hot component.

^dThe column density is estimated under the LTE approximation with $T_{\text{ex}} = 15$ K.

^eFollowing the method described by Fuente et al. (2014), we estimate the averaged column density N by summing up the column densities of extended ridge (N_{er}), compact ridge (N_{cr}), plateau (N_{p}), and hot core (N_{hc}). A filling factor of 0.44 is assumed only for the hot core, since Tercero et al. (2010), Esplugues et al. (2013a) and Marcelino et al. (2009) assumed the source diameter of the hot core to be 10" and the source size of other components to be larger than 15". Namely, $N = N_{\text{er}} + N_{\text{cr}} + N_{\text{p}} + 0.44 \times N_{\text{hc}}$.

^fFollowing the method described by Fuente et al. (2014), we estimate the averaged column density N by summing up column densities of extended ridge (N_{er}), compact ridge (N_{cr}), plateau (N_{p}), outer hot core (N_{ohc}), and inner hot core (N_{ihc}). A filling factor of 0.44 and 0.22 is assumed for the outer hot core and the inner hot core, respectively, since Esplugues et al. (2013b) assumed the source diameter of outer hot core and inner hot core to be 10" and 7", respectively. Namely, $N = N_{\text{er}} + N_{\text{cr}} + N_{\text{p}} + 0.44 \times N_{\text{ohc}} + 0.22 \times N_{\text{ihc}}$.

^gEstimated from ^{13}C bearing species with assumption that $^{12}\text{C}/^{13}\text{C} = 50$.

^hThe column density estimated by Fuente et al. (2014).

A. Expanded Spectra

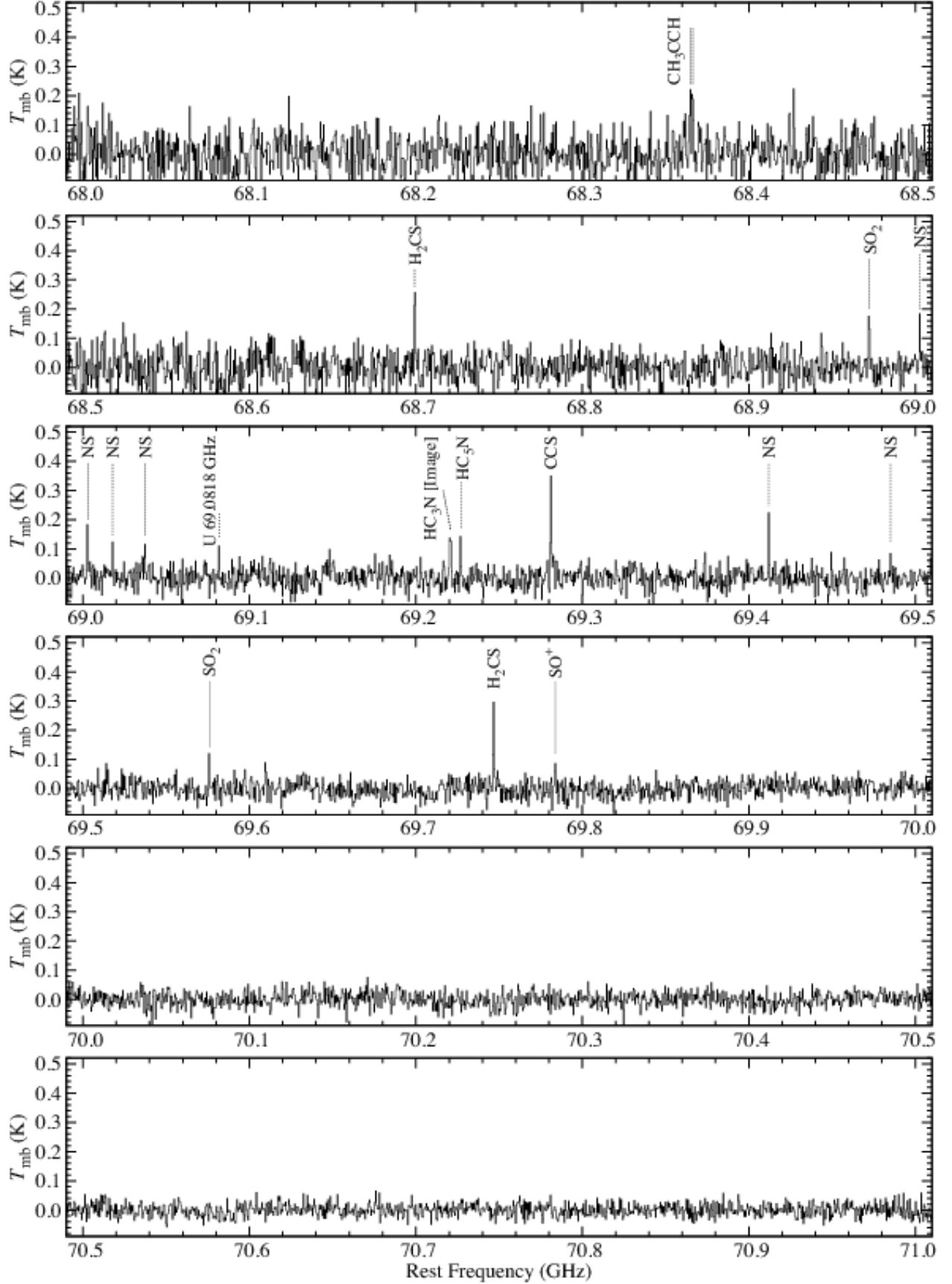


Fig. A.1.— Spectra of NGC 2264 CMM3 in the 3 and 4 mm band. The frequency resolution is 0.5 MHz. The T_{mb} is in units of mJy beam $^{-1}$ K.

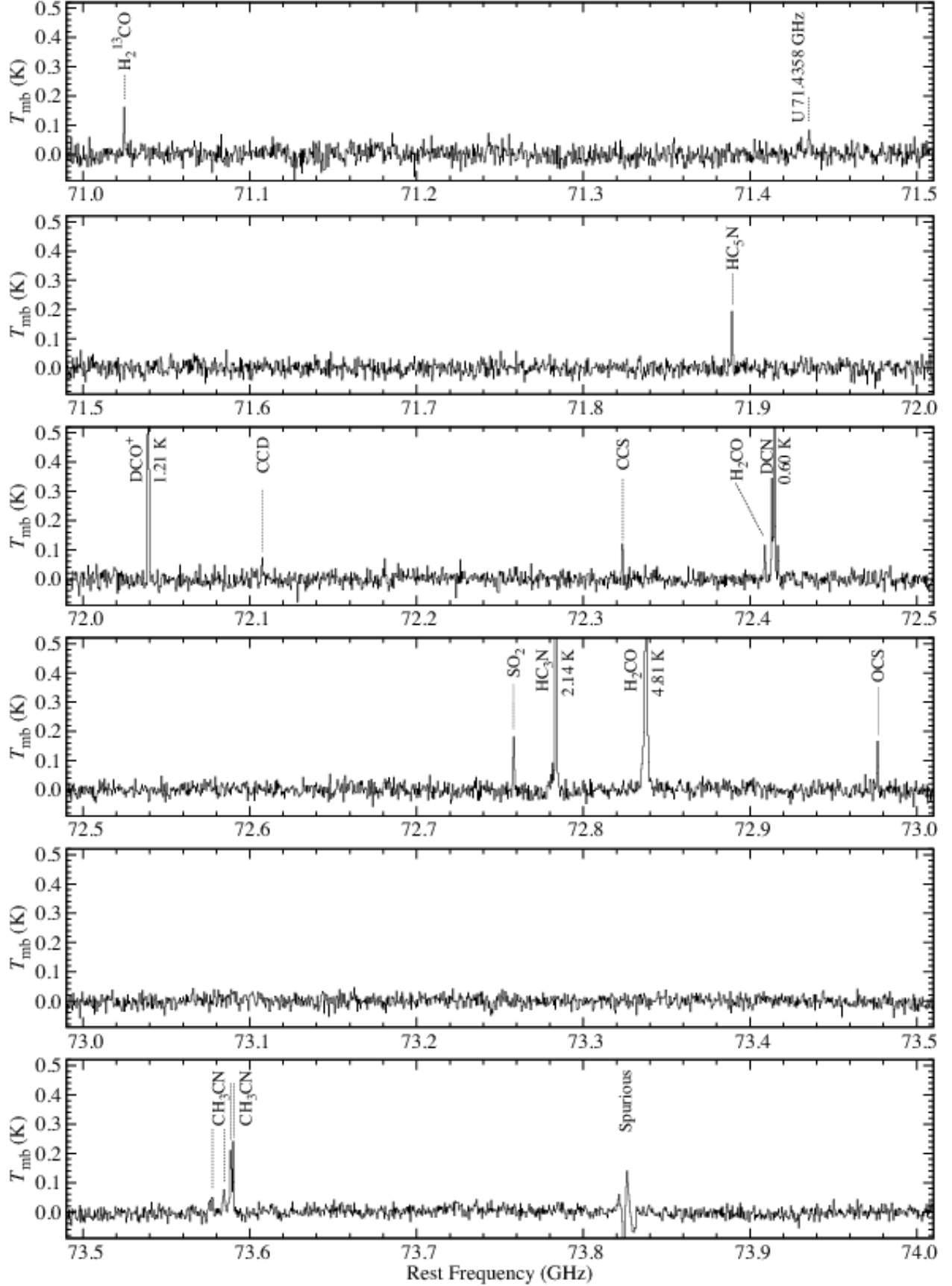


Fig. A.1.— *Continued*

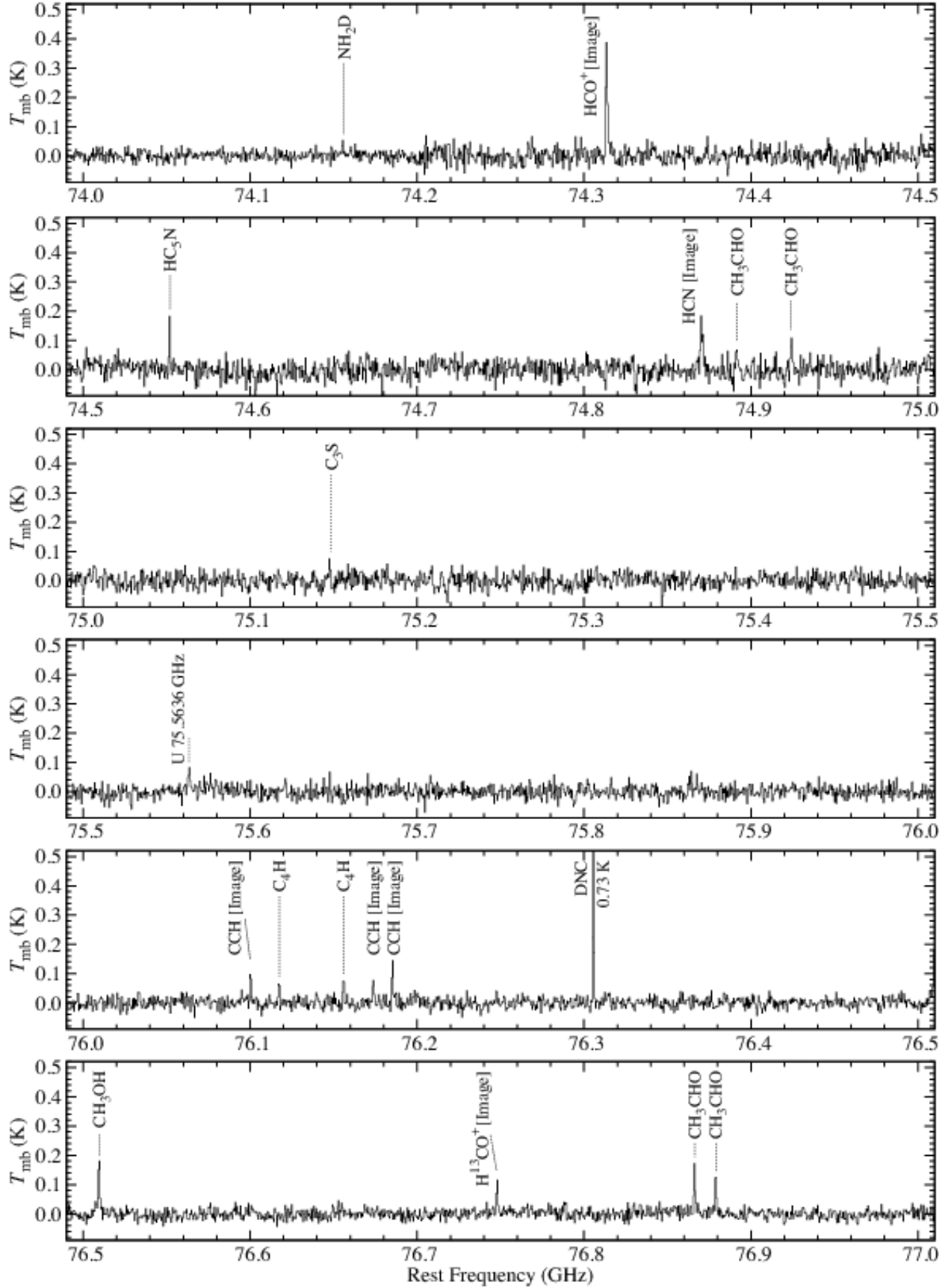


Fig. A.1.— *Continued*

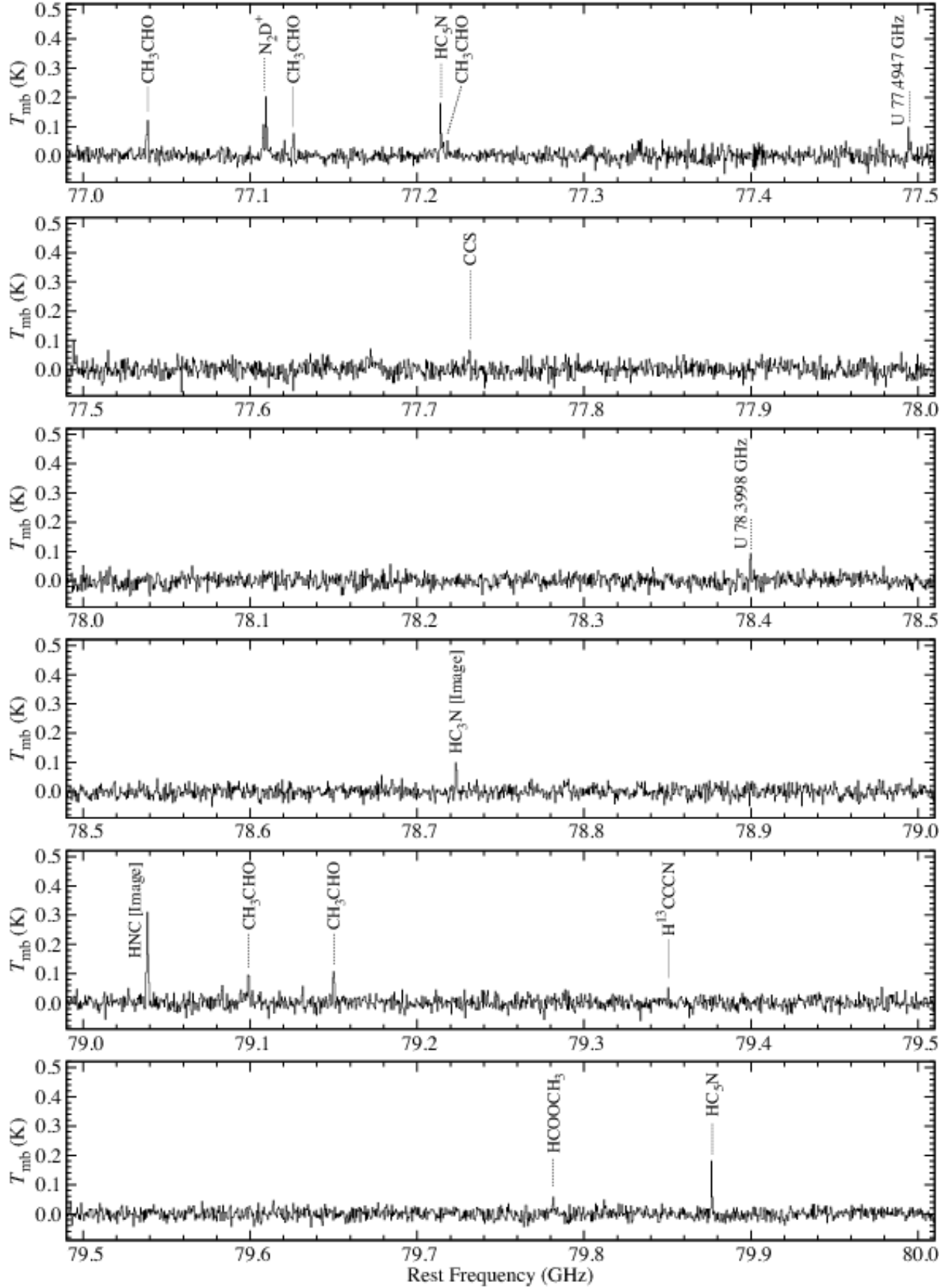


Fig. A.1.— *Continued*

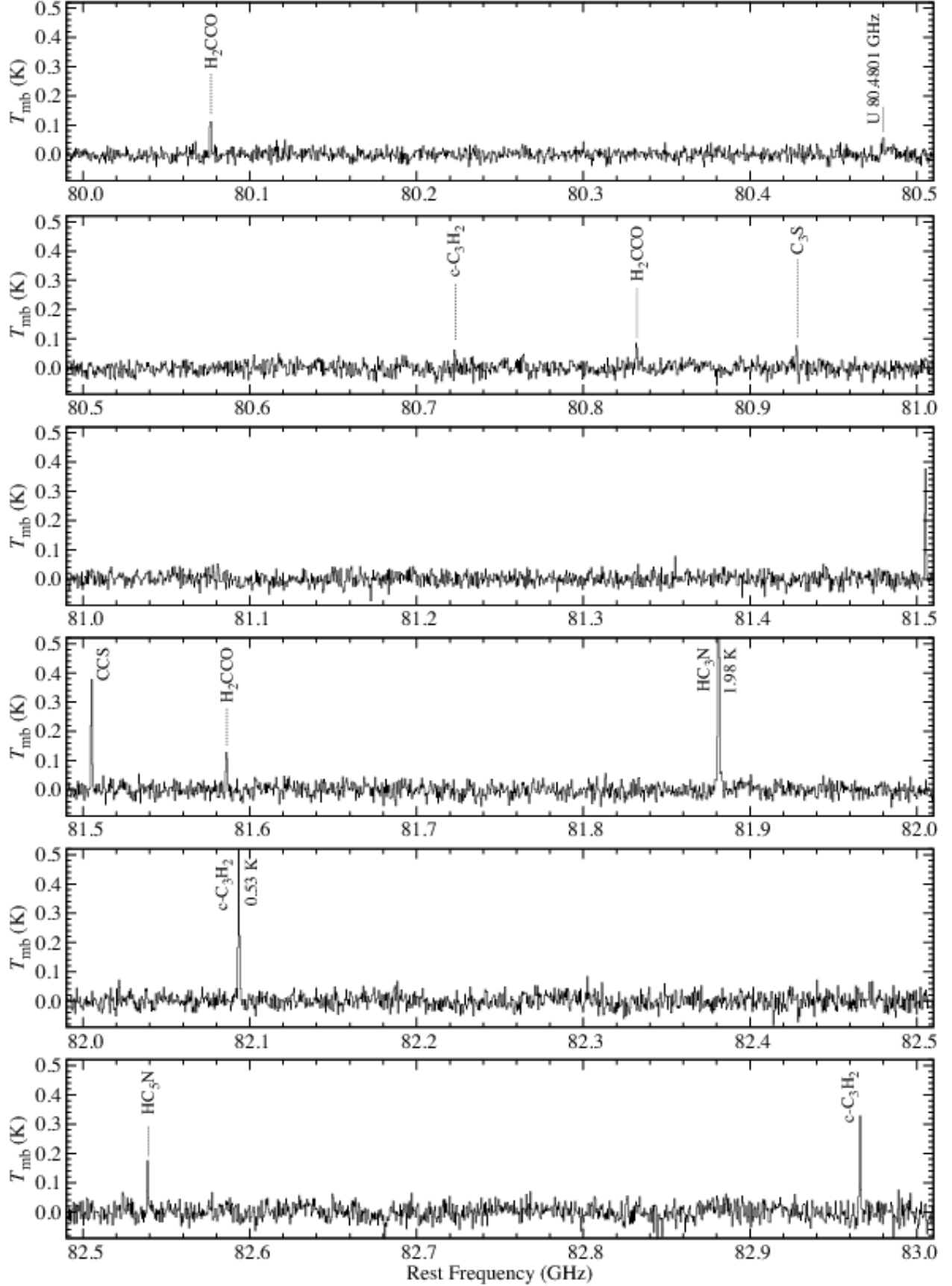


Fig. A.1.— *Continued*

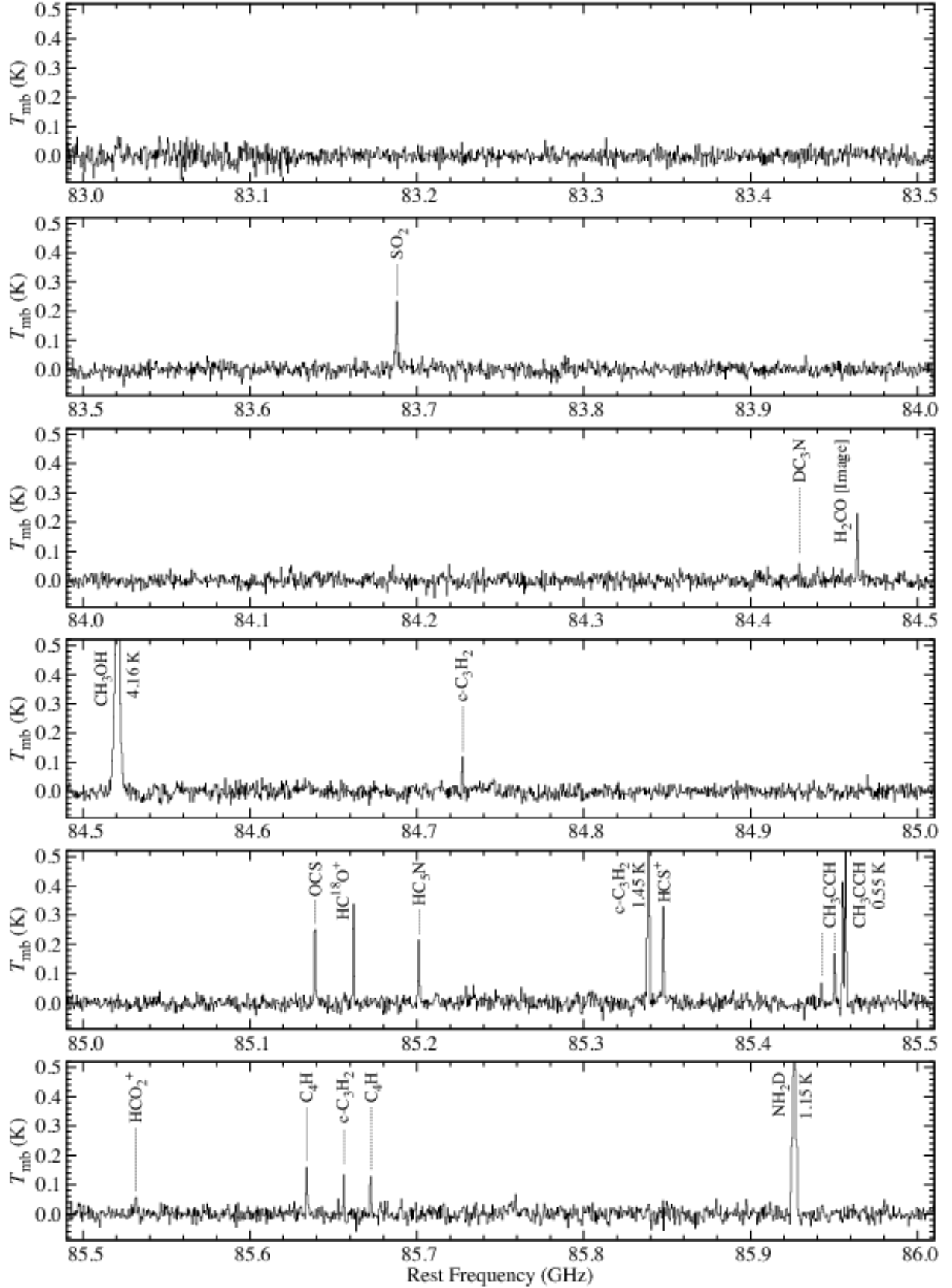


Fig. A.1.— *Continued*

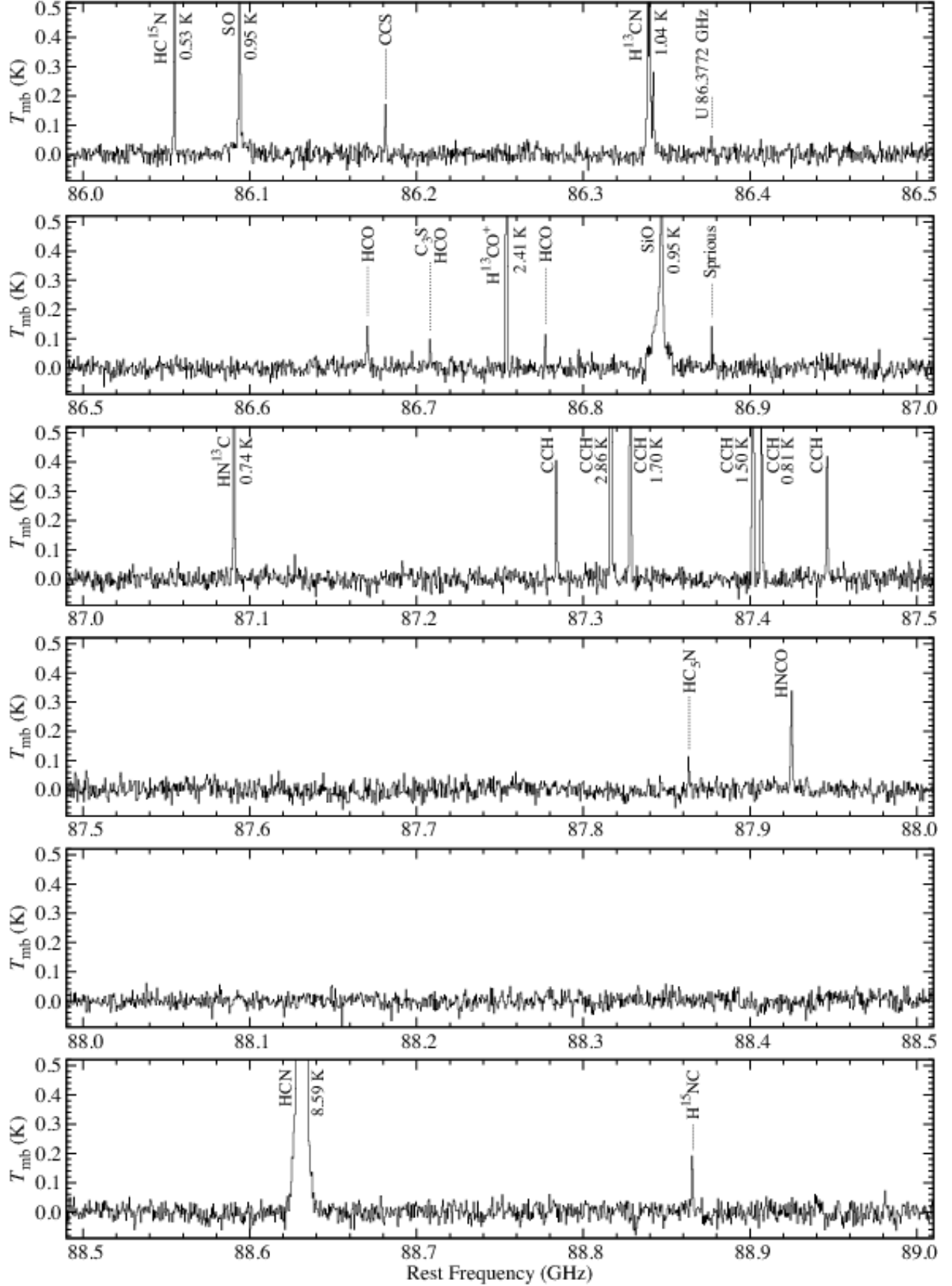


Fig. A.1.— *Continued*

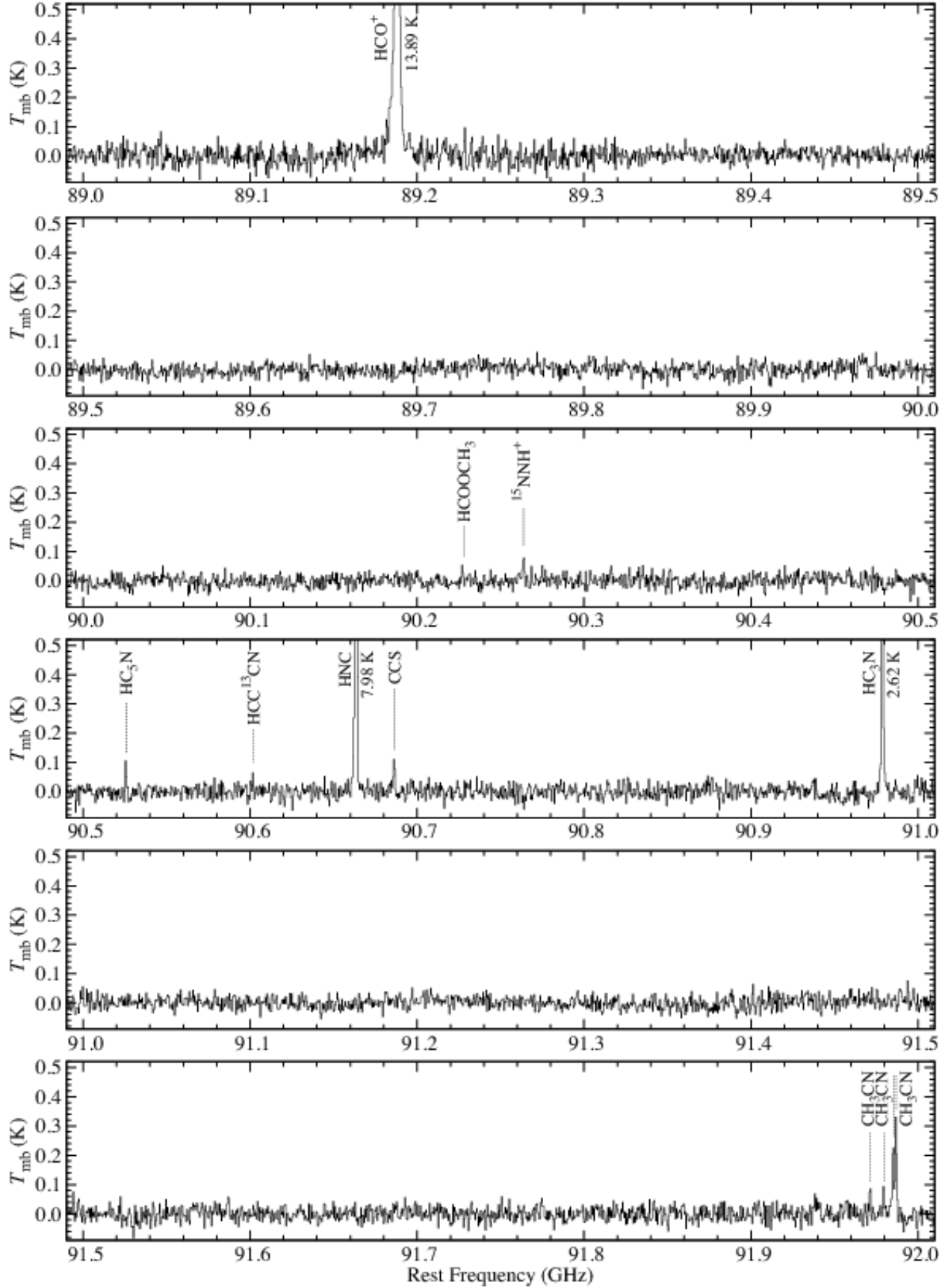


Fig. A.1.— *Continued*

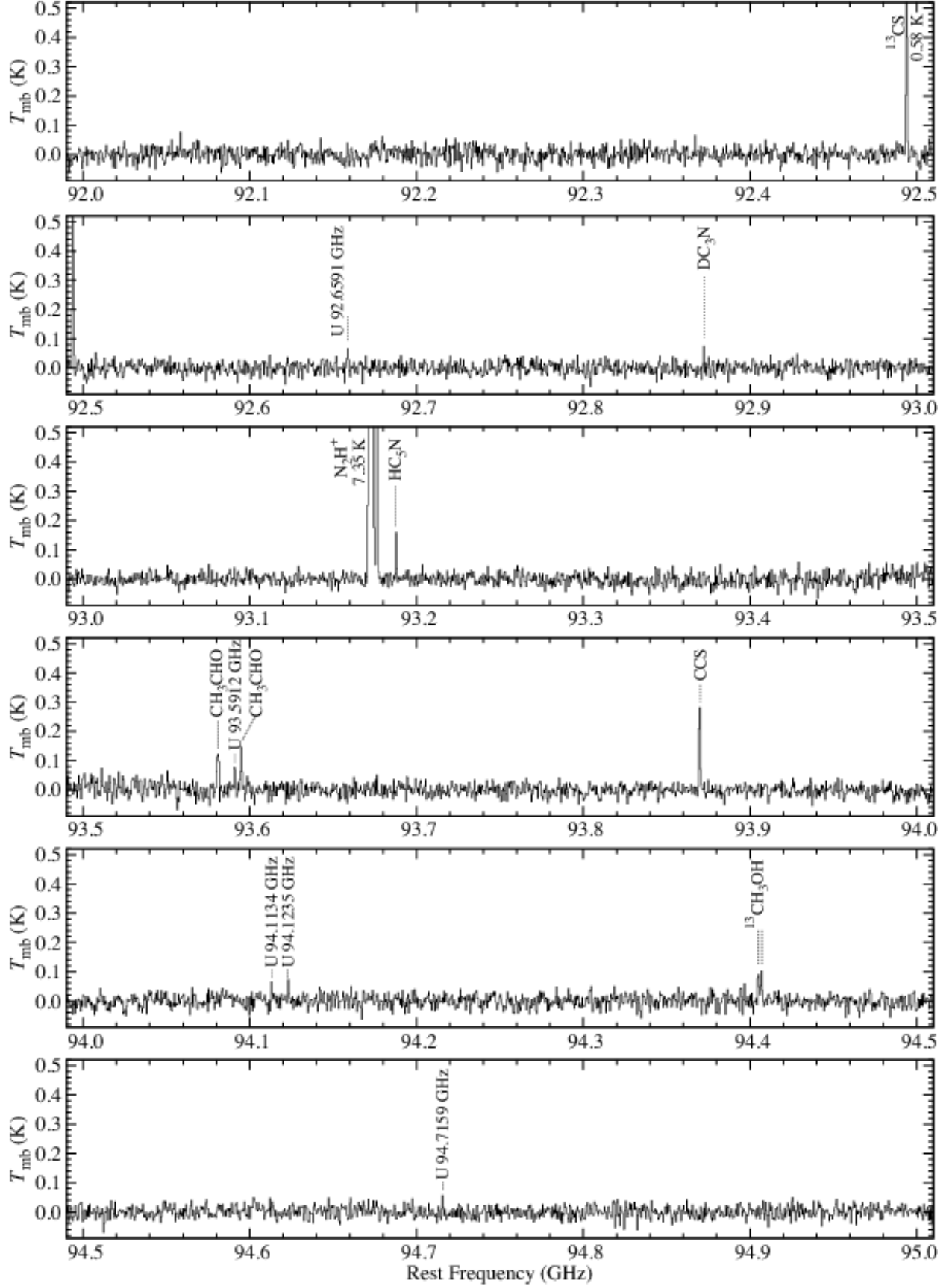


Fig. A.1.— *Continued*

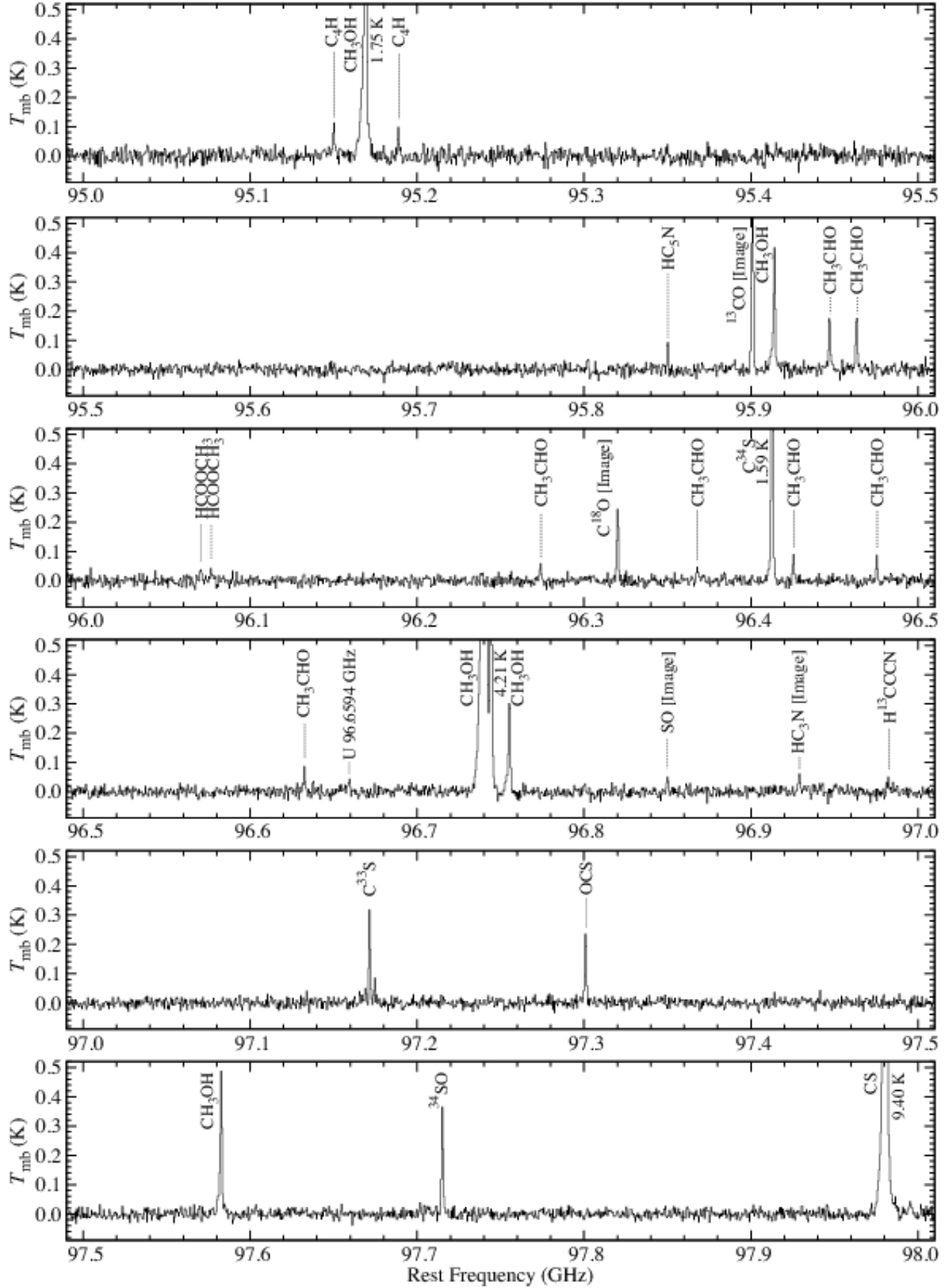


Fig. A.1.— *Continued*

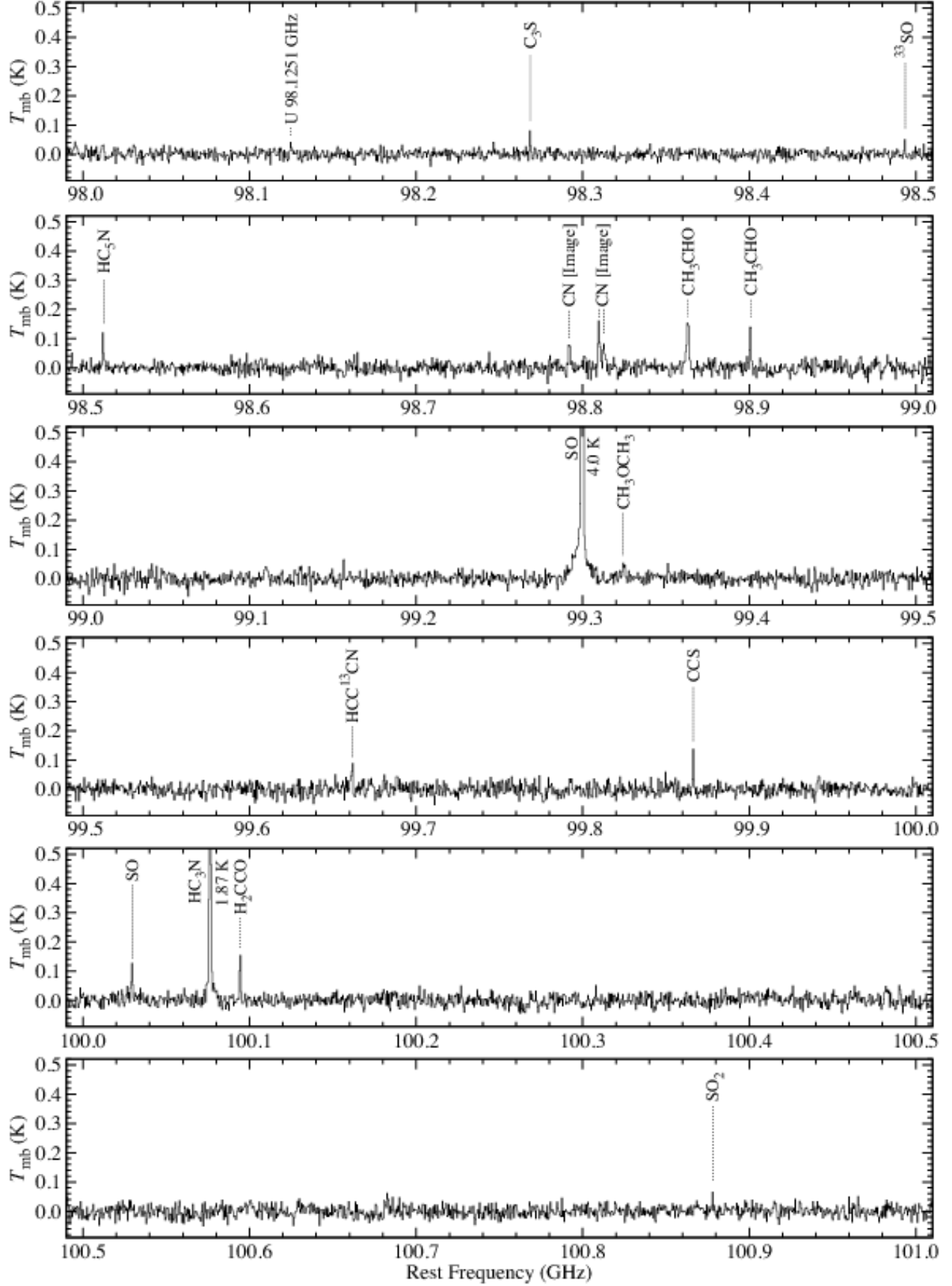


Fig. A.1.— *Continued*

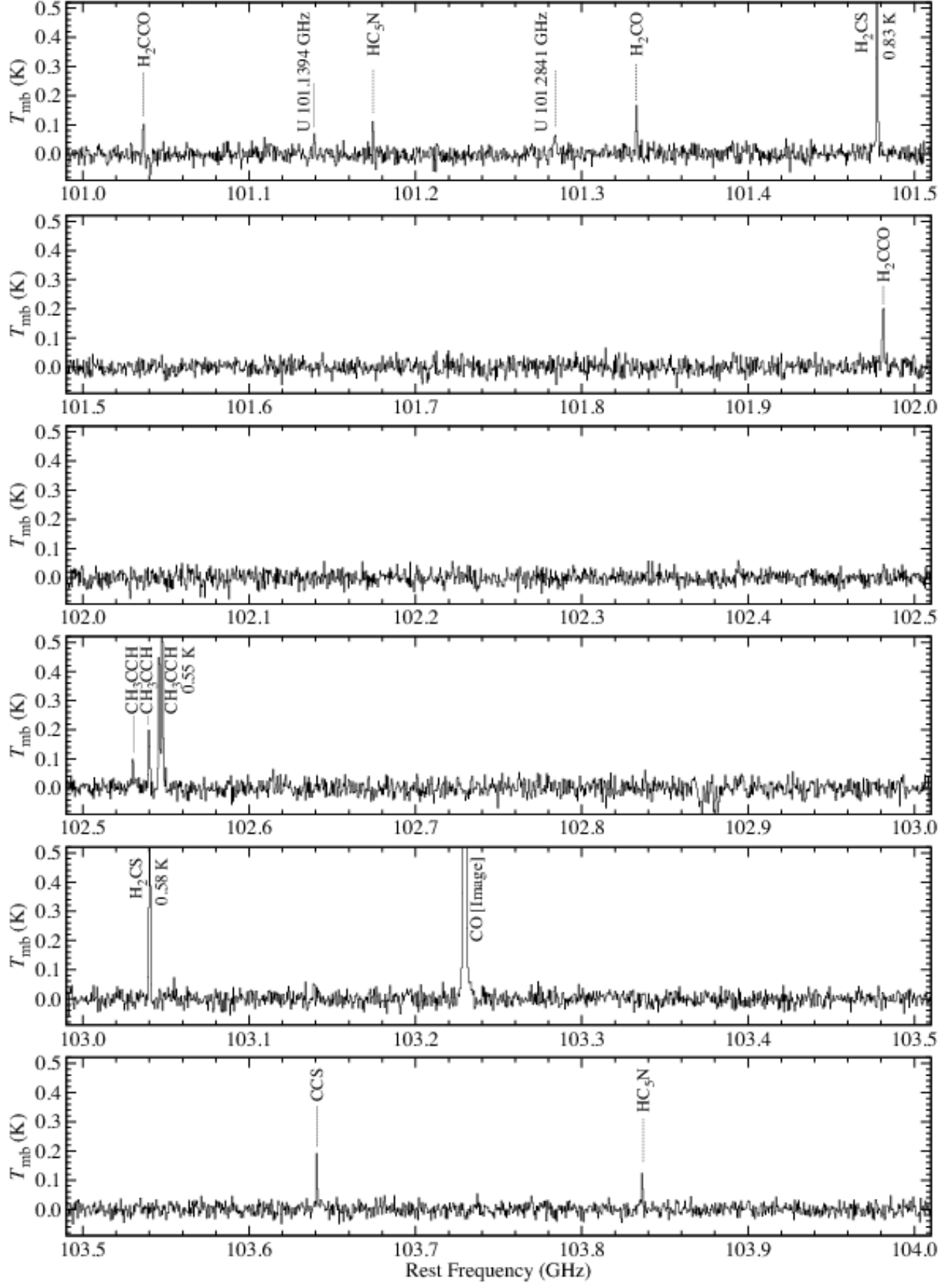


Fig. A.1.— *Continued*

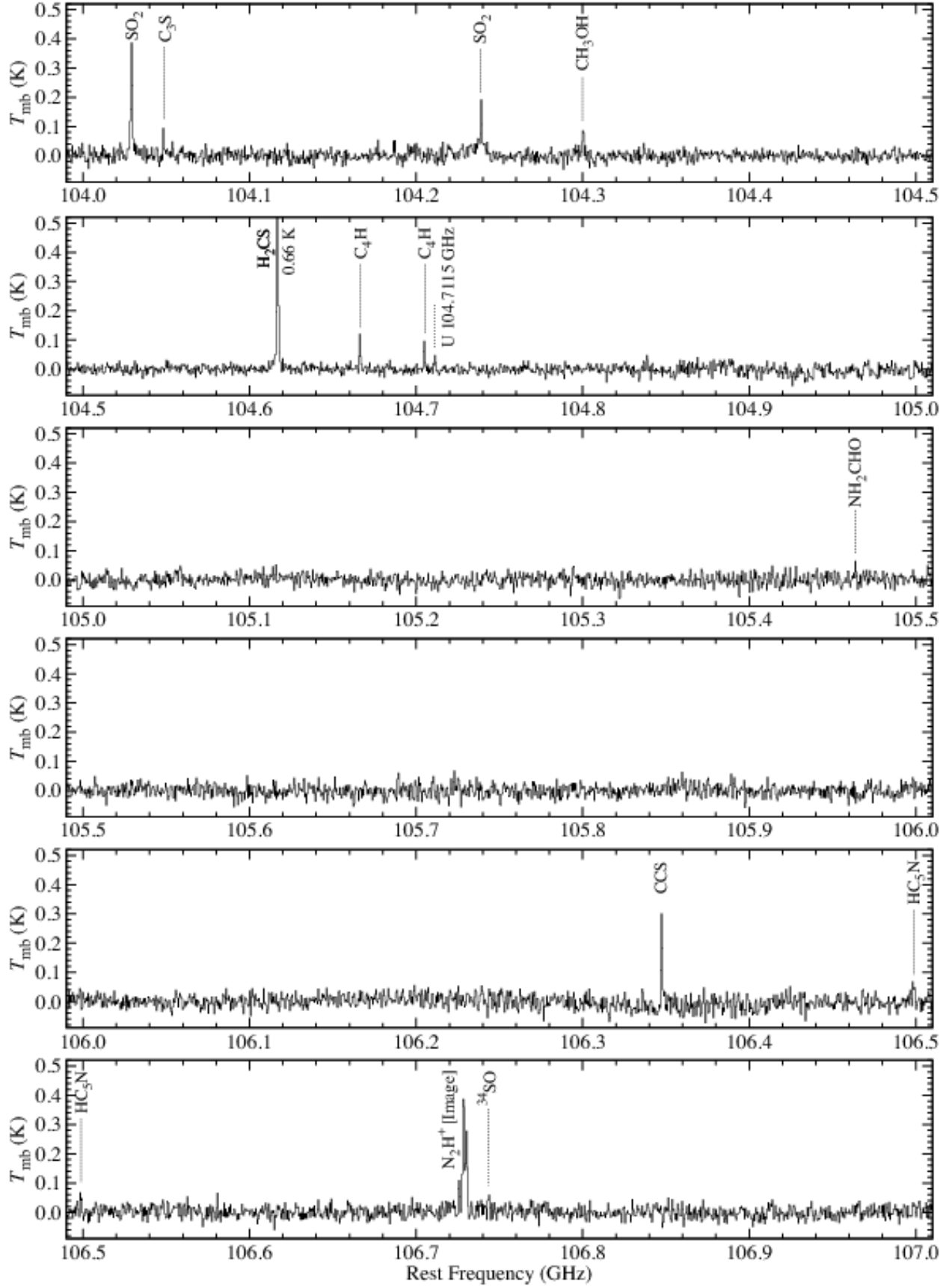


Fig. A.1.— *Continued*

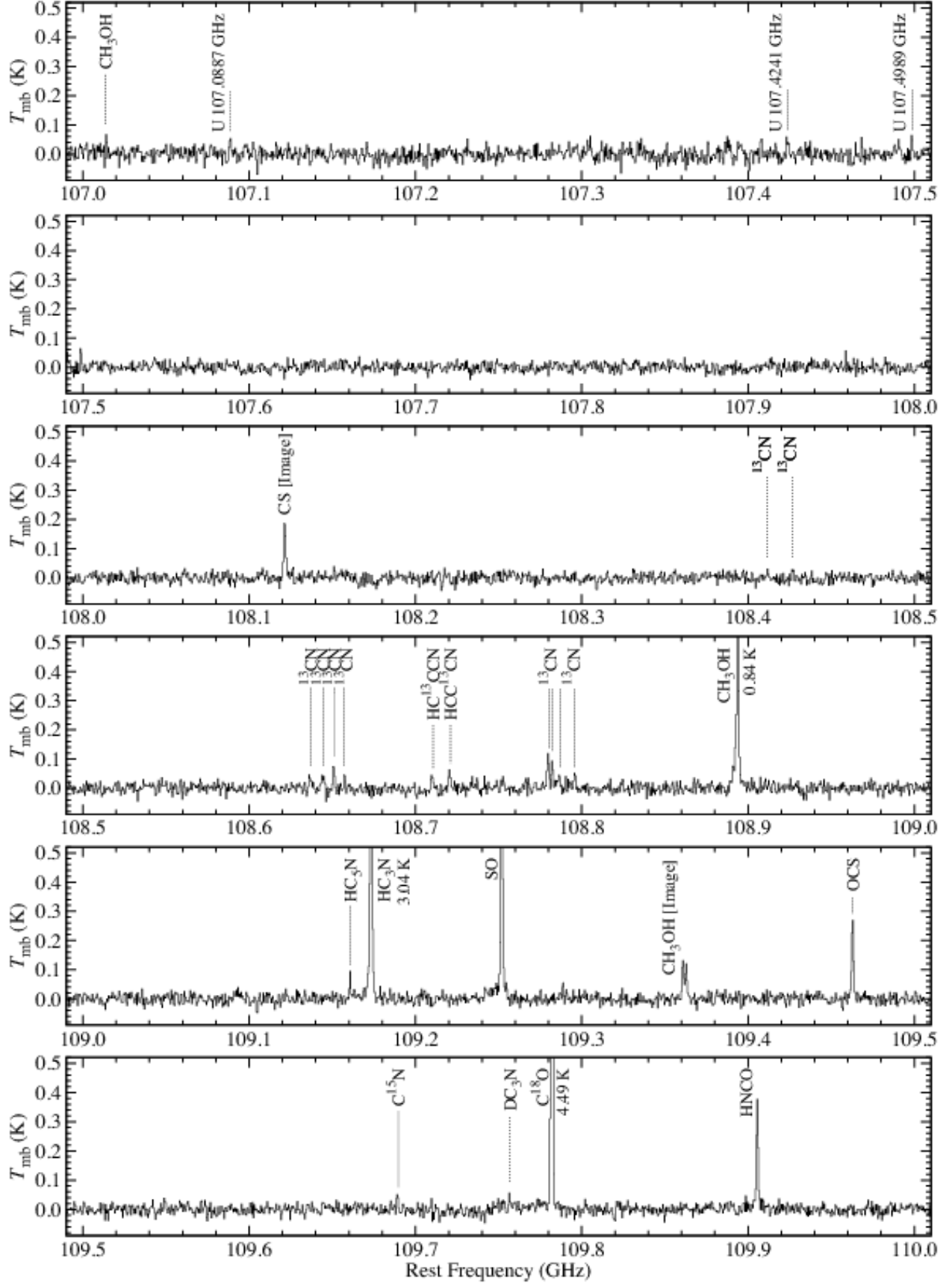


Fig. A.1.— *Continued*

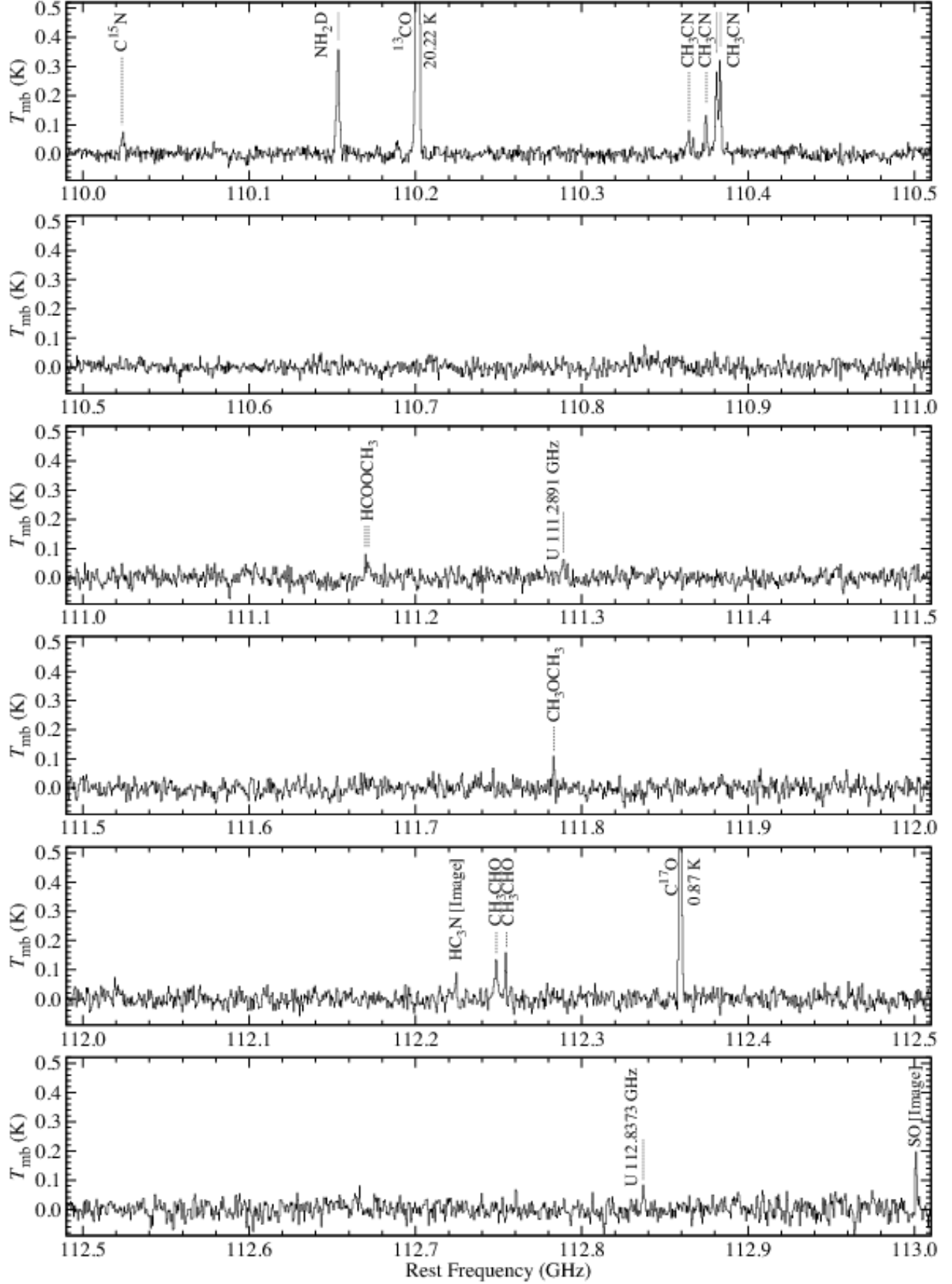


Fig. A.1.— *Continued*

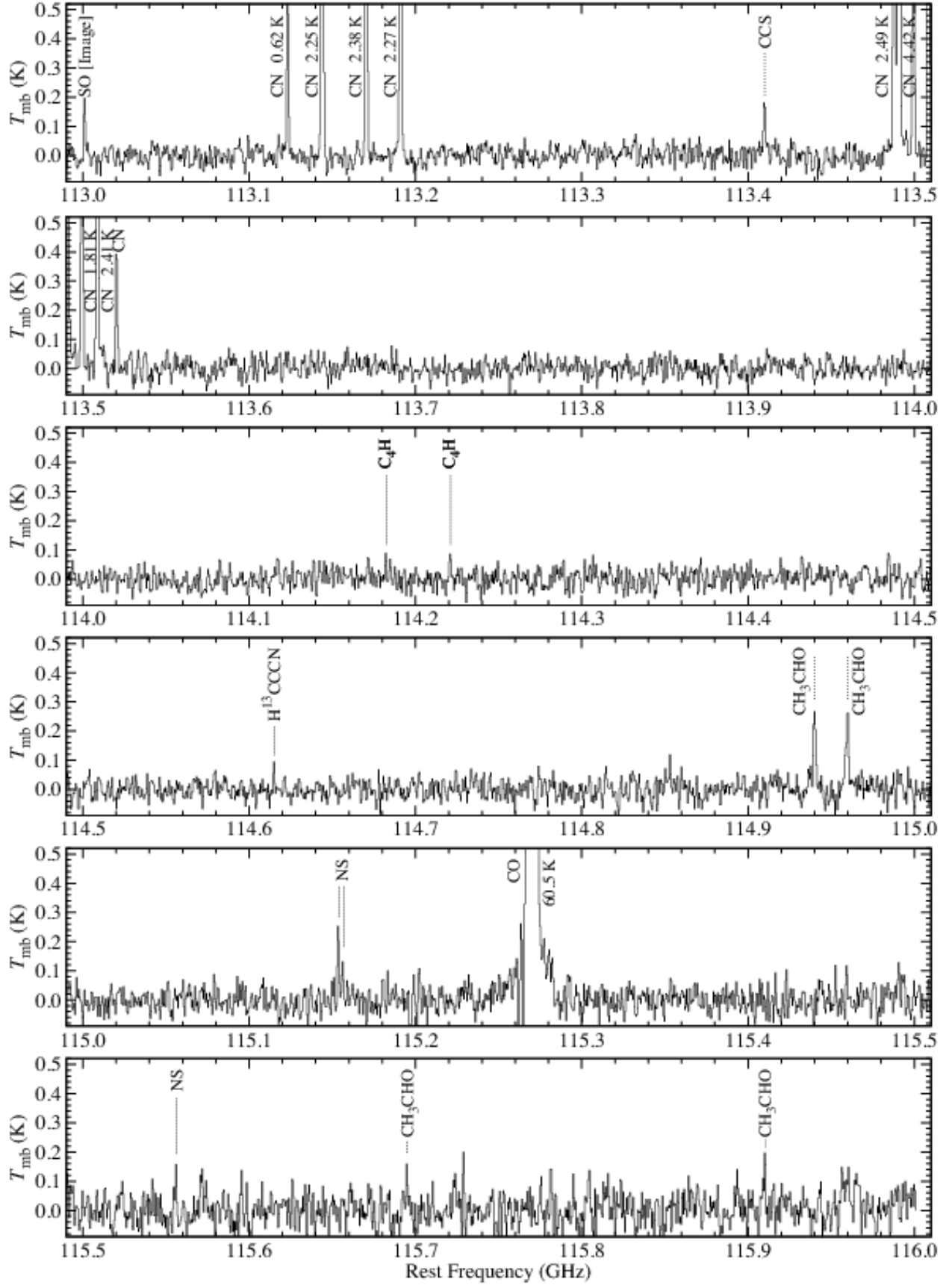


Fig. A.1.— *Continued*

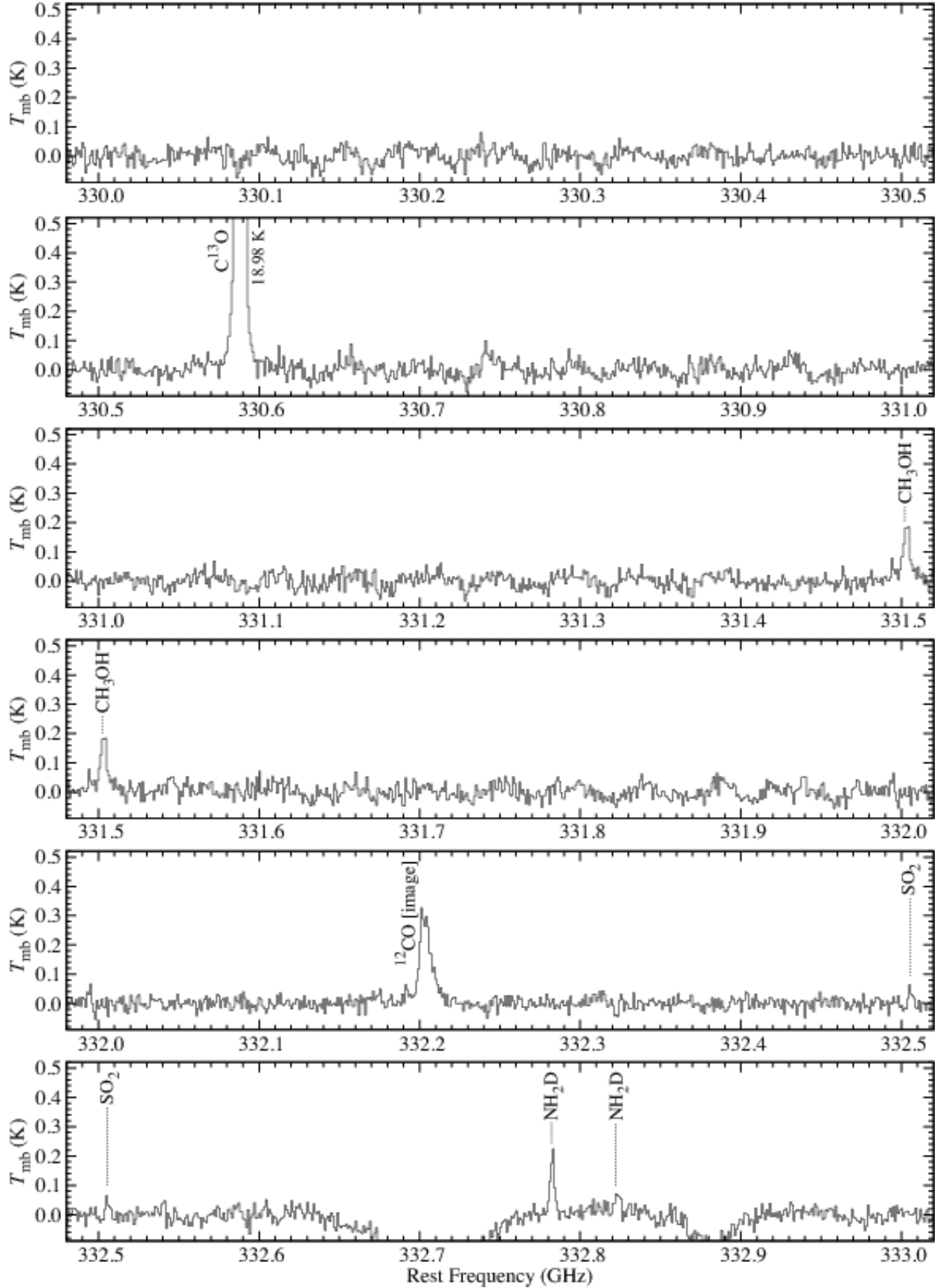


Fig. A.2.— Spectra of NGC 2264 CMM3 in the 0.8 mm band. The frequency resolution is

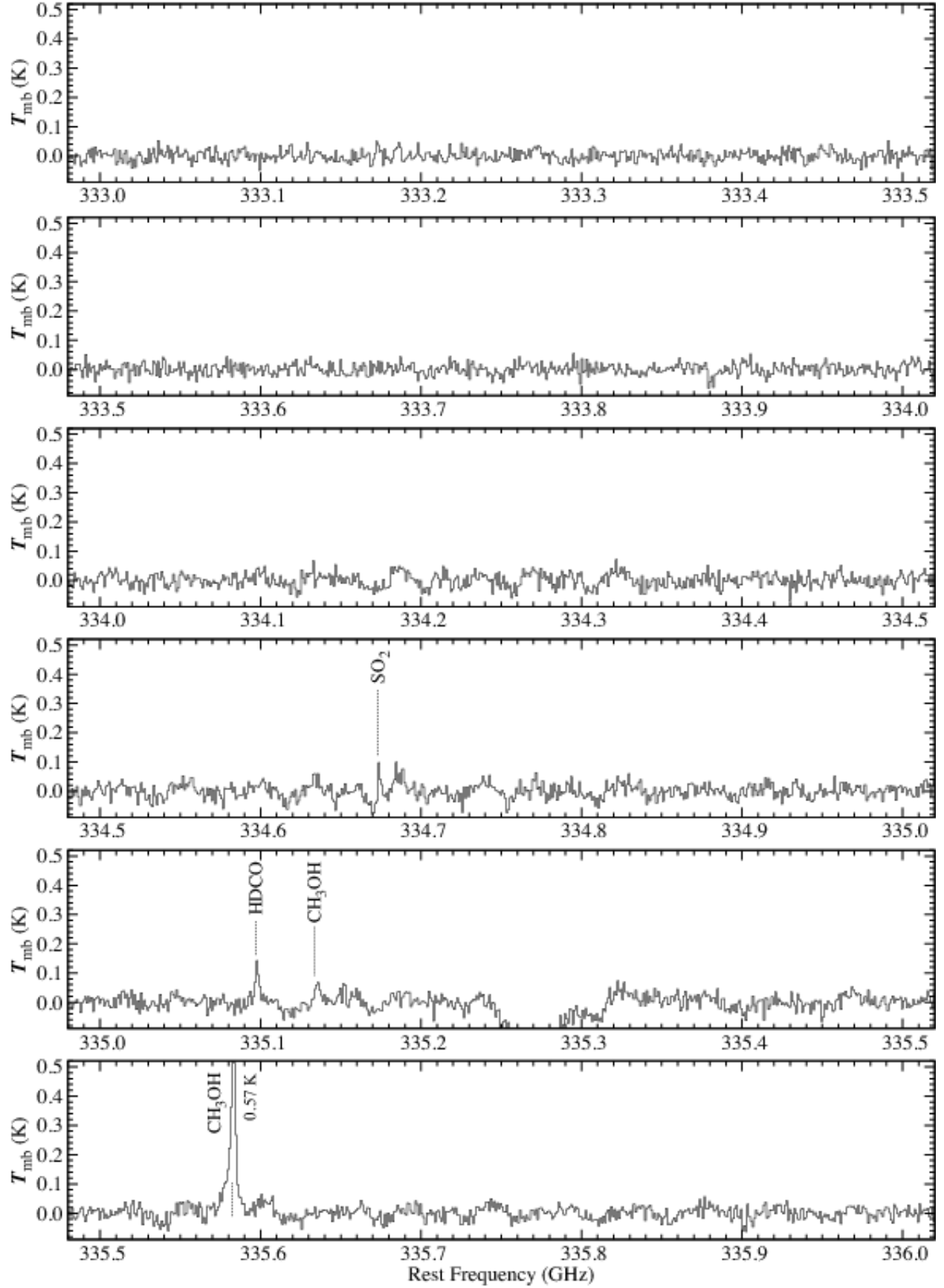


Fig. A.2.— *Continued*

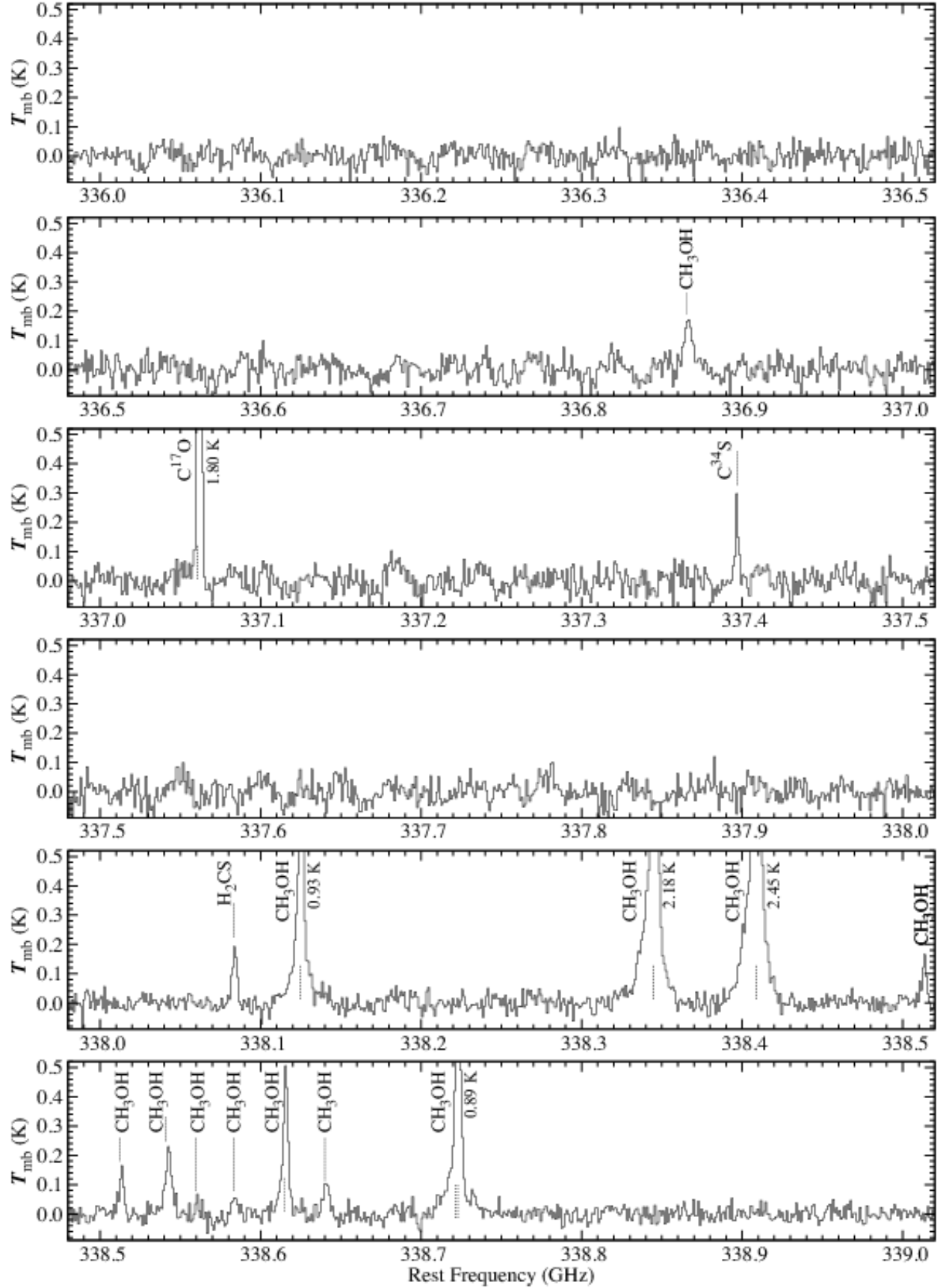


Fig. A.2.— *Continued*

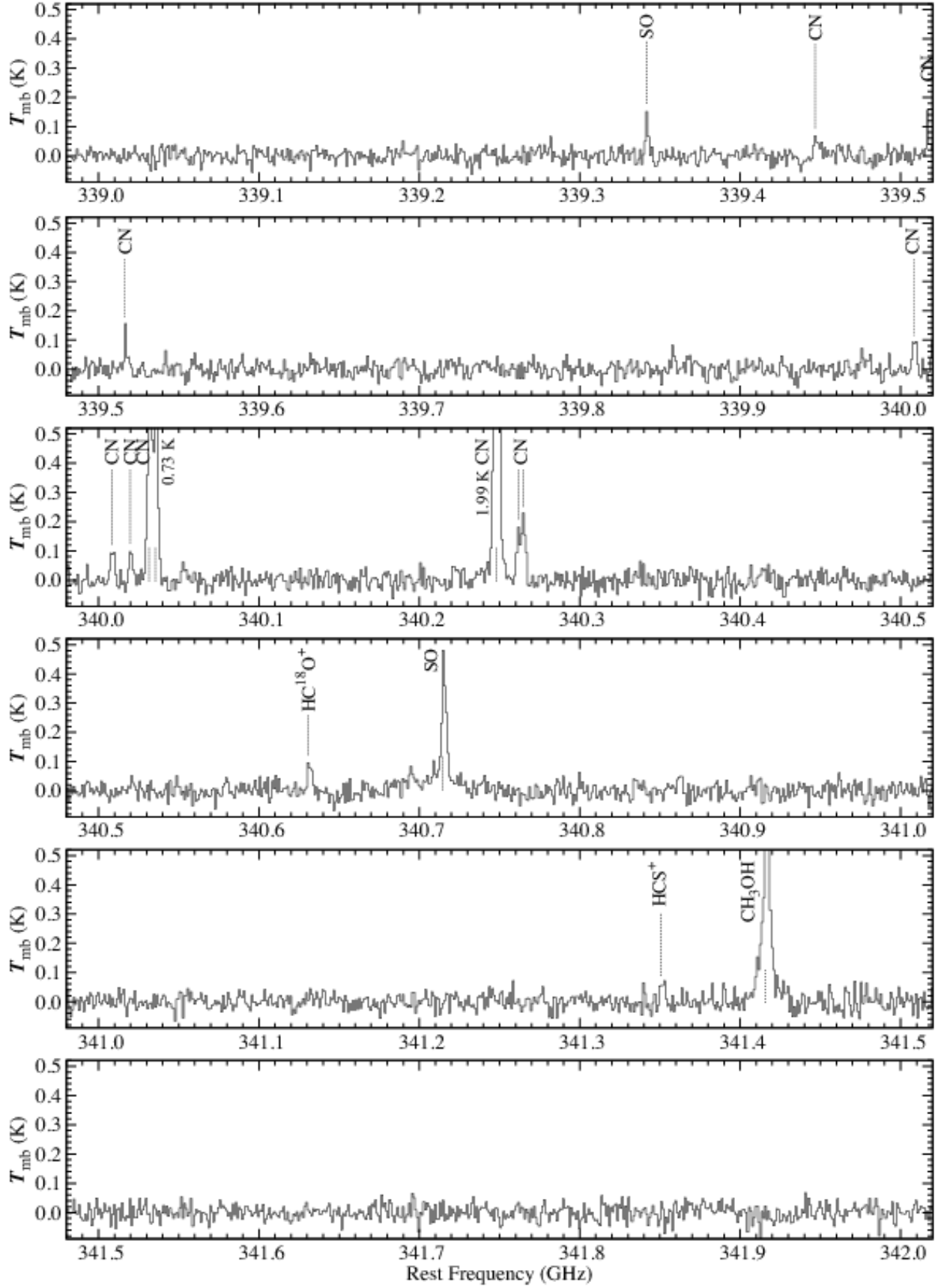


Fig. A.2.— *Continued*

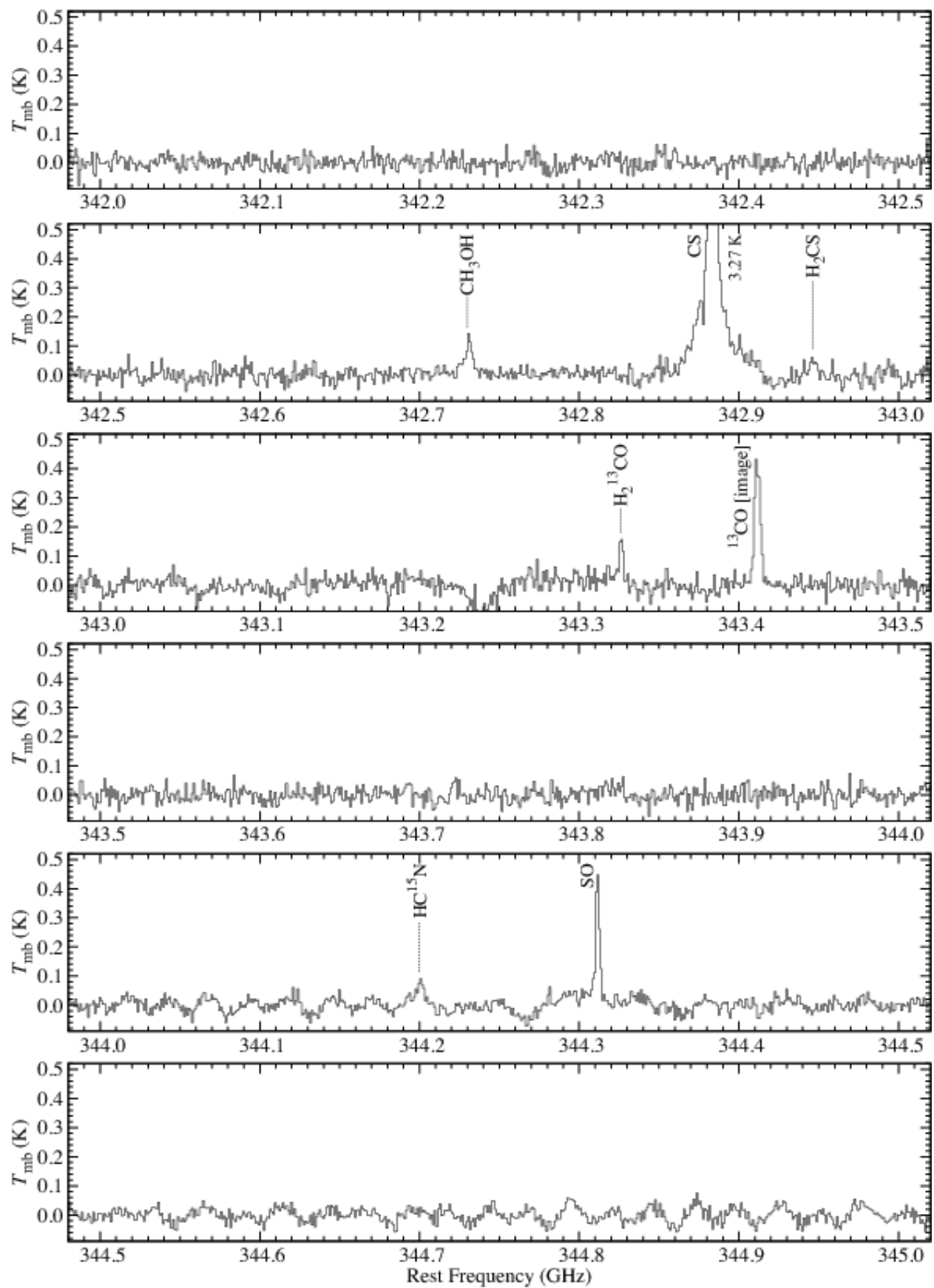


Fig. A.2.— *Continued*

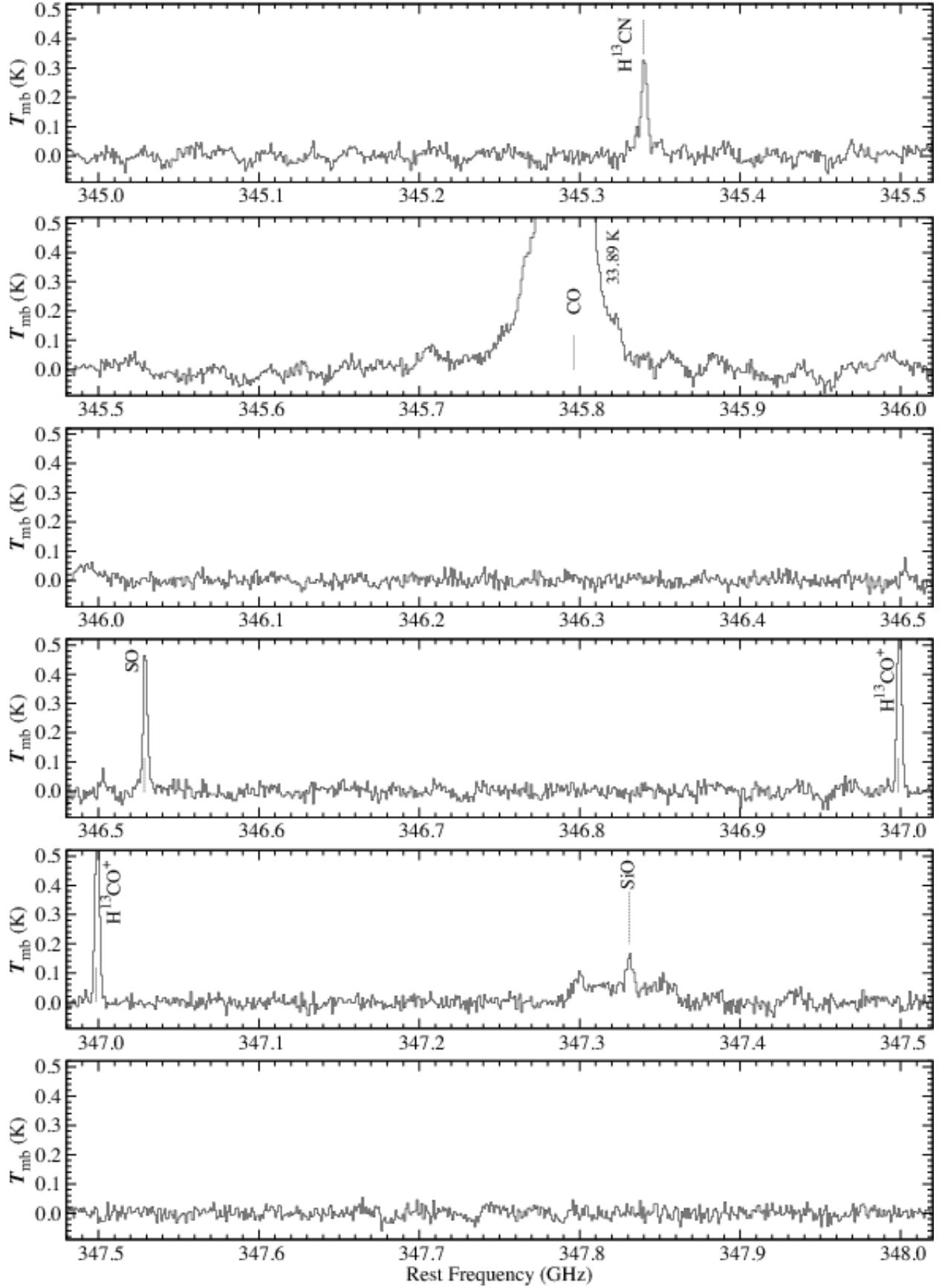


Fig. A.2.— *Continued*

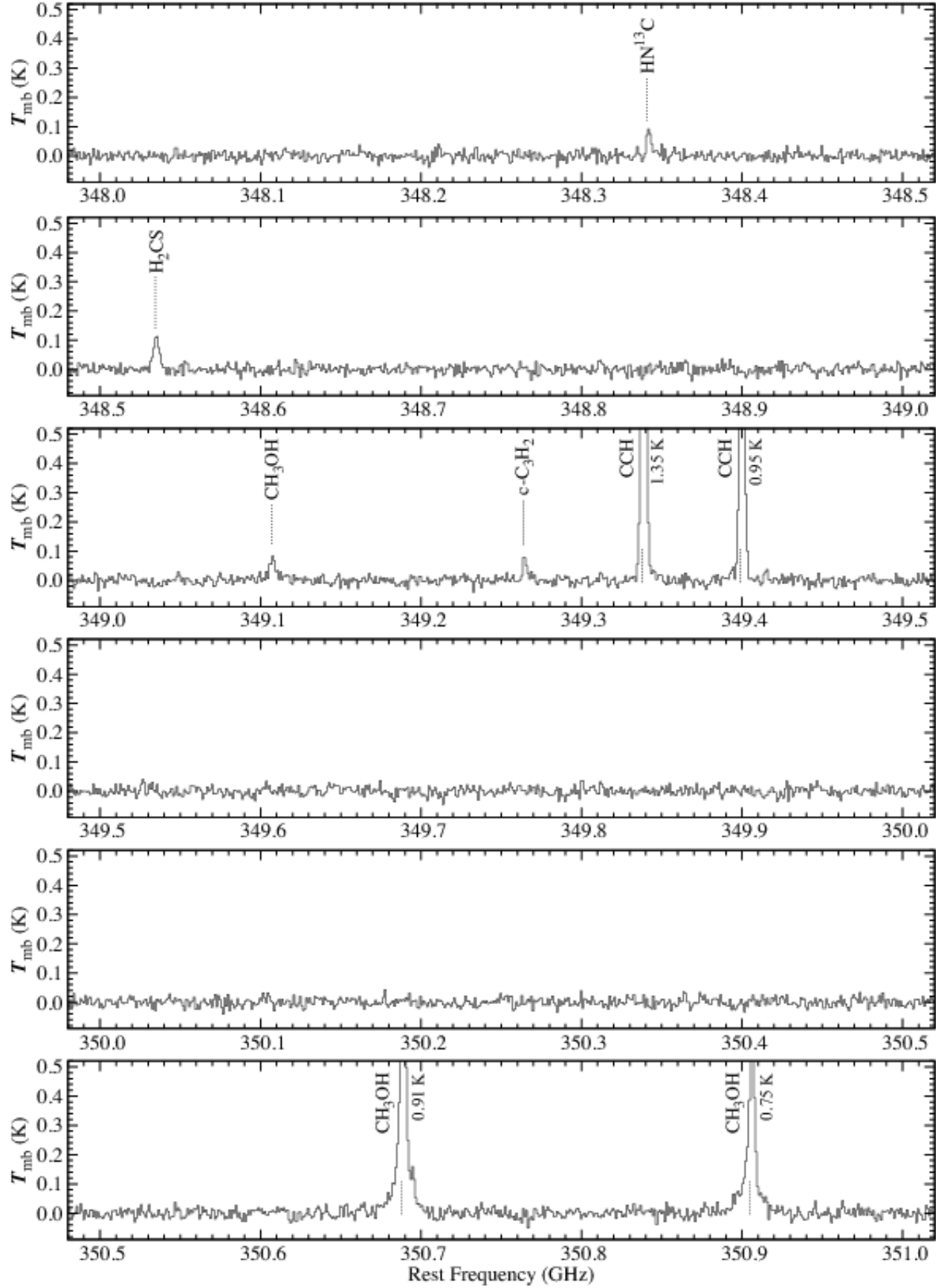


Fig. A.2.— *Continued*

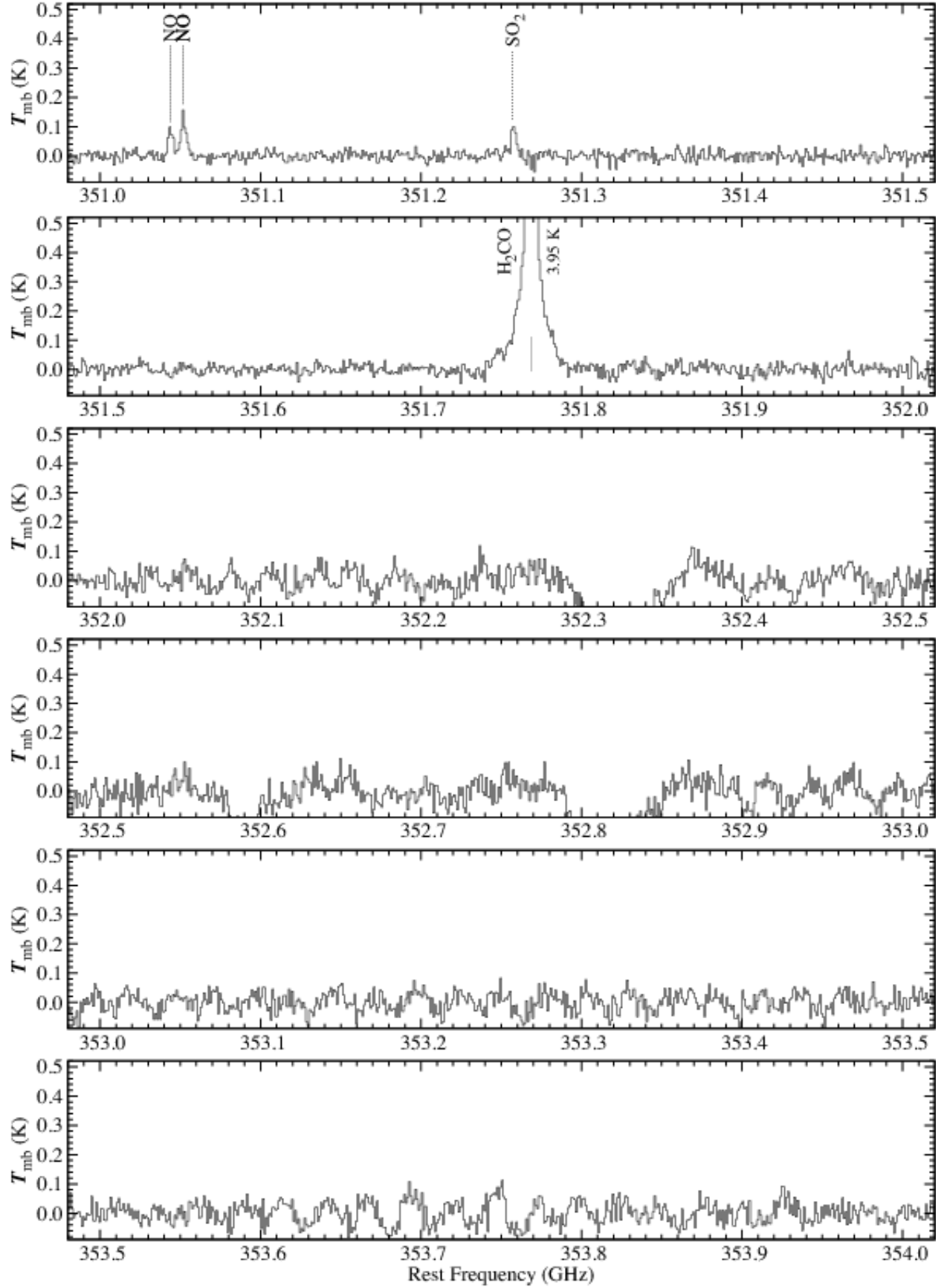


Fig. A.2.— *Continued*

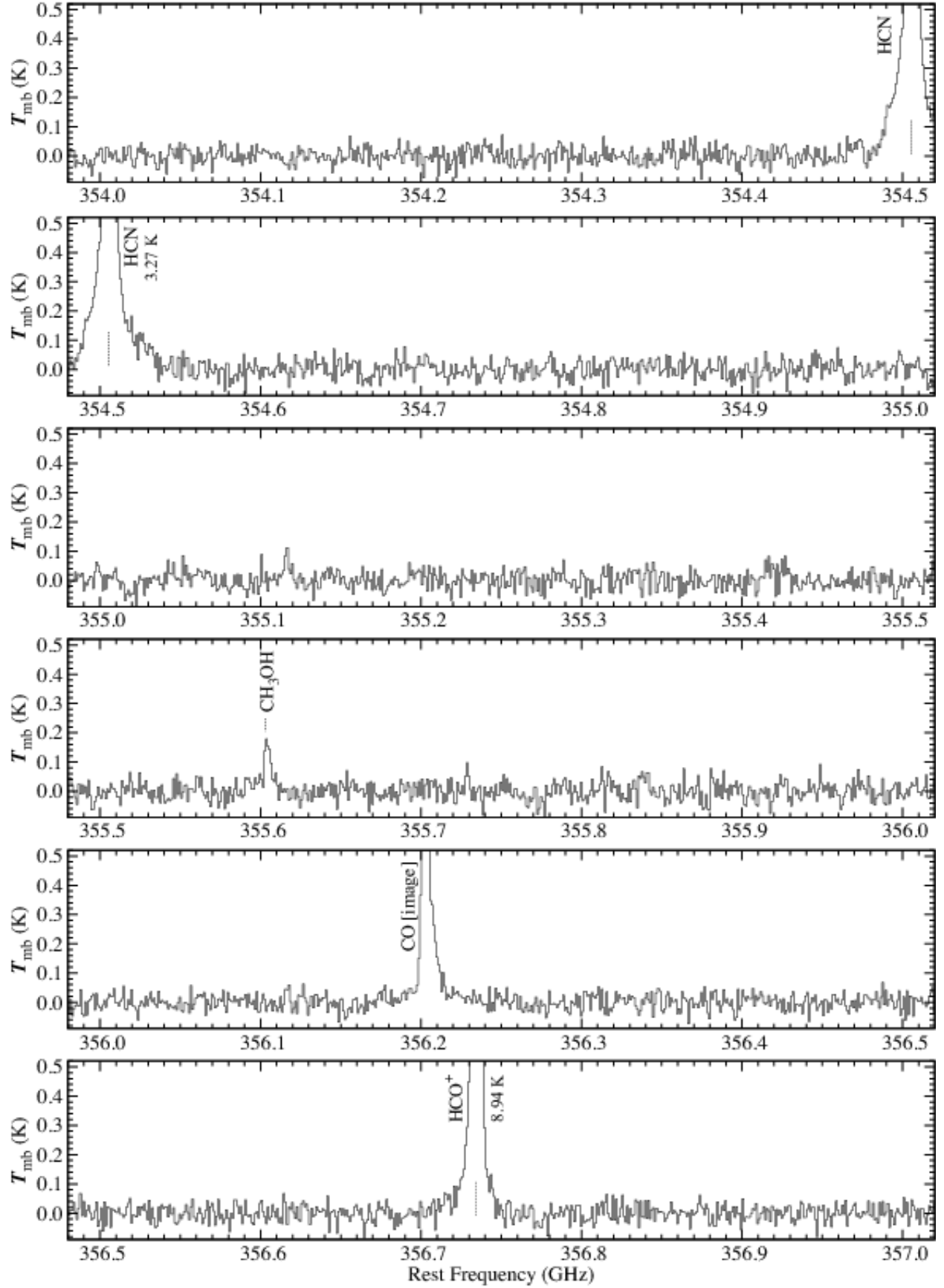


Fig. A.2.— *Continued*

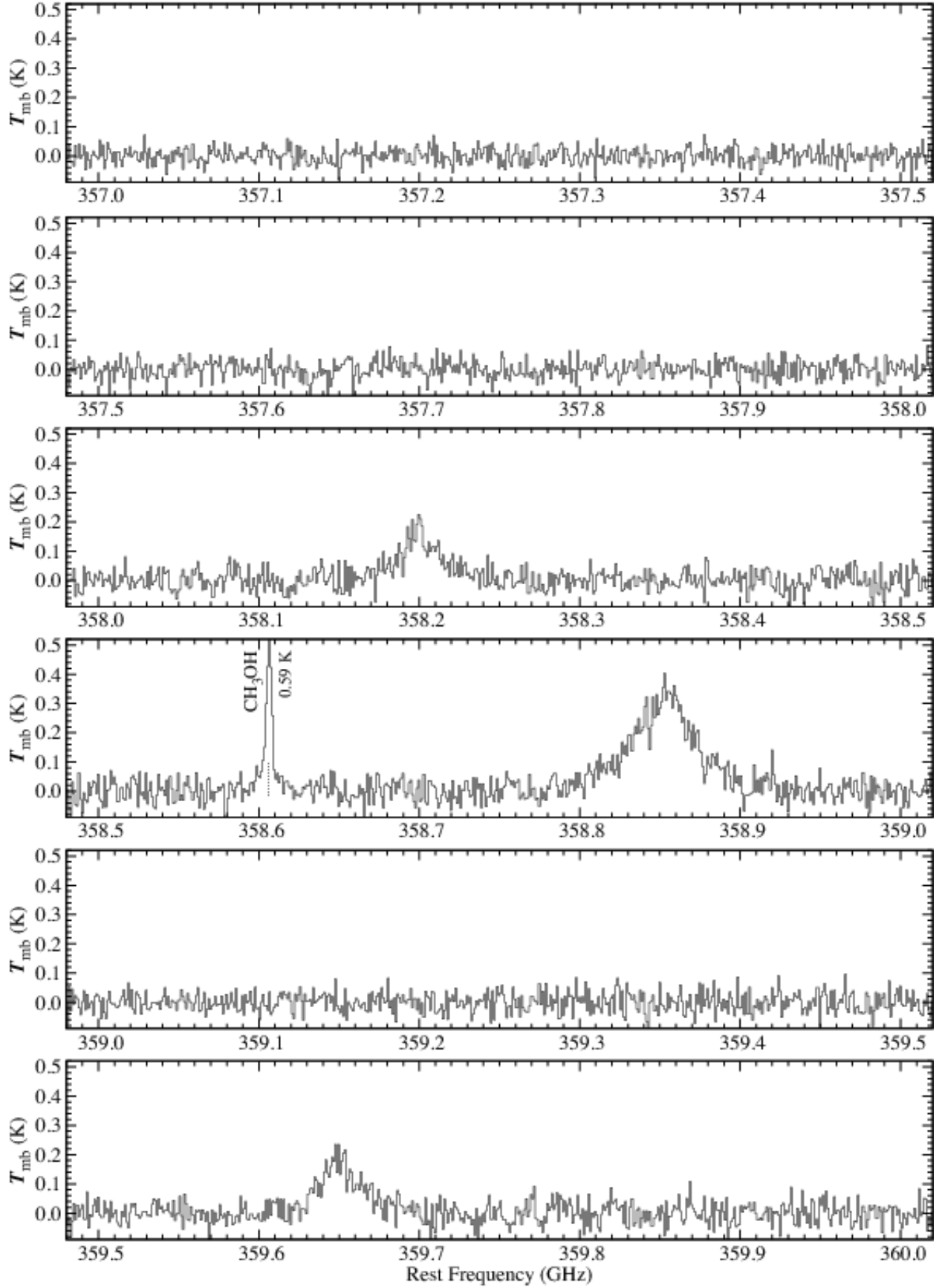


Fig. A.2.— *Continued*

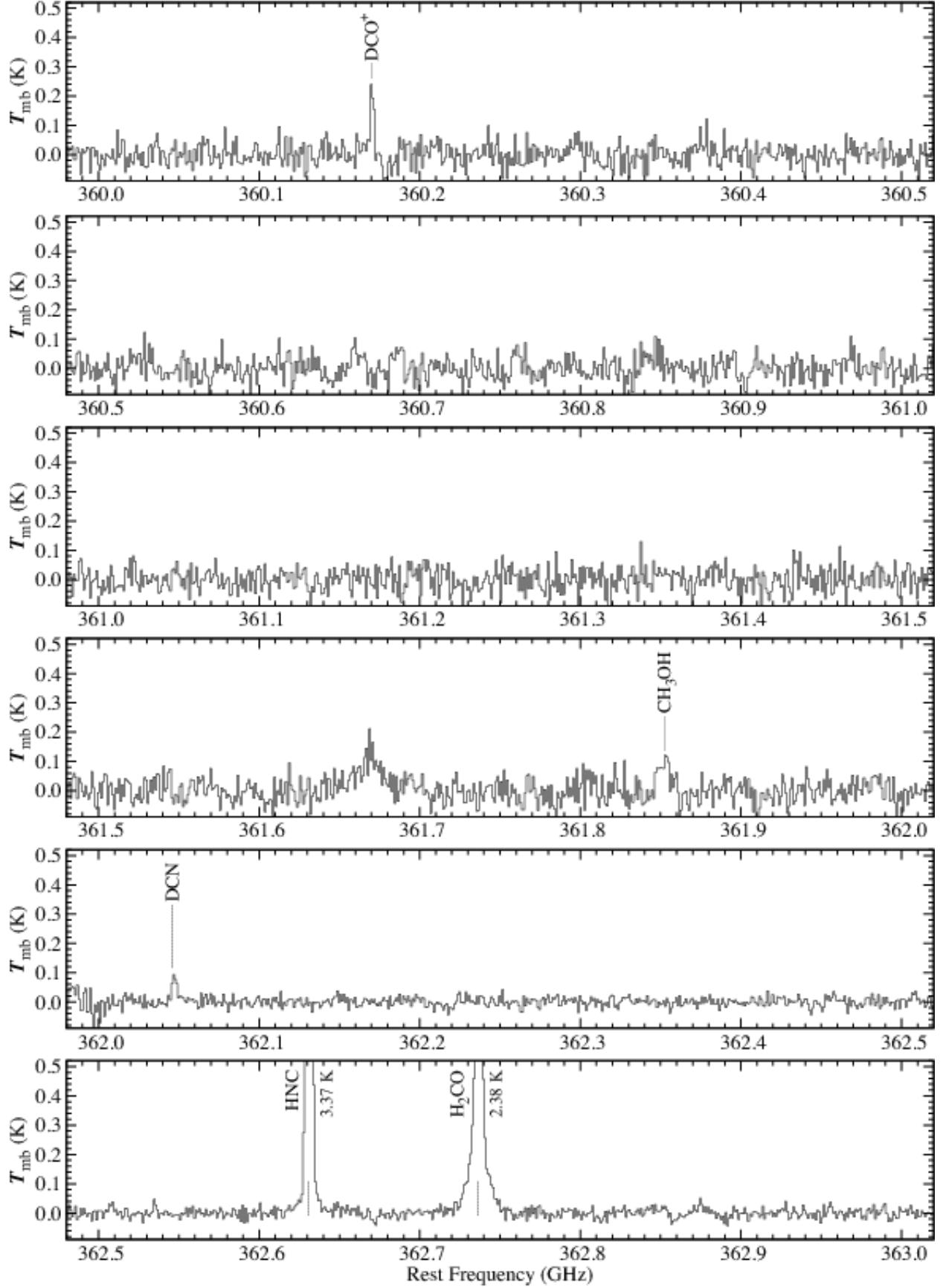


Fig. A.2.— *Continued*

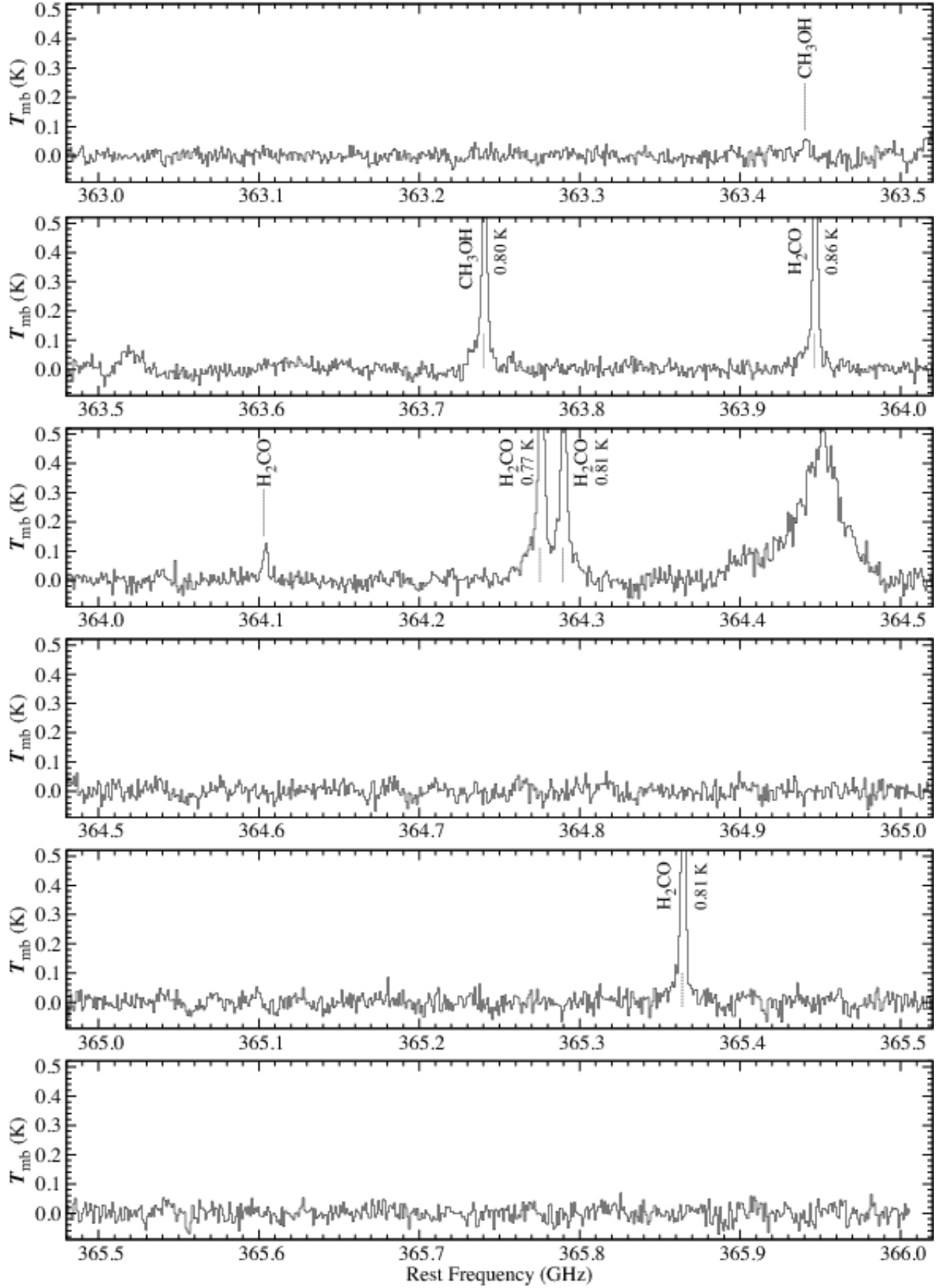


Fig. A.2.— *Continued*